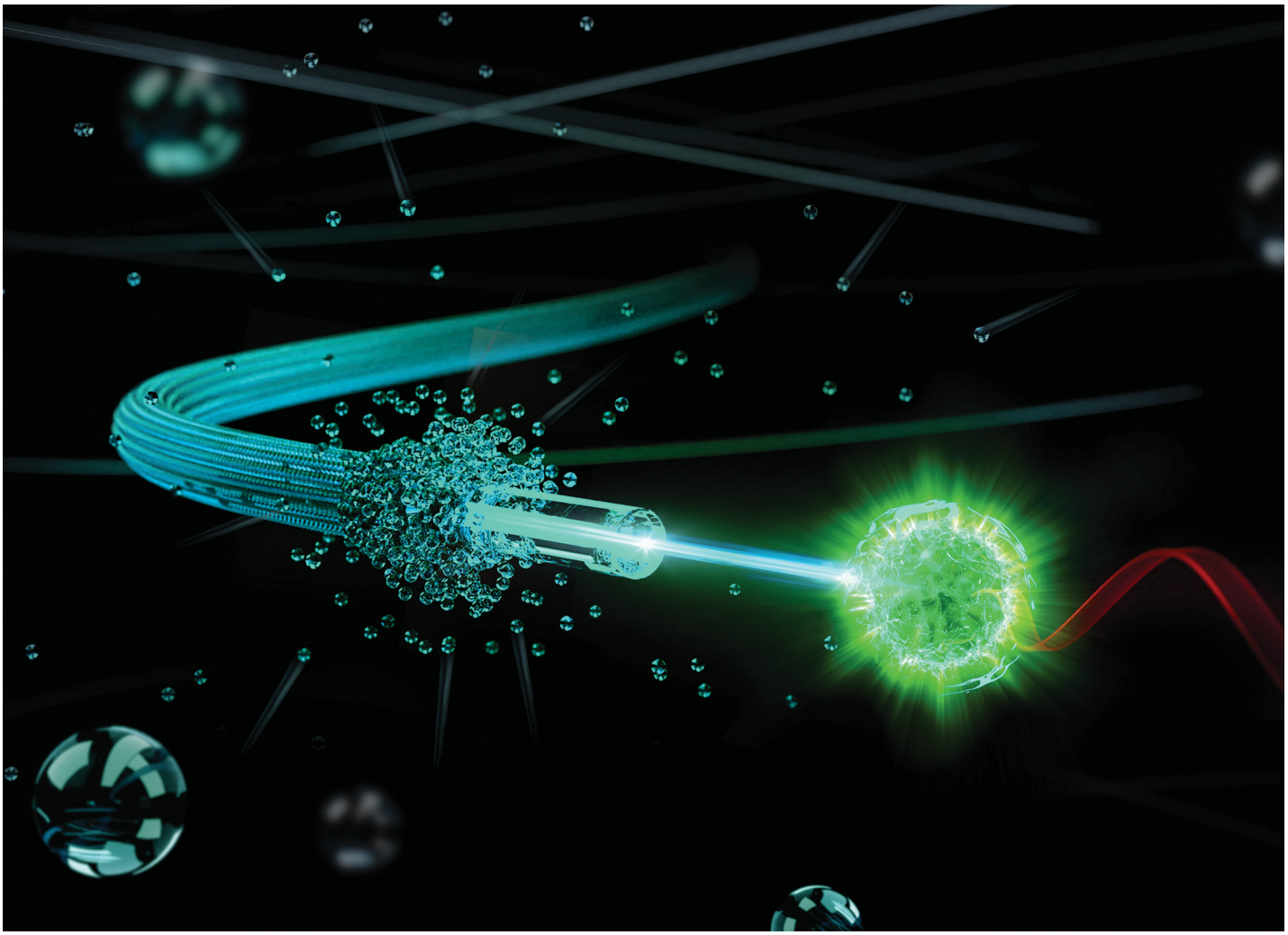


Showcasing research from Dr Mustafa Ordu's laboratory, National Nanotechnology Research Center (UNAM) and Institute of Materials Science and Nanotechnology, Bilkent University, Ankara, Turkey.

Hydrogel-integrated optical fiber sensors and their applications: a comprehensive review

The review article summarizes the recent advancement in hydrogel-based fiber optic sensing for biomedical and environmental applications. This work covers the fundamentals of hydrogels and their synthesis process, light-guiding and sensing mechanisms adopted by hydrogel-integrated optical fiber sensors, current progress in the fabrication procedures, and a brief evaluation of the applications of the hydrogel-integrated optical fiber sensors. The fundamental aim is to provide a comprehensive insight and future perspective about hydrogel-integrated optical fiber research for the multidisciplinary research communities.

As featured in:



See Mustafa Ordu *et al.*, *J. Mater. Chem. C*, 2023, **11**, 9383.

ROYAL SOCIETY OF CHEMISTRY

rsc.li/materials-c

Registered charity number: 207890

Journal of Materials Chemistry C

ROYAL SOCIETY OF CHEMISTRY

REVIEW

View Article Online
View Journal | View Issue

Check for updates

Cite this: J. Mater. Chem. C, 2023, 11, 9383

Hydrogel-integrated optical fiber sensors and their applications: a comprehensive review

Md. Sazid Bin Sadeque,[a] Hussain Kawsar Chowdhury,[a] Muzaffar Rafique,[a] Mehmet Atıf Durmuş,[a] Md. Kawsar Ahmed,[a] Md. Mehdi Hasan,[a] Aykut Erbaş,[ab] İbrahim Sarpkaya,[a] Fatih Inci[a] and Mustafa Ordu *[a]

Received 6th April 2023,
Accepted 9th June 2023

DOI: 10.1039/d3tc01206a

rsc.li/materials-c

Hydrogel-integrated optical fiber sensors have garnered momentous interest due to their optical properties, biocompatibility, and biodegradability. Integrating active materials with hydrogels facilitates hydrogels to be employed as a smart material that responds to external stimuli in biological or chemical media, allowing them to be a potential candidate for sensing applications. Although substantial research efforts have been made on integrating hydrogels with optical fibers, this field has never been reviewed extensively. In this paper, hydrogel-integrated optical fiber sensors are reviewed comprehensively, including the fundamentals of hydrogels, the synthesis process, and the working principle of various sensing methods. The light-guiding and sensing mechanism adopted by hydrogel-integrated optical fibers is discussed. The current progress in their fabrication procedures is categorized and explained. Finally, we have briefly evaluated the applications of hydrogel-integrated optical fiber sensors in various fields spanning from biosensing to environmental sensing.

Published on 13 June 2023. Downloaded by Bilkent University on 12/9/2023 12:01:00 PM.

1. Introduction

Hydrogels are three-dimensional networks of hydrophilic or charged polymer chains[1,2] that can adsorb large amounts of solvent and exhibit a high degree of stimuli-responsiveness. Due to their high water content, hydrogels demonstrate a close resemblance to the environment of living cells and tissues, which enables them to interact with biological systems without causing significant irritation, inflammation, or adverse reactions. Moreover, their softness, flexibility, and nontoxicity make them an ideal candidate for biocompatible materials.[3]

Their stimuli-responsive nature has led to extensive exploration of hydrogels for a broad range of applications, including biosensing,[4–6] environmental sensing,[7,8] bioelectronics,[9] tissue engineering,[10,11] artificial muscle development,[12] regenerative medicine,[13,14] cell separation,[15,16] brain function monitoring,[17,18] drug delivery,[19,20] photo-thermal therapy,[21] pharmaceuticals,[22] and diagnostics.[23,24] More recently, various hydrogel-based sensor platforms have been demonstrated to detect minuscule-level changes in glucose[28] and lactate concentrations[29] as well as in pH,[30] humidity,[31] and temperature levels.[32] By tailoring hydrogels' polymeric composition, physiochemistry, cross-linker density, and electrical charge of constituting polymer chains,[6] their viscoelasticity, molecular permeability, de/swelling kinetics, and responsiveness to various stimuli from light to mechanical forces[4] can be tuned further, and a new generation of hydrogel-based sensor systems can be constructed.

From a very general perspective, hydrogel-based sensors could be classified into two main groups: (i) stimuli-responsive and (ii) passive sensors. Stimuli-responsive hydrogel sensors can change phase and volume in response to exposure to a stimulus, while passive hydrogel sensors accommodate a responsive substrate in their matrices that can interact with input signals and produce output signals for detection.[24–28] The responsive components can be nanomaterials, biomolecules, and even living cells.[25]

Because of their large solvent content, hydrogels are optically transparent to a wide range of the optical spectrum, from visible to near-infrared (NIR) frequencies. For this reason, apart from the state-of-the-art applications mentioned above, hydrogels have been used to fabricate optical contact lenses that harvest the biocompatibility and gas-penetration capabilities of these polymeric networks.[1] More recently, beyond their conventional optical use in contact lenses, hydrogel-based optics[26,27] and photonics[28] have gained immense interest; hydrogel-based thin films, coatings, optical fibers, and waveguides have been explored as potential options for hydrogel photonics sensing, *i.e.*, photonic bandgap, plasmonic, and reflection and refraction index modulation-based sensors.[29,30]

[a] UNAM – Institute of Materials Science and Nanotechnology, Bilkent University, Ankara 06800, Turkey
[b] University of Silesia, Institute of Physics, Katowice Poland, Poland.
E-mail: ordu@unam.bilkent.edu.tr

Published on 13 June 2023. Downloaded by Bilkent University on 12/9/2023 12:01:00 PM.

An optical fiber generally consists of a core and cladding, where the refractive index (RI) difference between the core and the cladding confines light into the core and guides it through it. Any change in the properties of the propagation medium leads to variation in the output signal and provides sensing capabilities to such fibers. The flexibility, reliability, cost-effectiveness, and high sensitivity of optical fibers, while requiring a small molecular volume, have introduced the term "Lab-on-fiber".[31,32] Incorporating hydrogels into optical fiber structures further improves the sensitivity and selectivity of optical fibers[43] since hydrogels' refractive index is directly related to their structural and chemical composition. Indeed, hydrogels have already been utilized at fiber tips and fiber claddings and as Bragg grating and long periodic fiber grating.[31,33,34]

Hydrogels have been integrated with several nanomaterials to exploit various optical sensing principles as passive sensors, *i.e.*, change in the refractive index or transmission window, surface plasmon resonance (SPR),[35] localized surface plasmon resonance (LSPR),[36] Bragg grating sensor,[37] interferometry,[38] and fluorescence technique.[39] Although the number of efforts on integrating hydrogels with optical fibers has been surging in recent years, this field has never been reviewed extensively and hence a comprehensive look into the literature can benefit both new researchers and those who have been guiding the field. We note that while several reviews discuss hydrogel optics[40] and hydrogel-based sensors,[41–44] those discussions are rather brief and not comprehensive enough for hydrogel-integrated optical fibers, optical fiber sensing principles, and their applications.

This review covers the progress of hydrogel-integrated optical fiber fabrication for chemical/physical sensing applications (Fig. 1). The manuscript is organized into four main sections. The first section focuses on hydrogel synthesis, including

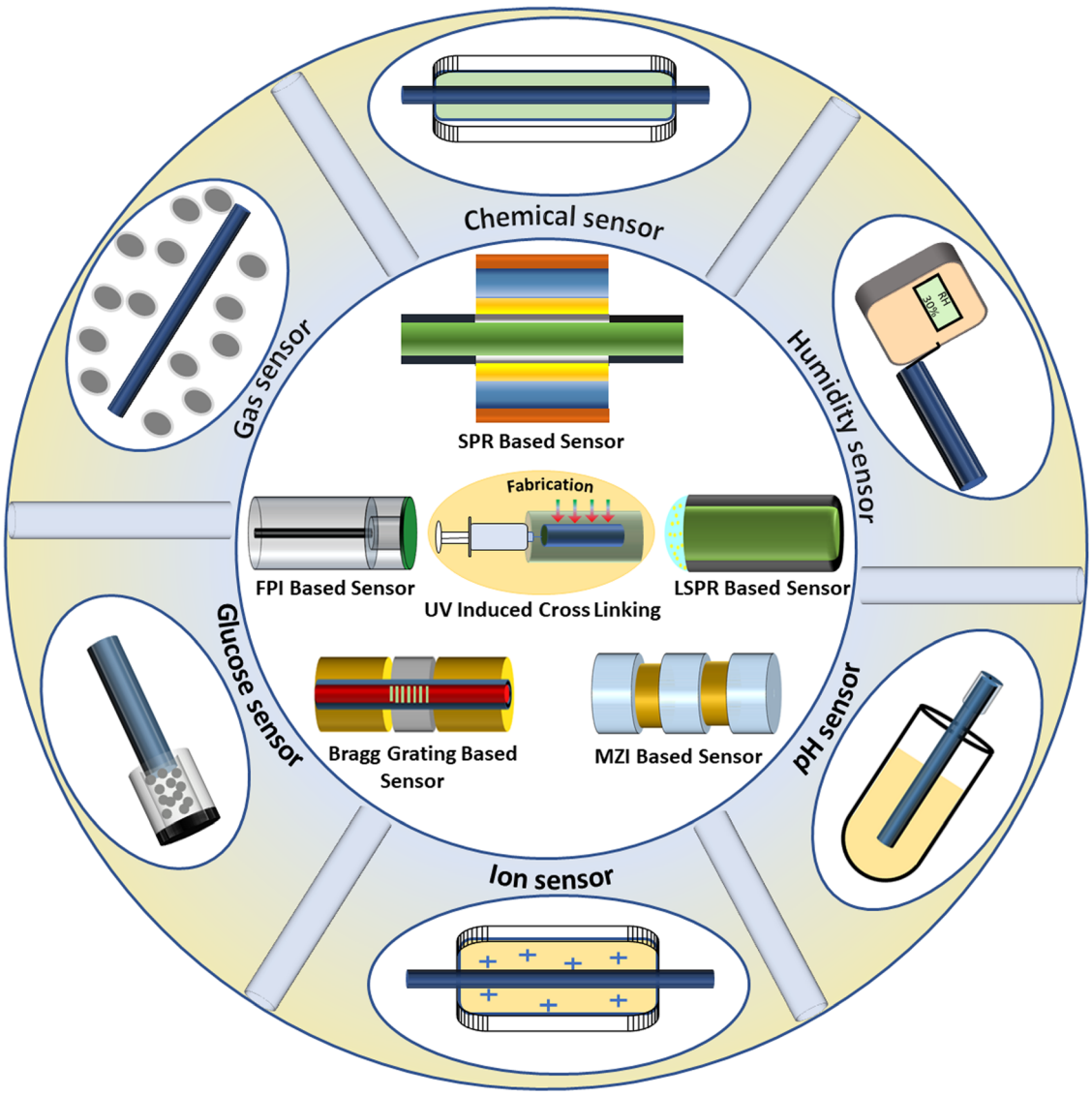


Fig. 1 Illustration of the fabrication methods of pure optical waveguides and optical sensors (SPR, LSPR, FPI, MZI and Bragg grating based sensors) and the major applications (glucose, pH, humidity, ion, gas and chemical sensing) of hydrogel-integrated optical fiber sensors.

 This journal is © The Royal Society of Chemistry 2023

Published on 13 June 2023. Downloaded by Bilkent University on 12/9/2023 12:01:00 PM.

physical and chemical cross-linking, comparative discussions on hydrogels, aerogels, and xerogels, and a brief discussion of the phase separation process of hydrogels. In the following section, the light-guiding principle of optical fibers is briefly discussed. The later section describes various optical sensing principles implemented in hydrogel optical sensing and the effect of nanomaterial incorporation in hydrogel matrices to improve their sensitivity. Next, various hydrogel-integrated optical fiber fabrication technologies and the hydrogel integration protocols that have been reported in the literature so far are extensively covered. The following section provides a detailed review of sensing applications, including biosensing and environmental sensing. Finally, the review concludes by providing an outlook on the development of the field and research gaps for future direction.

2. Overview of hydrogel structures

2.1. Synthesis of hydrogels

Hydrogels' tendency to contain large amounts of solvent in their pervaded volume is a consequence of their hydrophilic polymers, which prefer interactions with polar solvents, such as water, more than they do with themselves. Thus, hydrogel chains host hydrophilic groups, such as –COOH, $–NH_2$, $–CONH_2$, and –OH, attached to polymer chains, while crosslinkers connect chains and provide the nodes for the polymer network (Fig. 2a(i and ii)). Polymer chains can be cross-linked through relatively weak physical interactions such as hydrogen bonding, electrostatic interactions, hydrophobic interactions, crystallization, or relatively strong covalent bonds to form hydrogels. In general, the crosslinker's physiochemical properties and relative density (with respect to polymer chain monomers) control water-absorption levels and mechanical properties as well as optical properties of hydrogels.[45–48] Below, we will briefly overview the strategies used to obtain hydrogel networks along with their resulting mechanical properties.

2.1.1. Physically cross-linked hydrogels. The following section investigates the underlying physical mechanisms which are responsible for the formation of hydrogels. Physical crosslinking between polymer chains occurs due to weak molecular interactions such as hydrogen bonding, electrostatic interaction, hydrophobic interactions, and crystallization.[49] Hydrogen bonding provides a means of crosslinking between polymer chains and biomolecules, while electrostatic interactions occur between charged species and polyelectrolyte chains. On the other hand, the utilization of amphiphilic block copolymers or the integration of hydrophobic copolymers onto polysaccharide gives rise to hydrophobic interactions. Physically cross-linked hydrogel networks are generally weaker than their chemically cross-linked counterparts.[50]

Hydrogen bonding. The hydrogel structure can be synthesized through hydrogen bonding between synthetic polymer chains or biomolecules. The hydrogen bond occurs due to weak interactions between strongly electronegative atoms such as O, N, *etc.* These atoms can act as hydrogen acceptors. On the other hand, hydrogen atoms that are covalently bonded to another strong electronegative atom with lone pair of electrons act as hydrogen donors. In hydrogels, polymer chains can be cross-linked through multiple hydrogen bonds. The general schematic of hydrogen bonding is represented in Fig. 2b(i), where red atoms are the donors of lone electron pairs and gray atoms (hydrogen) are the acceptors to form a hydrogen bond. For example, ureidopyrimidinone (UPy) moieties can act as physical crosslinkers[51] by forming hydrogel bonds if chains are end-functionalized by UPy. UPy functional groups can form up to four hydrogen bonds between polymer chains and the formation of bonds occurs when the polymer solution is heated.[51] Similarly, synthetic hydrogels can be formed from dimethylacrylamide (DMAA) and methacrylic acid using hydrogen bonding between DMAA and the carboxylic acid group on methacrylic acid.[50] These hydrogels are pH sensitive and have a high refractive index, which makes them useful for photonics applications.[30]

Furthermore, hydrogels can also be obtained by introducing cross-linking through biological compounds, such as nucleobase pairs, that can make hydrogen bonds among themselves.[49,52] Similarly, other biomolecules, such as polypeptide chains, can self-assemble into stable β-sheet nanofibers, which are hydrogen bond-driven secondary structures. If the concentration of the nanofibers is above a critical value, these fibers can also form a hydrogel-like structure.[53]

Moreover, hydrogels can be synthesized from polymeric solutions that can undergo a crystallization transition. Low molecular compounds such as surfactants or amphiphilic peptides can assemble into crystalline structures in a solution.[54] If these groups are incorporated into chains, when the solution is allowed to cool, chains can form network structures through intermolecular interactions between crystals. The crystallization process can be affected by various factors such as temperature, solvent type, and cooling rate.[55] For example, poly(vinyl alcohol) (PVA) hydrogels are formed when water freezes; the temperature drop causes PVA chains to segregate and form high-concentration regions of PVA.[56,57] PVA chains then form strong hydrogen bonds with each other causing crystallization. These crystallized regions act as physical cross-linkers of the PVA hydrogel. The mechanical and biocompatibility properties of the crystallizing hydrogel such as PVA may depend on various factors such as type of polymer, polymer molecular weight, temperature, time of freezing, and the number of freezing cycles.[56,57]

Electrostatic interactions. Electrostatic interactions occur between species carrying a net charge, such as macromolecular chains bearing charged moieties and weak or strong polyelectrolyte chains (*i.e.*, charged polyions). The strength of such interactions depends on the charge valency and distance between the charged groups. Polymer chains with oppositely charged complementary functional groups like carboxylic acids and amines form polypeptide networks that can form complexes *via* electrostatic interactions.[49] These complexes can result in a network structure (Fig. 2b(ii)). Similar cross-linking

Published on 13 June 2023. Downloaded by Bilkent University on 12/9/2023 12:01:00 PM.

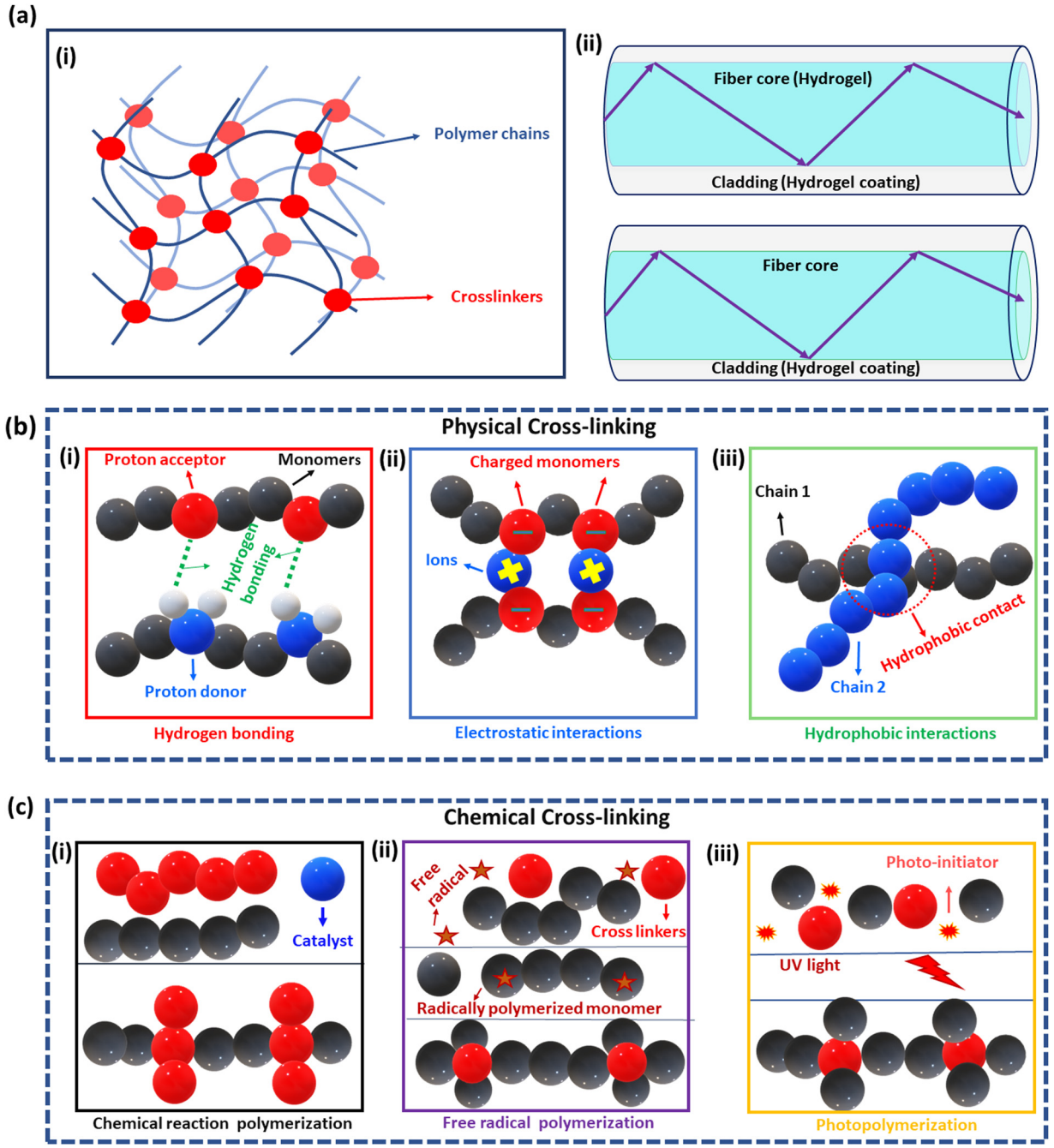


Fig. 2 Structure and synthesis of hydrogels. (a) Hydrogel formation for optical fiber applications: (i) crosslinking of polymer chains for hydrogel formation and (ii) usage of hydrogels as the core/cladding (above) and cladding (below) of an optical fiber. (b) Physically crosslinking methods used for formation of a hydrogel: (i) cross-linking of polymeric chains *via* hydrogen bonding to form a hydrogel, (ii) cross-linking *via* electrostatic interactions between charged polymeric chains and ions, and (iii) cross-linking through hydrophobic interactions between polymeric chains. (c) Hydrogel formation by chemically crosslinking methods: (i) crosslinking of two polymers (black and red) using chemical reaction in the presence of a catalyst (blue), (ii) free radical polymerization of polymers (black) with crosslinkers (red) initiated by free radicals (stars), and (iii) polymerization of photosensitive monomers (black) with photo-initiators (red) under UV light.

or bridging between multiple chains can form *via* multivalent ionic species, such as Ca^{2+}, Fe^{3+}, Zn^{2+}, *etc.*, to form hydrogels.[49] For instance, a weak polyelectrolyte such as poly(acrylic acid) (PAA) becomes negatively charged if its carboxylic acid monomers lose hydrogen ions when the pH of the medium is high. The carboxylic group, $-COO^-$, can bind with Fe^{3+} ions and form a network structure. Another example of hydrogels formed from multivalent cations is the one formed from alginate and Ca^{2+}. Alginate is formed from alginic acid, which comprises of a large amount of carboxylic acid functional groups. They can

 This journal is © The Royal Society of Chemistry 2023

Published on 13 June 2023. Downloaded by Bilkent University on 12/9/2023 12:01:00 PM.

electrostatically bind with Ca^{2+} ions, leading to alginate solution gelation. Alginate hydrogels are used as drug-delivery carriers, artificial tissues, and organs.[58,59]

Hydrophobic interactions. Hydrophobic interactions arise due to the water-repelling tendency of the chemical group and play a vital role in biological processes such as protein folding, biomolecular complexes, *etc.*

Amphiphilic block copolymers composed of hydrophobic and hydrophilic groups can form hydrogels through hydrophobic interactions if the polymer solution is heated.[61] Since hydrophobic interactions are of entropic nature, through heating, hydrophobic interactions become more dominant and lead to cross-links when the polymer solution reaches a critical gel concentration (Fig. 2b(iii)).[49] An example of amphiphilic block copolymers is the poly(*N*-substituted acrylamide) and poly(vinyl ether)-based copolymer. These thermo-responsive polymers undergo a reversible sol-gel transition through hydrophobic interactions when heat is applied and the temperature goes below or above the critical temperature.[60–62] Moreover, hydrophobic copolymers can be grafted to polysaccharides such as chitosan, hyaluronic acid (HA), dextran, and pullulan to form a temperature-sensitive hydrogel through hydrophobic interactions.[63]

Precise engineering of hydrogels with tailored properties encompassing mechanical strength, responsiveness to external stimuli, and biocompatibility requires understanding these mechanisms, which may enable novel prospects for their multifaceted applications.

2.1.2. Chemically cross-linked hydrogels. The following discussion will discuss chemically cross-linked hydrogels encompassing various mechanisms involved in their formation. Chemically cross-linked hydrogels form *via* strong covalent bonds between polymer chains. The process by which covalent bonds form between macromolecular chains can either be by chemical reaction of functional groups or by free radical polymerization of vinyl monomers along with cross-linking agents.[49] Chemical reactions such as ''click'' chemistry, Schiff-base reactions, and condensation reactions offer advantages such as high reaction rates, high chemical yield, and mild reaction conditions that enable formation of hydrogel networks with desirable properties. On the other hand, free radical polymerization utilizes vinyl monomers and cross-linking agents to form hydrogels. Additionally, photopolymerization offers a technique for synthesizing hydrogels using photosensitive monomers and UV light exposure, which is advantageous in controlling the coating thickness of the optical fiber. Chemically cross-linked hydrogels can have excellent thermal stability, mechanical strength, and surface chemistry. Also, these properties can be optimized according to the application for which they are being used.

Cross-linking by chemical reactions. Polymer chains can be cross-linked by chemical reactions such as ''click'' chemistry, Schiff-base reactions, and condensation reactions to form hydrogels.[64] These chemical reactions are advantageous due to high reaction rates, high chemical yield, fewer chemical byproducts, and mild reaction conditions.[64] Fig. 2c(i) represents crosslinking of two polymers (black and red) using chemical reaction in the presence of a catalyst (blue).

An example of a ''click'' reaction is azide–alkyne cycloaddition, which occurs between azide and alkyne groups. Hydrogel networks of HA can be synthesized by using azide-functionalized groups as crosslinkers and Cu^{2+} as a catalyst.[65] Mechanical properties of such hydrogels can be altered and optimized by varying the alkyne/azide ratio. Schiff-base reactions facilitate amine-functionalized and aldehyde functional groups to obtain an imine bond. Hydrogels synthesized *via* Schiff-base reactions usually contain amine and aldehyde groups, which are abundant in human blood, making these hydrogels highly biocompatible and useful for biomedical applications. Schiff-base reactions can also be implemented for polymers with an amine group, such as chitosan (biopolymer rich in an amine group), and crosslinkers with difunctionalized aldehyde groups, such as glutaraldehyde.[66] Moreover, Schiff-base reactions can also occur between two types of polymers which contain amine and aldehyde groups. For instance, an injectable hydrogel can be synthesized by mixing four-arm poly(ethylene glycol) (PFA) with aldehyde groups and four-arm poly(ethylene glycol)-*b*-poly(L-lysine) (PPLL) with amine groups.[67] Imine hydrogels are pH sensitive. Therefore, properties such as mechanical strength, swelling kinetics, degradation, *etc.*, can depend on pH levels. Furthermore, the Schiff-base reaction benefits the dynamic equilibrium between imine linkages and reactants (amine and aldehyde groups) so that the hydrogel can have self-healing properties.

Condensation reactions can also be used to synthesize hydrogels. They utilize carboxyl groups and an amine or hydroxyl functional group to form an amide and an ester bond, respectively. Under suitable coupling conditions, reagents such as *N*,*N*-(3-dimethylaminopropyl)-*N*-ethyl carbodiimide (EDC) and polymers with a carboxyl group and amide (or hydroxyl) groups can result in a hydrogel network through a condensation reaction. Such condensation reactions can also lead to a hydrogel by utilizing alginate with a carboxyl group and diamino-terminated PEG with amine groups in the presence of EDC.[68] Changing the crosslinker's (diamino-terminated PEG) concentration and molecular length can alter the mechanical and optical properties of such hydrogels.

Cross-linking by free radical polymerization. Chemically cross-linked hydrogels are commonly produced by using free radical polymerization.[69] To obtain a crosslinked network, this method mainly requires vinyl monomers such as PAA, styrene, vinyl chloride, *etc.*, in the presence of a cross-linking agent. Free radical polymerization goes through three stages: initiation, propagation, and termination. Initiators such as potassium persulfate (KPS), ammonium persulfate (APS), and benzoyl peroxide are used to start the polymerization reaction by radically polymerizing the vinyl monomers in the presence of a cross-linking agent to form a cross-linked hydrogel. As more monomers become cross-linked, the polymer solution's

Published on 13 June 2023. Downloaded by Bilkent University on 12/9/2023 12:01:00 PM.

viscosity increases, ultimately leading to gelation. At the same time, the polymerization process terminates. Homopolymer (single same monomer unit) and copolymer (two or more different monomer units) hydrogels are often produced using free radical polymerization. Fig. 2c(ii) represents free radical polymerization of polymers (black) with crosslinkers (red) initiated by free radicals (stars). A common example of homopolymer hydrogels is poly(*N*-acryloyl glycinamide) thermo-responsive hydrogel, which is synthesized from the *N*-acryloyl glycinamide (NAGA) vinyl monomer with two amides separated by carbon in the side chain.[70] However, copolymer hydrogels allow more tailoring ability as compared to homopolymer hydrogels. Poly(*N*,*N*-diethyl acrylamide-*co*-methacrylic acid) is a well-known example for pH-thermo-responsive hydrogel copolymers synthesized from *N*,*N*-diethyl acrylamide and methacrylic acid (MAA) monomers in the presence of the *N*,*N*′-methylenebis acrylamide (MBAm) crosslinker using free radical polymerization.[71]

The reversible addition-fragmentation chain transfer (RAFT) polymerization technique can also be used for the controlled synthesis of hydrogels. The RAFT polymerization technique uses a RAFT agent, solvent, monomer, and initiator. The synthesis of polymer chains is controlled using a RAFT agent, which serves as a mediator between growing polymer chains and the initiator. The RAFT polymerization technique can be used to construct hydrogel-based microfibers.[72]

Cross-linking by photopolymerization. In this method, photosensitive monomers are used to synthesize hydrogel structures for optical fiber applications. The photosensitive monomers are mixed with a photo-initiator to form a solution and when the solution is exposed to UV light, a polymerization reaction leads to a hydrogel, which can be used as a coating on the surface of optical fibers.[34,73,74] Fig. 2c(iii) represents polymerization of photosensitive monomers (black) with photo-initiators (red) under UV light. The swelling and deswelling of the hydrogel can control the thickness of the optical fiber cladding. This method can be used for large-scale industrial applications, especially for the uniform and controlled coating of optical fibers. The optical fiber core can also be synthesized using hydrogels. For example, poly(ethylene glycol) combined with diacrylate (PEGDA) has been used to create an optical fiber core because of its high refractive index, which causes light to be total internally reflected in the optical fiber core.[75] Hydrogel-based optical fibers are used for measuring glucose and metal concentrations.[75,76]

2.2. Mechanical properties of hydrogels

The mechanical properties of hydrogels can be modeled by employing rubber elasticity and viscoelasticity theories.[77] These theories encompass time-dependent and time-independent relaxation of the polymer chains' orientation and structure, including polymeric materials' elasticity, flow, and molecular motion. By considering these theories, one can investigate the mechanical behavior of the polymer structure, effective molecular weight between cross-links, and information on the elastically active chains.

When gels are in a rubber-like regime (swollen state), they behave similarly to a rubber whose mechanical properties mainly depend on the polymer network structure.[78] Rubber-like hydrogels are composed of cross-linked networks with large free space. When an external stimulus is applied, the hydrogel's chains respond by changing the conformation. The viscoelastic response of hydrogels depends on the nature of the mechanical stimuli applied to the system, while their mechanical response depends on time-dependent stress and strain.[78] The mechanical properties of the hydrogels can be modified by controlling three factors: (i) monomer composition, (ii) cross-linking density, and (iii) polymerization conditions.

2.2.1. Effect of monomer composition. The strength of the hydrogel is directly related to the composition of the comonomer used to prepare the hydrogel. The use of heteropolymers has been reported to increase the physical strength of the final product.[79] For instance, replacing acrylate monomers with methacrylate monomers along a copolymer chain can increase the stiffness of the polymer backbone since methacrylate monomers give rise to more hydrophobic interactions as compared to acrylate monomers because of methyl groups. The mechanical properties of the hydrogel can also be altered by adding more hydrophilic groups in the hydrogel's polymer network, as in the case of replacing 2-hydroxyethyl methacrylate (HEMA) with methacrylic acid.[78] In contrast, HEMA copolymers and methyl methacrylate (MMA) copolymers have the same mechanical strength in their unswollen state, but when *N*-vinyl-2-pyrrolidone (NVP) is added to these copolymers, their mechanical strength is reduced significantly. This change also increases the degree of swelling of the hydrogel since NVP is a highly hydrophilic moiety.[78]

2.2.2. Effect of cross-linking density. The hydrogel's mechanical strength is often correlated with the cross-linking density.[80] The mechanical strength of the hydrogel increases with the increase in cross-linking density.[79] As the number of cross-links increases, the hydrogel's polymer chains can be more restrained, causing the hydrogel to increase its Young's modulus, which is directly related to the mechanical strength.[79]

2.2.3. Effect of polymerization conditions. In polymer chemistry, polymerization conditions such as temperature, solvent type, or how much solvent is used during the polymerization reaction determine the mechanical strength of the hydrogel.[79] To illustrate, cross-linking agents tend to form cycles instead of cross-links when a larger amount of solvent is used during polymerization, decreasing the number of cross-links in the hydrogel and reducing mechanical strength. Furthermore, the type of solvent (*e.g.*, ionic strength of aqueous solution or pH) used during polymerization can also change the copolymer structure, affecting the Young's modulus, which is a direct measure of mechanical strength.[79] The effect of polymerization conditions on the properties of the hydrogel was reported based on the copolymerization of HEMA and 2-dimethylaminoethyl methacrylate under different pH conditions and volume fractions of solvent.[81] An increase in the

 This journal is © The Royal Society of Chemistry 2023

Published on 13 June 2023. Downloaded by Bilkent University on 12/9/2023 12:01:00 PM.

swelling ratio by 400% was observed, which resulted from the structural change of the polymer network.[81]

2.3. Swelling properties of hydrogels

One of the notable features of hydrogels is that they can absorb large amounts of water. Since hydrogels consist of hydrophilic functional groups, they form hydrogen bonds with water molecules. As a result, water is absorbed and the polymer network prevents water from leaving the hydrogel structure. The swelling of hydrogels depends on factors such as polymer type, salt concentration in the medium, cross-linking density, and synthesis state. Swelling is directly affected by the functional group used in synthesizing the hydrogel.

The swollen state of a hydrogel is characterized by the swelling ratio. The swelling ratio (SW) is defined as

$$\mathrm{SW} = (W_{\mathrm{swollen}} - W_{\mathrm{dry}})/W_{\mathrm{dry}} \times 100$$

where W_{swollen} and W_{dry} represent the weight of the swollen and dry state of the hydrogel, respectively.

As the concentration of crosslinkers increases, the swelling ratio decreases and *vice versa*. The swelling ratio of the hydrogels may also depend on the chemical nature of the crosslinker. The swelling ratio is sensitive to external stimuli like electric field, mechanical deformation, exposure to light, and magnetic field.[71,82–85]

2.4. Stimuli-sensitive properties of hydrogels

Hydrogels can swell or deswell (changing their phase or volume) as a response to changes in the surrounding environmental conditions such as temperature, pH, *etc.*[5–7] When the physicochemical conditions are altered, the hydrogel structure responds to these changes by changing its structure or swelling ratio by changing the water intake and conformation of polymer chains to maintain its balance between elastic energy and osmotic stress.[86]

2.4.1. pH-Sensitivity. Many hydrogels exhibit pH-responsive swelling behavior. They can undergo significant volume changes in response to changes in the pH of the surrounding environment. This swelling behavior is often due to the ionization of functional groups present in the hydrogel network. If the polymer network is composed of acidic functional groups such as carboxylic acid or sulfonic acid, they will lose the hydrogen ions in case of pH change. As a result, the polymer backbone becomes ionized. On the other hand, if the polymer network consists of basic groups, such as amine, which accept hydrogen ions in the medium, it facilitates the polymer network's ionization. The charges on the polymer chains give rise to electrostatic repulsion between the monomers, which, along with the osmotic pressure of ions, stretches the polymer chains further. Under these conditions, polyelectrolyte hydrogels (consisting of many acidic or basic functional groups) can swell or de-swell in response to pH changes. For example, hydrogels of *N*,*N*′-dimethyl aminoethyl methacrylate (DMAEM) and methyl methacrylic acids show pH-sensitive swelling behavior. Such hydrogels exhibit a low swelling ratio at neutral pH, but at acidic pH, the swelling ratio increases.[87]

2.4.2. Thermo-sensitivity. Depending on the constituent polymer network, hydrogels can undergo a reversible volume phase transition in response to changes in temperature. These hydrogels are called thermoresponsive hydrogels. They can significantly change their swelling behavior as the temperature crosses a specific transition point known as the lower critical solution temperature (LCST) or upper critical solution temperature (UCST). The water solubility of the hydrogel changes if the temperature varies; this effect depends on the nature of the constituting polymers.[84] Polymers whose water solubility decreases as the temperature increases exhibit lower critical solution temperatures (LCSTs).[84] Therefore, LCST polymers swell as the temperature of the surrounding decreases and de-swell with the increase in temperature; they are also known as negative thermo-responsive systems. On the other hand, polymers with upper critical solution temperatures (UPSTs) show increased water solubility when the temperature is raised. Hence, UPST hydrogels swell with the increase in temperature and shrink at low temperatures and they are also known as positive thermo-responsive systems.[84] The temperature change can affect the refractive index of the optical fiber sensors in which hydrogels are incorporated, which allows the optical fiber to be considered for various biological sensing applications.[88,89]

2.5. Comparative discussion on hydrogels, aerogels, and xerogels

Aerogels and xerogels are light solid materials with highly porous structures and surface areas constructed from the drying of gels. Both these materials possess excellent properties such as thermal insulation, catalytic activity, and energy storage.[90,91] Although aerogels and xerogels are similar in some ways, they have some key differences. Aerogels are relatively lighter (density around 0.03 g cm^{-3}) than xerogels (density around 0.1–0.6 g cm^{-3}).[92] The pores in aerogels are more open (interconnected porous structure) relative to the xerogels. In other words, aerogel pores are smaller and isolated from each other. This means that aerogels have a much larger surface area than xerogels, making them useful for catalytic applications. One of the key distinctions between aerogels and xerogels is the production method used to dry the gel.

Aerogels are fabricated from the displacement of solvent content from the gel (polymer and a suitable solvent) under supercritical drying, where the gel is placed inside a high-pressure (50–100 atm) batch reactor and exposed to a supercritical fluid (SCF) such as methane, carbon dioxide, ammonia, and argon.[93] During the process, the batch reactor's pressure and temperature are maintained above the critical pressure and temperature of the SCF used. The solvent in the pore will dissolve in the SCF, and the SCF diffuses from the pores, leading to solvent-free aerogels.[93] The advantage of using a SCF is that it does not allow the coexistence of liquid and vapor. Hence, it reduces the capillary stress and surface tension in the pore walls, which avoids the collapse of the gel network during solvent removal.[94] The solvent is replaced by air while the polymer network structure is maintained. Therefore, aerogels

Published on 13 June 2023. Downloaded by Bilkent University on 12/9/2023 12:01:00 PM.

have very low density and high surface area; they can be modified with hydrophilic and hydrophobic elements to be applicable for different applications. Aerogels are used for various applications such as thermal insulators, controlled drug delivery, oil spill cleanup, micro-filters, *etc.*[94]

On the other hand, xerogels are prepared from the evaporation drying of wet gels under ambient conditions. Unlike aerogels, xerogels shrink and do not maintain their expanded polymer network conformation because capillary forces arise from surface tension induced in the liquid surface of the pores at the solid–liquid–vapor interface on the pore walls. The collapse of the pore walls can be avoided if capillary forces induced on the pore walls are reduced.[94] Chemical treatment of pore-wall surfaces with a nonpolar solvent before actual drying can reduce further condensation because of surface charges.[95] This method is relatively more time- and cost-efficient than supercritical drying and is used in the mass production of aerogels.

2.6. Optical applications of hydrogels

Like many other materials, hydrogels can also interact with light and behave differently depending on environmental conditions. Light can be reflected, transmitted, or scattered from a hydrogel surface depending on the type of hydrogel and wavelength of light. As the light propagates through the material, it loses its intensity upon interacting with the material due to light absorption and scattering. Typically, the optical loss in hydrogel-based optical fibers is in the range of tens of dB cm^{-1}, which is much higher than that found in the case of solid-state materials, like silica.[29,96] However, solid-state materials have higher refractive indices than hydrogels if the refractive index of water is considered as the baseline. A significant difference between the refractive indices of a solid-state material and water makes them problematic because of the coupling losses.[29,96] Furthermore, a considerable portion of solid-state materials are incompatible with the biological environment. This makes hydrogels a strong fit for optical-based biological applications.

2.7. Mechanism of hydrogel's phase transition

Various hydrogel-based sensors employ phase transition-induced optical property change as a sensing parameter. Hydrogels can undergo volume phase transition (VPT)[44] between various swelling states when they experience changes in environmental conditions or external stimuli. The phase transition mechanism in hydrogels can vary depending on the specific type of hydrogel and the triggering factors involved. For hydrogels that are sensitive to changes in ionic strength, a change in the concentration of ions in the surrounding environment can lead to changes in electrostatic interactions within the hydrogel network, resulting in swelling or deswelling.[86] pH-Sensitive hydrogels can undergo volume changes in response to pH variation. For instance, some hydrogels can swell or shrink when the pH crosses a certain threshold due to the ionization or deionization of the polymer network's acidic or basic functional groups.

In case of a change in the concentration of a specific analyte, the osmotic pressure generated (Π) forces the hydrogel to change volume until it reaches an equilibrium condition. Total osmotic pressure Π_T in the hydrogel is expressed as the volume derivative of Gibbs free energy difference between the reference state (*e.g.*, solvent-free) and phase transitioned (*e.g.*, swollen) hydrogel. The change in total free energy is associated with the free energy of mixing ΔG_M, the free energy of electrostatic interactions ΔG_I, and the free energy of crosslinking (elastic free energy) ΔG_E:

$$\Pi_T = \Pi_M + \Pi_E + \Pi_I$$

Under equilibrium conditions, the osmotic pressure associated with mixing Π_M, the electrostatic osmotic pressure Π_I, and the elastic restoring force osmotic pressure Π_E balance one another.[97–99] Even in high ionic strength solutions, localization of charge can lead to a large change in ΔG_M.[100,101] Further, elastic free energy ΔG_E variation can occur due to changes in cross-linking density (*e.g.*, in physically cross-linked hydrogels mentioned in Section 2). Moreover, ionic free energy ΔG_I can also change due to variations in the ionic conditions inside the hydrogel and in the environment.[102,103]

The Donnan effect describes the uneven distribution of charged particles (ions) across a semipermeable membrane. When charged polymer chains and ions are present in the hydrogel or the surrounding solution, they can create an imbalance in ion concentrations. Although constrained backbone charges (of the polymer chains) cannot freely move across the hydrogel, water and free ions can diffuse across the hydrogel until a chemical equilibrium is established. When the hydrogel composed of charged chains is immersed in a solution, the Donnan effect leads to an unequal distribution of ions inside and outside of the hydrogel. This uneven distribution creates an osmotic pressure difference in the hydrogel and leads to a solvent intake, which causes a volumetric phase transition. Moreover, phase transition can also occur due to other stimuli-responsive transitions, such as due to light, temperature, and electric and magnetic fields, which can change the crosslinking density or ionization levels in the hydrogel.

3. Optical fiber guiding mechanism

Light bends away from the normal when it passes from a higher refractive index (n_1) medium to a lower refractive index medium (n_2). The refraction of light is governed by Snell's law, which depends on both media's incident angle and refractive indices. While propagating through a high refractive index to a low refractive index medium, beyond a specific angle, the refraction no longer occurs and the light is completely reflected back to the high refractive index medium, as presented in Fig. 3a. This specific incidence angle is called the critical angle (θ_c) and the phenomenon is known as total internal reflection (TIR).

 This journal is © The Royal Society of Chemistry 2023

Published on 13 June 2023. Downloaded by Bilkent University on 12/9/2023 12:01:00 PM.

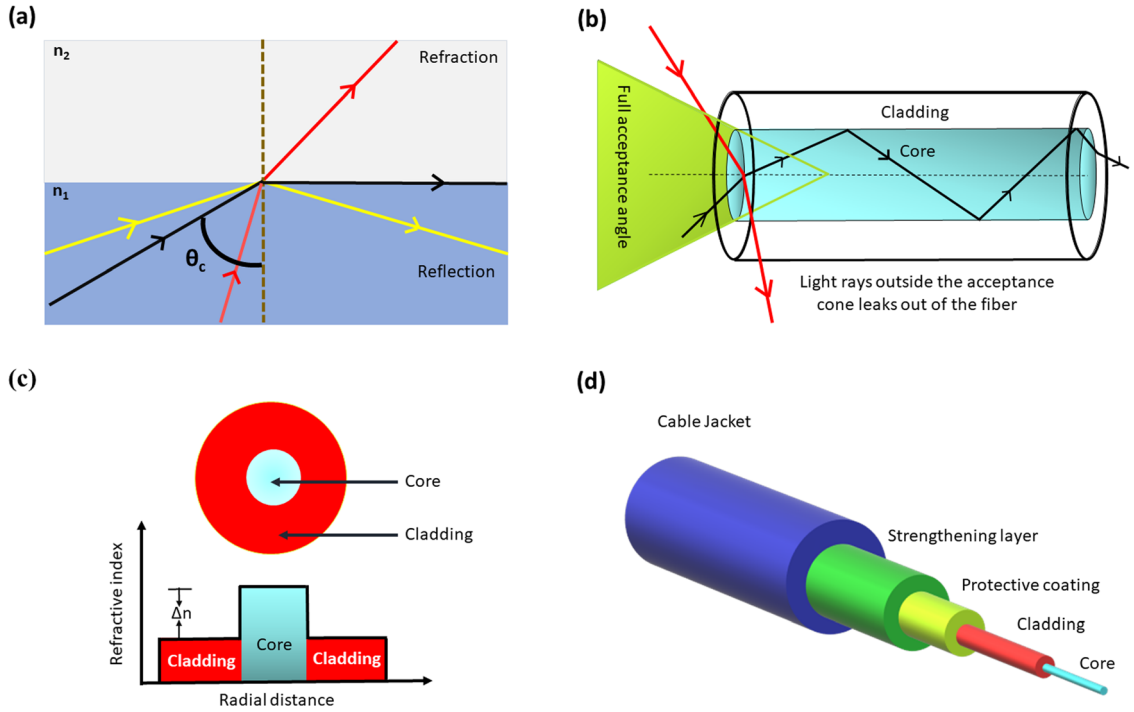


Fig. 3 Guiding mechanisms of an optical fiber. (a) Total internal reflection at the interphase of two different media, (b) acceptance angle of an optical fiber, (c) refractive index profile of a step-index optical fiber and (d) optical fiber structure with protective layers.

For a core-clad optical fiber, the incident light will escape the core when the incident angle (θ_i) is smaller than the critical angle (θ_c). In contrast, light reflects back to the same medium if $\theta_i > \theta_c$.[104] This feature is achieved by coupling light into the core from a light source within the acceptance angle for that designed fiber (Fig. 3b). Thus, the light gets confined in the core and travels along the fiber. There is a difference in the refractive index between the core and the cladding material. The refractive index of the core has to be higher than that of the cladding material for light confinement in the core (Fig. 3c). A coating protects the core and clad regions from environmental effects and prevents physical/chemical damage (Fig. 3d).

Hydrogel-integrated fiber optic manufacturing technology mainly adopts this core-clad profile due to its simple structure and potential for functionalization of the core.[34,73,105] Even though there have been several efforts to integrate hydrogel-based materials with novel photonic bandgap (PBG) fibers,[88,106,107] these have achieved limited popularity due to the complex manufacturing process of PBG fibers.[108]

4. Sensing principles of hydrogel-integrated sensors

The application of a hydrogel coating can improve the sensing capabilities of fiber-based sensing devices, while the integration of nanomaterials into these developed structures can lead to even increased sensitivity of hydrogel-integrated sensors. The concepts of various hydrogel-coated optical fiber-based sensing techniques and the impact of nanomaterials on sensing performance will be outlined in this section.

4.1. Surface plasmon resonance sensors

SPR is an optical measurement technique to obtain information about optical changes such as the refractive index of thin material layers in response to molecular interactions.[109–112] It is an optical technique that utilizes the interaction between light and electrons in metals to measure the refractive index change in the thin metal layer, enabling it to be implemented in various optical sensing applications. When light stimulates the surface of a material (*i.e.*, metals), the electrons in the conduction band interact with the incident photons. The resonance between the oscillation of these electrons and the electric field of the incident light is called surface plasmon resonance.[113] Due to the resonance, energetic plasmonic electrons can be formed through non-radiative excitation. The basic schematic of the working principle of SPR is depicted in Fig. 4a. In more detail, the incoming light passing through a high refractive index glass prism at a specific angle can interact with the delocalized electrons in the metal layer and initiate plasmonic electron propagation, which is parallel to the surface.[109] The intensity of the reflected light is affected by this propagation,[114] and this influence can be monitored for sensing purposes.

Plasmons can be classified into two categories: (i) the propagating surface plasmons and (ii) the localized surface plasmons.[115,116] Measuring the changes in the reflected light's intensity, angle, or spectrum facilitates SPR-based detection in various applications.[109] The general applications are pH

Published on 13 June 2023. Downloaded by Bilkent University on 12/9/2023 12:01:00 PM.

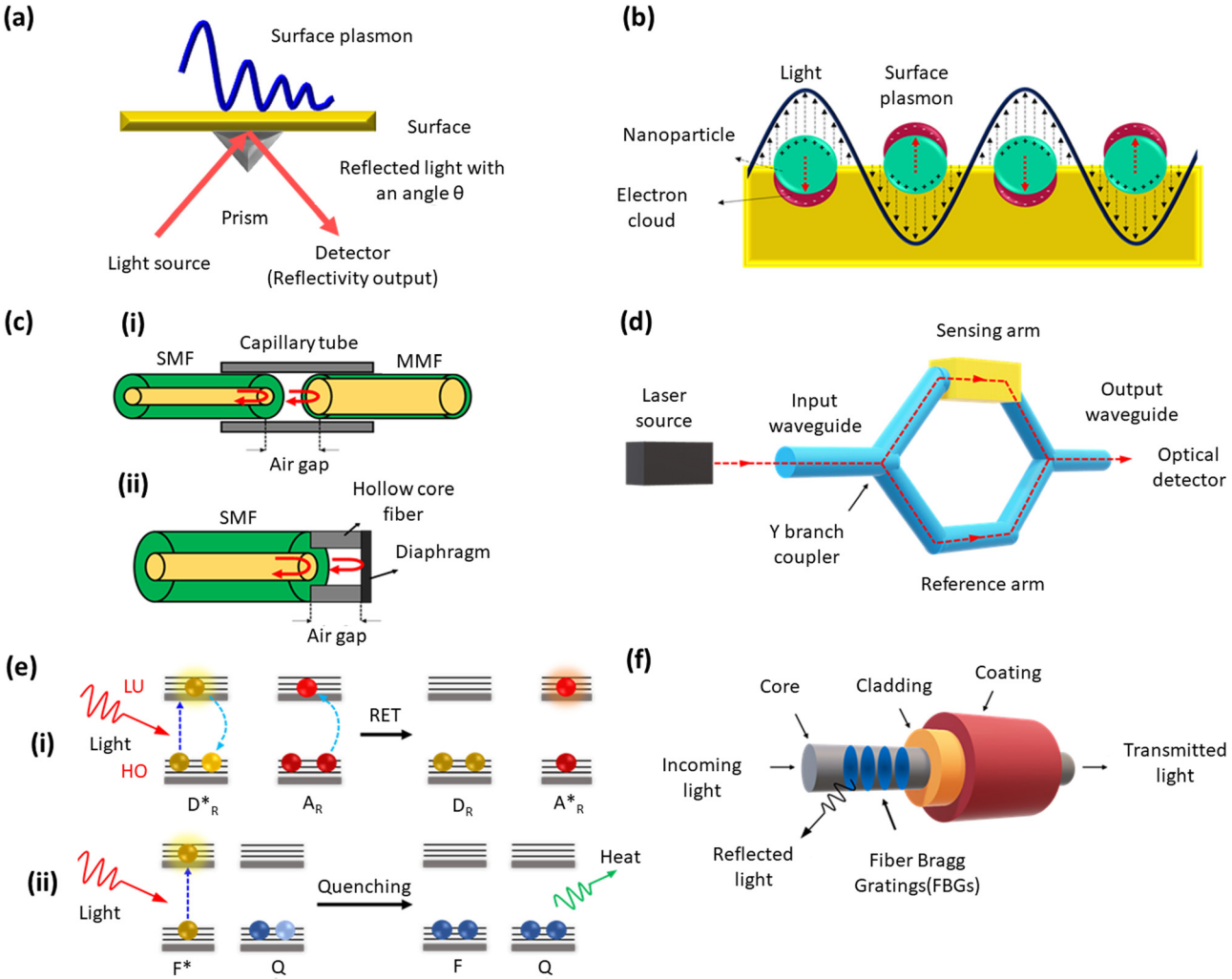


Fig. 4 Sensing principles of hydrogel-based optical fibers: (a) surface plasmon resonance (SPR), (b) localized surface plasmon resonance (LSPR), (c) Fabry–Perot cavities: (i) fiber air gap-based cavity and (ii) diaphragm based cavity, (d) Mach–Zehnder interferometer-based sensor, (e) fluorescence sensing mechanisms: (i) resonance energy transfer (RET) mechanism and (ii) quenching mechanism (F: fluorophore, Q: quencher) and (f) Fiber–Bragg grating sensor.

sensing,[117–119] temperature sensing,[118,120,121] RI sensing,[121,122] and ion concentration sensing.[123,124] The optical fiber integrated SPR sensors demonstrate advantages in the detection process along with high spatial resolution, on-line distributed measurement, remote sensing, and low cost.[125] Hydrogel coating can further improve the SPR effect on optical fiber-based sensors. It provides diffusion control in biological applications and increases sensor reusability and provides protection by trapping substances such as enzymes.[126] However, the metal layers used to obtain plasmons could be damaged during those applications. Thus, a hydrogel coating can facilitate protection while increasing sensitivity by having a fast response.[35] Furthermore, nanoparticle integration with hydrogel coatings can also help to increase the signal rate. In addition, the hydrogel's protection feature can prevent metal nanoparticle contamination, which can also contribute to the formation of localized surface plasmons. Therefore, in such systems, LSPR formation can be achieved by metal nanoparticle-trapped hydrogel coatings on the metal film, which facilitates the formation of SPR and enhances the sensitivity of the sensor.[35,127–129]

4.2. Localized surface plasmon resonance sensors

The improved form of SPR, known as LSPR, is brought on when light interacts with the metal nanoparticles in the system, which are smaller than the wavelength of the incident light. In contrast to SPR, LSPR does not require prisms or crucial angles, indicating that its system is less complicated, more compact, and more vibration-resistant.[130] The basic working principle of LSPR is demonstrated in Fig. 4b. When light strikes a nanoparticle, the electron cloud becomes displaced, which leads to Coulomb attraction between electrons and nuclei. The oscillation brought on by this ensuing force is known as localized surface plasmon (LSP), and LSPR is realized by the resonance of LSPs.[130] There are mainly two effects that can be considered for LSPs: the enhancement of the electric field at the surface of a particle and the optical extinction peak of the

 This journal is © The Royal Society of Chemistry 2023

Published on 13 June 2023. Downloaded by Bilkent University on 12/9/2023 12:01:00 PM.

particle at the resonant frequency of the LSPs, which is mainly dependent on the refractive index change of the medium.[9] LSPs demonstrate sharp spectral absorption, scattering peaks, and electromagnetic field enhancements upon combining the resonances with noble metal nanostructures.[130,131] The wide range of application areas[132–136] of optical fiber-based LSPR sensors are mainly dependent on the integration of nanoparticles to have the LSP effect, and the studies of the last decade show it clearly.

Fibers can be coated with hydrogels and various metal nanoparticles to improve the sensitivity and enhance the signal properties of the LSPR-based fiber sensors. At the same time, trapping of nanoparticles inside the hydrogel coating ensures protection from detrimental environmental effects such as contamination, making the sensor more effective. On the other hand, the concentration of the trapped material can also affect the efficiency of the sensor. A recent study has shown that the sensitivity of a hydrogel-coated LSPR-based sensor is directly proportional to the concentration of the doped gold nanoparticles (GNPs) due to the LSPR effect being dependent on it.[137]

4.3. Interferometer-based sensing systems

Interferometry can be described as the use of wave interference to obtain characteristic information about materials with the help of devices known as interferometers. Although several types of interferometers have been proposed to date, Fabry–Perot and Mach–Zehnder interferometers are the most extensively used in fiber optic-based sensing applications.

4.3.1. Fabry–Perot interferometer. Fabry–Perot interferometers (FPIs) are generally constructed by using two planar and parallel semi-transparent reflective mirrors to bounce the trapped beam multiple times between the mirrors.[138] During each mirror bounce, some part of the beam becomes transmitted, which offsets the beam to obtain an interference pattern utilizing the interaction between these offset beams and multiple reflections.[139] This linear optical resonator forms a high-resolution interference pattern which is advantageous for optical spectrum analysis and resonant mode characterization.[138,140] Fig. 4c shows the schematic of an optical fiber-based Fabry–Perot cavity. As seen from the figure, the location of the Fabry–Perot cavity can influence whether the type of interferometry is extrinsic or intrinsic. The gap between two fibers (SMF and MMF), as shown in Fig. 4c(i), indicates an extrinsic type of FPI formed between two reflecting surfaces.

On the other hand, an FPI of an intrinsic type is indicated by the cavity between the SMF fiber and a diaphragm, as shown in Fig. 4c(ii). This principle forms the basis of sensing applications involving the integration of fibers. These applications can be exemplified as gas sensing,[141,142] temperature sensing,[142–144] wave velocity measurements,[145] humidity sensing,[146] and various other fields.

Many sensing applications use hydrogel-coated optical fibers in FPIs owing to the tunable properties of hydrogels. These application areas generally focus on detecting the optical properties caused by the interaction between the hydrogel and the target agents.[26,147,148] The detection of these modified optical properties caused by the mechanical and structural changes of hydrogel coatings is realized by measuring the unique interference spectrum change provided by the Fabry–Perot cavities. However, a general limitation is the thickness of the hydrogel layer, which can affect the beam's diffraction, reflection, and transmission, which can further affect the properties of the interference fringes. Considering the direct proportionality between hydrogel thickness and the period of the fringes, it can be concluded that both the thickness and the density of the fringes can increase or decrease simultaneously.[26,149] Therefore, an FPI-based sensing system's sensitivity generally depends on the hydrogel layer's thickness. Furthermore, nanoparticles or nanostructures can be integrated further to enhance the sensitivity of the hydrogel-coated FPI-based sensors.[150,151] The use of nanoparticle-trapped hydrogel films with different material variations can significantly enhance the features of fiber-based FPI sensing systems.

4.3.2. Mach–Zehnder interferometer. In the Mach–Zehnder interferometer (MZI), the interference pattern is obtained by two beam splitters that divide and recombine the beam into one of the outputs with a 180° or 0° phase shift. The reflection efficiency of the final beam-splitter depends on the relative phase of the beam that has followed the two paths.[152] Thus, the output of the interferometer has two beams with a relative phase shift, and a sample can be detected by measuring this sample-induced phase-shifting phenomenon (Fig. 4d). Moreover, MZIs can be used in various sensing applications with the combination of optical fibers, such as temperature sensing,[153–155] RI sensing,[153,154,156] axial strain sensing,[153,157] curvature sensing,[158,159] and pH sensing.[160]

The integration of hydrogel fibers can improve the optical sensing capabilities of MZI sensors, including an increase in the sensitivity of detection of changes such as the refractive index change. The general characterization of these sensing systems can be done by measuring the RI change,[161] the interference wavelength response,[88] or the optical transmission change,[89] which are caused by the mechanical change of the hydrogel medium. Hence, the characterization is done by simply detecting the spectral response of the MZI system.

The sensitivity and response time can be improved for the existing MZI-based sensing systems by developing hydrogel coating media. However, the nanoparticle-integrated hydrogel-coated fiber-based MZI sensing systems are yet to be studied in sensing applications. As nanoparticles or biomaterials trapped in hydrogel media can enhance the sensing capabilities, using hydrogels with nanoparticle integration in MZI-based sensors may further increase sensitivity.

4.4. Fluorescence-based methods

Due to its superior sensitivity, fluorescence spectroscopy has been preferred and utilized in various applications.[162,163] It provides an opportunity to achieve high-intensity spectra for low-level light and electronic impulse detection by measuring

Published on 13 June 2023. Downloaded by Bilkent University on 12/9/2023 12:01:00 PM.

the signal independently from the initial beam or reference beam.[164]

The fluorescence sensing method involves observing the changes in the optical characteristics of fluorescent materials, such as intensity, wavelength, anisotropy, or lifetime.[164] Fig. 4e describes the two different mechanisms of fluorescence-based sensing. The basic working principle of fluorescence spectroscopy-based sensing mainly involves either resonance energy transfer (RET) or quenching. In the case of the RET mechanism (Fig. 4e(i)), the excess energy of a donor (excited: *) particle (D_R) is transferred to an acceptor (A_R) particle in the form of an imaginary emitted photon.[165] During the RET, an electron in the acceptor particle reaches a higher excited-state orbital while the excited electron in the donor particle returns to the ground state. The acceptor particle does not need to be fluorescent, and in both scenarios, the fluorescence intensity of the initially excited molecule decreases.[164] Sensing is performed by monitoring the fluorescence intensity, which varies due to the transfer between the donor and the acceptor.

On the other hand, the quenching phenomenon (Fig. 4e(ii)) essentially indicates the release of the electrical energy of the fluorophore as heat across the sensing system, which is also used in various reported sensing applications. Due to the highly confined electron clouds, during quenching, the fluorophore and quencher must come into molecular contact at the van der Waals radii in order for their electron clouds to interact.[164] The excited electron in the lowest unoccupied (LU) state of the fluorophore returns to the ground state during the contact and releases the energy as heat. The crucial distinction between these two mechanisms is that RET results from long-range dipolar interactions between the donor and the acceptor. In contrast, short-range interactions between the fluorophore and the quencher cause quenching. The information that can be detected in each process is impacted by the distance dependence between RET and quenching.

Despite the growing popularity, hydrogel-coated fiber-based fluorescence sensors still have some drawbacks, such as fluorescence intensity fluctuations and environmental change dependence that might lower their sensitivity. Nearly all of the current studies focus on enhancing the characteristics of these sensors, such as their sensitivity, reusability, and cost. As a platform for fluorescence excitation and collection, the hydrogel-coated fiber, together with the fluorescent components, serves as a major component of the fluorescence sensor. The extensively reported pH detection applications can be improved by using hydrogel fibers, which offer a diffusible environment for H^+ ions in these pH-sensing applications.[166–169] Furthermore, metal–organic frameworks (MOFs) can also be used along with hydrogel coatings to further improve the fluorescence-based sensors. Their adjustable luminescence and adaptive functionality can provide benefits while being protected with hydrogel coatings in specific applications such as substance detection.[39] Research on this design utilizing various materials may yield even more benefits and sensors with improved capabilities. Although some reports use QD[74] integrated hydrogel fibers, to the best of our knowledge, there are still no reports of fluorescence sensors based on nanoparticle-integrated hydrogel fibers.

4.5. Fiber Bragg grating sensors

Optical communication and sensing systems frequently employ fiber Bragg gratings (FBGs) fabricated by stacking Distributed Bragg Reflectors (DBRs) in a small portion of an optical fiber.[170] A periodic variation of the refractive index along the fiber core with DBRs is the key to achieving the reflection of a particular wavelength and variation in periodicity specifies the wavelength. When broadband light passes through the FBG, only a specific wavelength gets reflected while the remaining part gets transmitted.

The straightforward UV patterning of gratings offers a significant degree of freedom in choosing the patterned sensing region, which is used in the fabrication process of FBGs.[171] The sensing mechanism (Fig. 4f) involves detecting the reflection spectrum change of an FBG, which varies due to the microscopic deformations that causes a non-uniform strain spread along the entire length of the grating.[170] This particular phenomenon can be applied to various sensing applications.[172–175]

As demonstrated in the other sensing concepts, using stimulus-responsive hydrogel coatings can also improve the efficiency of FBG-based sensors. The application area of the FBG sensors generally includes ion concentration,[176,177] pH,[178,179] and salinity detection.[180] The hydrogel-based FBG sensors have been studied and developed during the last decade. The primary objective of these studies is to address the challenges in the existing FBG sensors, such as thermal sensitivity, challenging discrimination of the wavelength shift, and diagonal strain sensitivity. Further improvements in the sensitivity can be made by using long-period fiber gratings (LPFGs) along with hydrogel coatings in FBG-based sensing systems.[181] Recent studies have shown that a proper etching of LPFGs can boost the sensitivity of FBG-based sensing platforms.[177,182]

5. Hydrogel-based optical fiber manufacturing process

5.1. Hydrogel optical fiber as a pure optical waveguide

Hydrogels have shown great promise to find a biocompatible light-guiding medium as an alternative to conventional solid-state materials such as glasses and inorganic plastics. One of the initial methods to utilize hydrogels as light guiding media implemented a poly(ethylene glycol) diacrylate (PEGDA) integrated slab waveguide where a glass mold was used to form a planar waveguide of uniform refractive index for light guiding in a biological medium which had a limited distance light-guiding capacity of 10 cm. The light guiding efficiency of this planar waveguide was insufficient to achieve organ scale light guidance.[183]

The first efficient light guiding through a hydrogel medium was realized with a step-index optical fiber in a two-stage core-clad fabrication process using a platinum-cured silicone tube

 This journal is © The Royal Society of Chemistry 2023

Published on 13 June 2023. Downloaded by Bilkent University on 12/9/2023 12:01:00 PM.

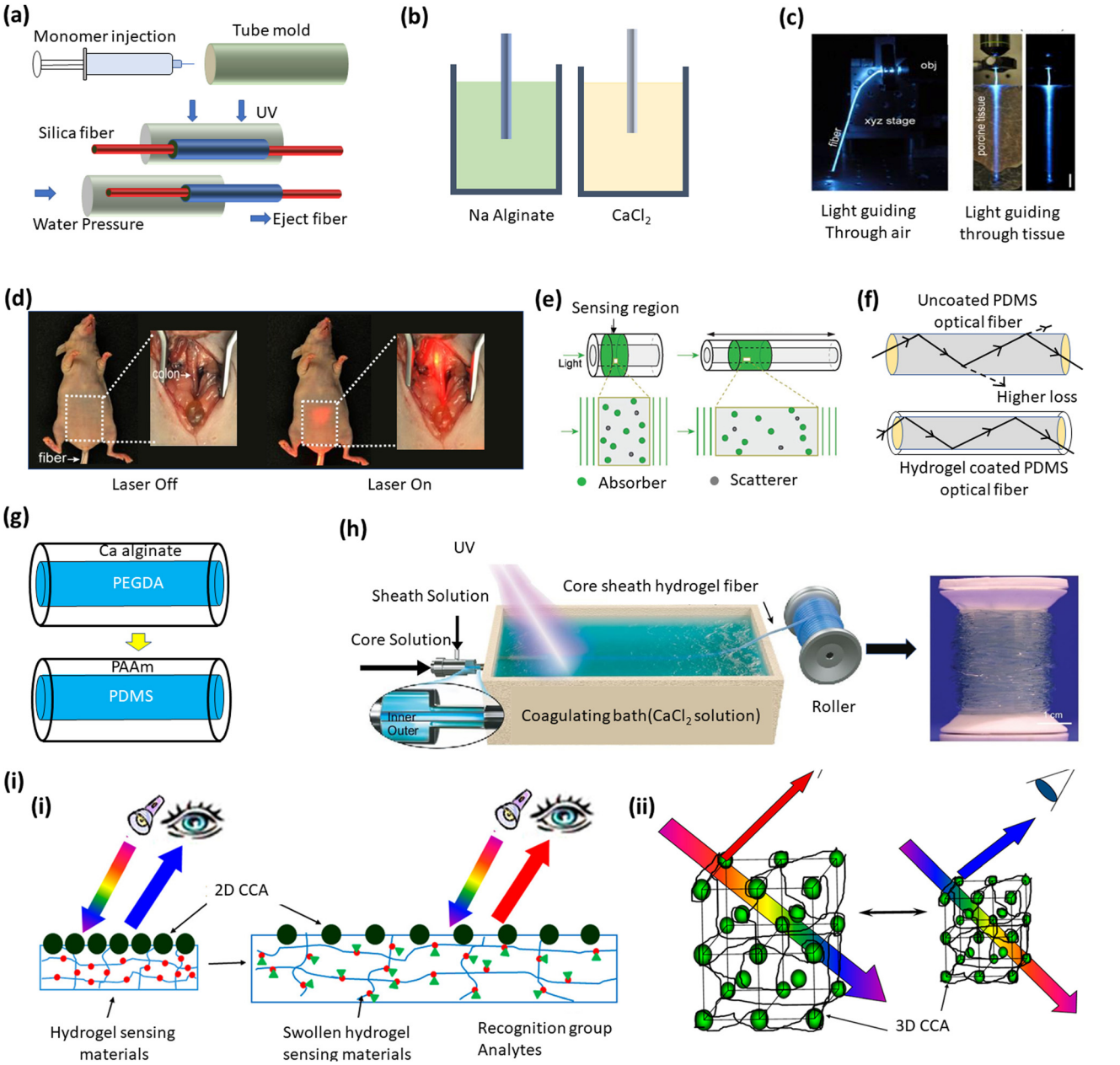


Fig. 5 Hydrogel-based pure optical waveguides. (a) Fabrication procedure of the hydrogel optical fiber core, (b) Ca alginate deposition on a bare fiber core, (c) demonstration of blue light (492 nm) guiding through the hydrogel optical fiber between two thin porcine tissue slices, (d) light guidance from rectum to the colon of an anesthetized mouse, confirmed by abdominal laparotomy. (c and d) Reproduced with permission from ref. 34, Copyright © 2015 John Wiley & Sons, Inc. (e) Hydrogel-based strain sensor. Reproduced with permission from ref. 73, Copyright © 2016 John Wiley & Sons, Inc. (f) Hydrogel-coated PDMS core optical fiber with increased light confinement in the core region, (g) alginate coating replaced by PAAm clad PDMS structure for lower loss, (h) continuous hydrogel optical fiber production through a dynamic wet spinning process (ILDWS) and collected fibers around a spool. Reproduced from ref. 201, Copyright © 2020 The Author. Published by Oxford University Press. (i) Hydrogel based (i) 2D and (ii) 3D photonic crystals by attaching 2D or 3D CCAs onto a hydrogel containing functionalized recognition groups. Reproduced with permission from ref. 44, Copyright © 2015 American Chemical Society.

as a mold.[34] Preparation of the precursor solution for core formation involved mixing PEGDA with 2-hydroxy-2-methyl-propiophenone in distilled water. The precursor was then injected into a platinum-cured silicone tube through a syringe and the precursor solution inside the tube mold was subjected to UV-induced photo-crosslinking (365 nm, 5 mW cm^{-2}) for 5 min (Fig. 5a). After swelling the tube mold in dichloromethane for 30 min, the core was extracted, washed in distilled water and finally immersed in sodium alginate (NaAlg) and then calcium chloride solution to form multilayer alginate cladding of 100–150 μm thickness (Fig. 5b). Here, Ca alginate was used for its superior biocompatibility, adhesion, and water-retaining

Published on 13 June 2023. Downloaded by Bilkent University on 12/9/2023 12:01:00 PM.

properties.[184–186] The fabricated hydrogel optical fiber showed excellent light-guiding properties with a propagation loss of 0.32 dB cm^{-1} in air and 0.42 dB cm^{-1} inside porcine tissue slices at 492 nm, while the reported loss of the core-only PEG fiber without alginate coating was 1.15 dB cm^{-1}.[34] The practicality of the designed sensor was demonstrated by light guiding through open air, through porcine tissue, and inside the colon of an anesthetized mouse (Fig. 5c and d).[34] However, one fundamental obstacle in the tube mold fabrication process is the surface roughness of the tube mold, which significantly increases the attenuation property of the fiber. Although PEGDA is extensively used for fabricating hydrogel sensors, its practicality is limited by the stiffness and incompatibility towards volumetric change-induced quantitative measurements.[34] However, this hybrid core gives rise to a higher 6 dB cm^{-1} loss in the visible range due to PBA-induced scattering losses.[76] Thus, a hybrid poly(acrylamide) (PAAm)-PEGDA core has been investigated with phenylboronic acid (PBA)[187] to bring flexibility into the structure.

A novel hydrogel-integrated strain sensor has been proposed based on integrating functional molecules like fluorescein with PAAm.[73] Strain sensing can be performed by the comparative attenuation study between a strained fiber and a fiber at rest using the Beer–Lambert law (Fig. 5e).[188] The fabrication process is similar to the PEGDA-integrated hydrogel optical fiber preparation method.[34] However, cross-linking the cladding material with the core is particularly challenging. Here, Ca^{2+} participates in ionic cross-linking with the alginate chain, which causes higher viscosity and makes it difficult to dip the core for the cladding deposition process. A possible remedy is to coat the core with the Na-alginate-PAAm hydrogel, where PAAm chains are cross-linked and well-dispersed while no cross-linking occurs in alginate chains;[189] effective bonding between the core and the cladding is ensured *via* EDC-NHS chemistry.[190,191] Finally, cladding was formed by immersion of the core in $CaCl_2$. The designed step-index optical fiber pressure sensor demonstrated superior stretchability and toughness properties where 700% of strain could be applied before relaxing it in multiple cycles (1% for silica fibers).

Recently, a hybrid PDMS-PAAm structure has been reported with a low attenuation loss of 0.25 dB cm^{-1} in the visible spectra, by replacing alginate coating.[192] The conventional hydrogel/alginate-integrated core-clad structure demonstrates superior light confinement properties compared to the core-only fiber (Fig. 5f) but cannot facilitate a high refractive index difference between the core and the cladding, which is necessary for low-loss TIR-based light guidance. PAAm is a transparent material with a low refractive index, while polydimethylsiloxane (PDMS) has a higher refractive index and the significant refractive index difference facilitates light confinement inside the core (Fig. 5g). The fabrication process involved a three-step preparation of the core, surface treatment of the PDMS core, and subsequent coating with transparent hydrogel cladding. However, coating PDMS with the hydrogel is challenging due to the hydrophobic nature of PDMS.[193] To facilitate PDMS coating, silane coupling agents were added to both PDMS and PAAm, as demonstrated in previous experiments.[194] The surface modification technique was also employed in PDMS with oxygen plasma treatment to improve the wetting ability of PDMS. During curing, the silane coupling agent forms a covalent cross-link between PDMS and hydrogel coating. Although the reported fiber achieved an optical loss as low as 0.25 dB cm^{-1} in the visible range, a higher refractive indexed bio-compatible material over hydrogel core can be an ideal candidate to further improve the guiding property deep into tissue.[195] There has been a significant achievement in reducing light-guiding loss through hydrogel optical fibers. Yet, continuous large-scale production of core-clad structures with the desired optical and mechanical properties is still challenging. For increasing production capacity, several continuous processes can be adopted.[196,197] Still, continuous production processes have several limitations, like poor processing of the stable cross-linked network after hydrogel gelation, the difference in rheological properties between core and cladding material, and the creation of a non-equilibrium state during fiber spinning.

Recently, wet spinning technology has been investigated to fabricate polymer fibers to overcome these limitations.[198–200] Even though other methodologies like micro-fluidic spinning and hydro-dynamic cross-linking spinning provide a better scope for structural design, scalable fabrication, and functionalization than wet spinning technology, those can only be adopted for producing single-phase hydrogel fibers (core only). Thus, integrated light-triggered dynamic wet spinning (ILDWS) has been adopted to fabricate a two-phase structure with superior mechanical and optical properties (Fig. 5h).[201] The process involves coaxially injecting the core (PEGDA + PAAm) and cladding (Na-alginate) precursor solutions through different nozzles of the core-sheath spinning needle into a coagulating bath containing $CaCl_2$. The cladding solution became gelled immediately after coming in contact with $CaCl_2$ through ionic cross-linking and the core solution was subjected to UV cross-linking at 360 nm in the presence of an initiator. This process ensured a uniform core-clad structure since spinning parameters can be controlled by monomer viscosity and extrusion speed. This superior control over the micro-structure resulted in a record-low 0.18 dB cm^{-1} propagation loss.[201] A similar methodology has been applied to produce a temperature-adaptive hydrogel fiber-based optical waveguide (THFOW) with a reported loss of 0.32 dB cm^{-1}.[202]

Although the step-index profile results in significantly low propagation loss, further development can be explored by adopting double clad guiding structures, gradient index profiles, or single mode fibers at sub-micrometer scale using fabrication techniques such as microfluidics and electrospinning as an adaptation of minimally invasive implantation techniques.[203] Moreover, hydrogels with highly stretchable and self-healing properties are reported for organohydrogel[204] fibers, but these properties are needed to be tailored into hydrogel-based pure optical waveguides since their attenuation is much less compared to other forms of hydrogels. Besides,

 This journal is © The Royal Society of Chemistry 2023

Published on 13 June 2023. Downloaded by Bilkent University on 12/9/2023 12:01:00 PM.

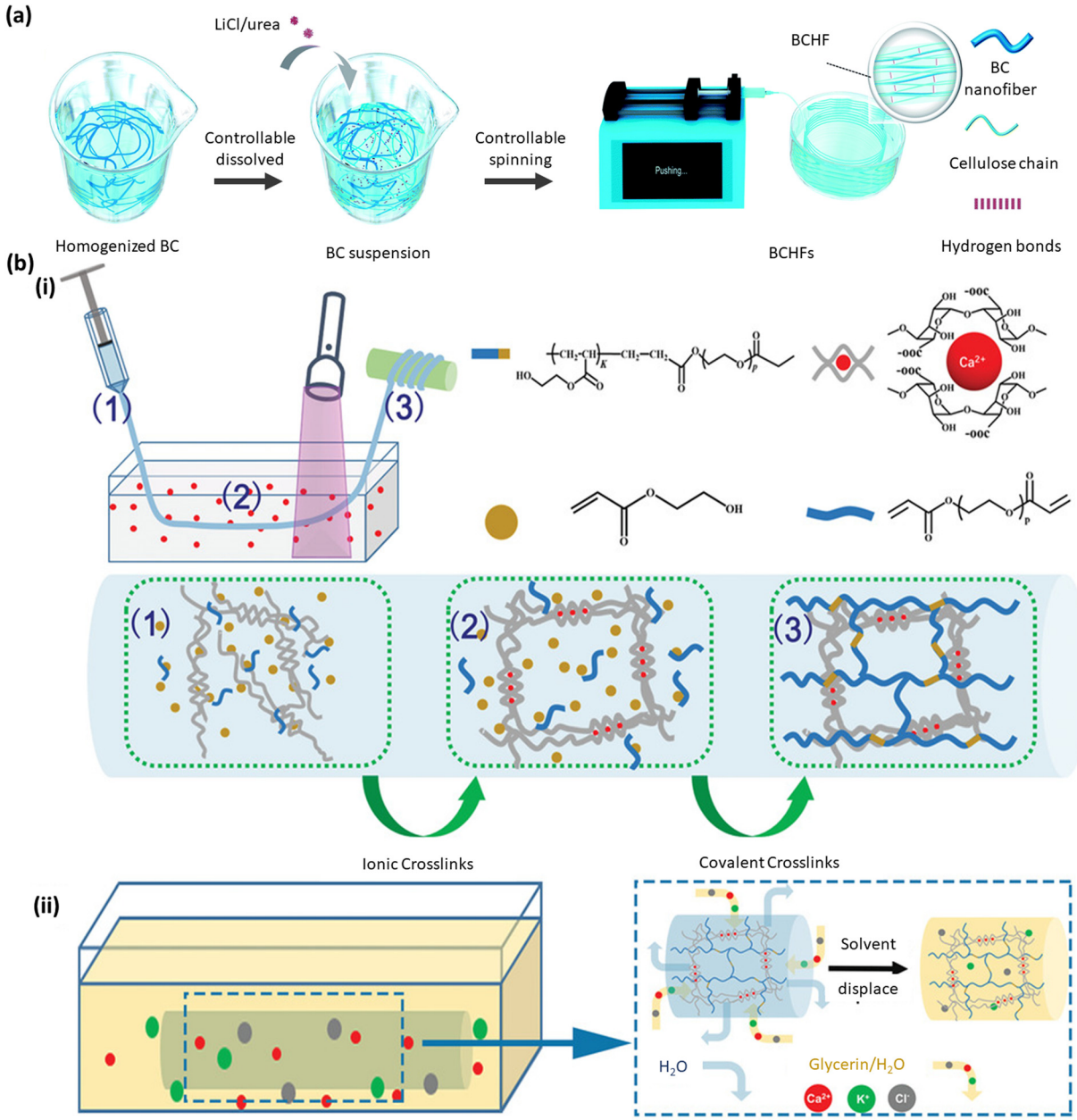


Fig. 6 Fabrication procedure of hydrogel-based optoelectronic fibers. (a) Wet spinning procedure of BCHFs using the nanofiber-rich BC suspension as a spinning solution and water as a coagulating bath. A dense hydrogen bond was formed between cellulose nanofibers and molecular chains leading to continuous BCHFs. Reproduced with permission from ref. 213, Copyright © 2021 Royal Society of Chemistry. (b) (i) Wet spinning process of an organohydrogel with the evolution of polymeric networks at different stages of the spinning process. (1), (2) and (3) represent the structural evolution at different stages during spinning including (1) spinning solution, (2) ion-crosslinked fiber, and (3) hybrid crosslinked fiber. (ii) Preparation of organohydrogel fibers by the solvent displacement method. Reproduced with permission from ref. 215, Copyright © 2020 John Wiley & Sons, Inc.

novel optical waveguides such as hydrogel-based hollow-core photonic crystal fibers (HCPCFs)[205] and negative curvature hollow-core fibers (NCFs)[206] can be investigated. There has been a significant advancement in photonic crystal-based 2D and 3D sensor structures.[207–209] Face-centered-cubic (fcc) crystalline colloidal arrays (CCAs) were incorporated within smart, responsive hydrogels to form 2D and 3D photonic crystal structures. The chemical recognition agents in the hydrogel structure actuate hydrogel volume changes. The change in the volume brought changes to array spacing, which shifted the diffraction wavelength (Fig. 5i(i and ii)).[44] A similar hydrogel-based photonic crystal fiber fabrication methodology can be implemented, bringing novel applications to this field. For example, cancer treatment with photothermal therapy (PTT) requires near-IR (NIR) radiation (700–2000 nm), which can be supported through PCFs. This NIR guiding is yet to be reported for step index-based hydrogel fibers, which only support visible spectra.[210]

Published on 13 June 2023. Downloaded by Bilkent University on 12/9/2023 12:01:00 PM.

Hydrogels have shown significant promise as biocompatible light guidance media with organ scale light guiding compatibility. However, challenges remain regarding surface roughness, core-clad cross-linking, and scalability for large-scale production. For superior light confinement, future research direction for continuous hydrogel optical fibers may explore double-clad and gradient index profiles, microfluidic and electro-spinning techniques, and incorporating photonic crystal structures.

5.2. Hydrogel-based optoelectronic fiber sensors

Hydrogel-based optoelectronic devices and sensors have the potential to draw significant interest among multi-disciplinary research communities due to their scope of integrating both optical and electrical applications in the same device.

Conductivity in a hydrogel can be brought by the movement of electrons or ions through the 3D network structure of the hydrogel. Hydrogel conductive fibers (CHFs) can transfer charge in three modes: electronic, ionic, and hybrid electronic-ionic.[211] Conductive filler-based CHFs mainly adopt electron conduction mechanisms. However, the lack of optical transparency and mechanical properties (increased Young's modulus and decreased stretchability) makes them unsuitable for optoelectronic devices. A flexible MXene integrated aerogel fiber with a 3D-oriented porous structure has been reported to demonstrate an electrical conductivity of 10^4 S m^{-1}, but the fiber shows large absorption in the near-infrared region of 750–850 nm due to the semimetallic LSPR effect of MXene.[212] In contrast, ionogel fibers, which consist of a 3D polymer network percolating through the ionic liquid (IL), achieve conduction through mobile ions. Ionic liquids participate in non-covalent interaction, facilitating uniform dispersion in the polymer matrix. Increasing the IL percentage can also result in superior conductivity. Even though ionogel fibers demonstrate lower conductivity, their superior optical transparency and stretchability make them an ideal candidate for hydrogel-based optoelectronic devices. Optoelectronic physiological probes, which have the potential to be used as a next-generation neural interface, enabling bio-ion conductivity and light-guiding performance, have been investigated. The continuous wet spinning of the natural bacterial cellulose hydrogel fiber (BCHF) without the necessity of additional cross-linking was reported for the first time by the dissolution and spinning process.[213] The process involved preparing a spinning dope by treating homogenized bacterial cellulose (BC) with LiOH/urea solution at −12.5 °C for 4 hr to get a transparent suspension containing nanofibers. OH^- ions of the alkaline solution break hydrogen bonds while BC's hydrophilic and hydrophobic segments interact with Li^+ and urea, respectively. Then the suspension was loaded into a syringe and continuously extruded into the water by an extruding pump to get continuous BCHFs. Here, the solvent of the BC was exchanged with a coagulation bath, promoting the rapid formation of hydrogen bonds between nanofibers and the cellulose macromolecular chain (Fig. 6a).[213] In this process, gelatinization occurred in the fiber. The cladding was obtained by inserting BCHF into 5 wt% gelatin hot solution and was cooled naturally to get a continuous core-clad structure. The attenuation of the fiber was recorded as 5.1 dB cm^{-1} at 515 nm, while ionic conductivity was reported to be 0.03 S m^{-1} which can reach up to 0.56 S m^{-1} in stimulated body fluid (SBF).[213]

Hydrogel-based fibers are needed to resist degradation of performance in extreme weather (*e.g.*, abnormal temperature and humidity) for their continued effectiveness in sensing. Noncovalently crosslinked hydrogel fibers present a drawback as they exhibit creep and hysteresis.[214] In this regard, ionically conductive covalently bonded organohydrogel fibers have attracted interest due to their negligible hysteresis and creep and thermal and hydration compatibility.[204,215] Previously reported covalently cross-linked hydrogel fibers executed cross-linking inside the tube mold in a stress-free environment. Even though UV-induced crosslinking increases the fabrication speed, it is still associated with poor mechanical properties. On the other hand, spinning is a dynamic process associated with drafting force (the force applied to stretch and align the hydrogel fibers as they are extruded from a spinneret or nozzle). To address these challenges, a hybrid crosslinked transparent organohydrogel has been reported.[215] Here, ionically cross-linked alginate was co-spun with covalently crosslinked PEGDA (Fig. 6b(i)) and the organohydrogel fiber was prepared by the solvent displacement method where the prepared fiber was immerged in glycerin : water (1 : 1) solution in the presence of $CaCl_2$ and KCl to replace part of the water from the hydrogel fiber by glycerin (Fig. 6b(ii)). The fiber was reported to exhibit stable mechanical performance maintaining stretchability up to 300% at subzero temperature, which can be attributed to the formation of a 3D covalent structure.

Recent advancements in the hydrogel-based optoelectronic field can pave the way for hydrogel-based optoelectronic devices and sensors with enhanced functionality and durability. However, the lack of optical transparency and mechanical properties in conductive filler-based hydrogel fibers remains a significant limitation. Additionally, improving the optoelectronic hydrogel fibers' creep, hysteresis and thermal stability is essential for their effective use in sensing applications.

5.3. SPR-based hydrogel optical fiber sensors

SPR-based sensing technology has shown great promise in chemical and biological sensing.[216,217] Several media have been investigated to excite surface plasmons at the metal–dielectric (sensing medium) interface, such as the high index prism and optical fibers.[218,219] Fiber optics-based SPR sensors have numerous advantages, such as miniaturized probes, low cost, and suitability for remote sensing and online monitoring applications. Thus, they are extensively used in pH, ethanol, and glucose monitoring because of hydrogel's swelling or deswelling in those media.[220–222] For instance, an SPR-based hydrogel-coated silica optical fiber with a 600 μm core size has been reported for pH measurements by modifying a plastic-clad silica optical fiber (PCS).[223] The fabrication procedure involved sharpening both sides of the fiber (for efficient coupling), removing 1 cm of the outer layer from the cladding and

 This journal is © The Royal Society of Chemistry 2023

Published on 13 June 2023. Downloaded by Bilkent University on 12/9/2023 12:01:00 PM.

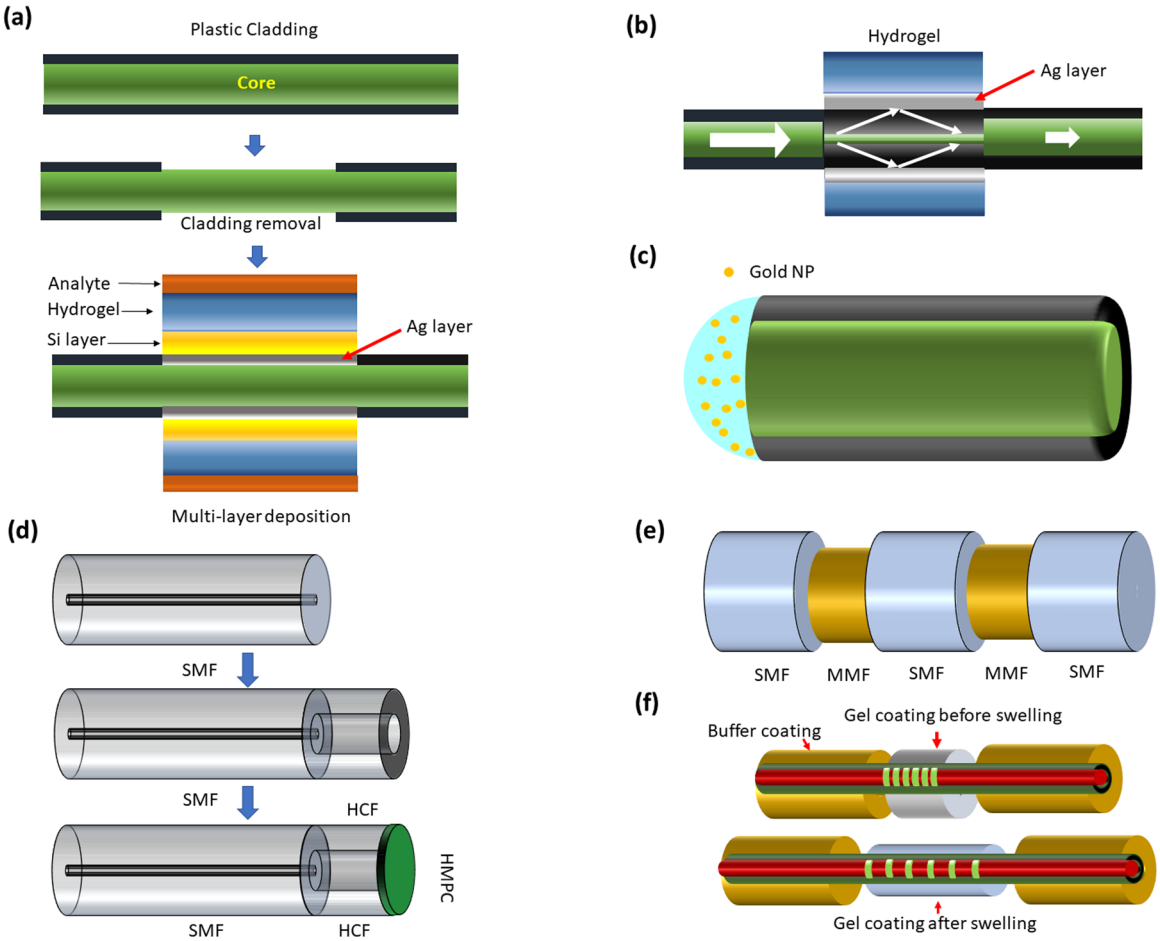


Fig. 7 Schematic illustrations for fabrication procedures of various hydrogel-based optical fiber sensors: (a) hydrogel-based SPR sensor. Reproduced with permission from ref. 220, Copyright © 2012 Elsevier Ltd. (b) Spliced MMF–SMF–MMF structure SPR sensor. Reproduced with permission from ref. 35, Copyright © 2018 Elsevier Ltd. (c) LSPR-based hydrogel fiber optic sensor with a functionalized tip. Reproduced from ref. 235, Copyright © 2017 The Author. Published by MDPI. (d) SMF–HCF–HMPA-based Fabry–Perot interferometry-based sensor. Reproduced with permission from ref. 147, Copyright © 2019 Elsevier Ltd. (e) SMF–MMF–SMF–MMF–SMF spliced structure for the Mach–Zehnder interferometry-based fiber optic sensor. Reproduced with permission from ref. 263 Copyright © 2019 The Optical Society. (f) Bragg grating-based hydrogel fiber optic sensor. Reproduced with permission from ref. 268, Copyright © 2016 SPIE.

cleaning the opened portion with dilute nitric acid, rinsing 4–5 times with de-ionized water and acetone, followed by ion bombardment in a vacuum chamber. Consecutive silver and silicon layer deposition was performed by thermal evaporation over the unclad core. The silicon layer over the metal layer increases sensitivity and protects silver from oxidation.[224,225] Silanizing with 3-trimethoxysilyl propyl methacrylate improved adhesion with the hydrogel. Lastly, a layer of the acrylamide (Am)-based hydrogel was deposited over silicon with ammonium persulphate as a chemical initiator and then UV-induced cross-linking was performed (Fig. 7a). A similar methodology has been adopted for hydrogel-integrated SPR sensors by coating silver, indium tin oxide (ITO; In_2O_3:SnO_2), aluminum, and smart hydrogel layers consecutively over an unclad core of an optical fiber.[223] Although ITO's low flexibility leads to damage during bending, integrating the ITO layer increases sensitivity. ITO enhances the evanescent field at the ITO–hydrogel interface, while aluminum contributes to detection accuracy.[226]

Earlier fabrication methodology of SPR-based optical fiber sensors employed cladding removal techniques to excite the evanescent wave for stimulating surface plasmon wave (SPW) propagation.[106,227] However, these studies demonstrated limitations such as poor structural strength and inadequate mechanical performance of the fiber.[228–230] One possible alternative to solve this problem was proposed which involved the utilization of the spliced multimode–single mode–multimode (MMF–SMF–MMF) structure which successfully stimulates SPW propagation along the interface between the cladding layer and the metal film[35] (Fig. 7b). In this method, Ag metal coating deposition over the MMF–SMF–MMF structure replaced the chemical vapor deposition technique, reducing the film coating cost significantly.[231]

There have also been several attempts to fabricate LSPR-based sensors to replace the complexity of the cladding removal process in SPR-based fabrication.[232–234] Instead of integrating noble metal nanostructures (NMNS) at the optical

Published on 13 June 2023. Downloaded by Bilkent University on 12/9/2023 12:01:00 PM.

fiber core-cladding interface, they were immobilized in a pregel solution containing the hydrogel monomer, which was later deposited at the tip of a step-index optical fiber (Fig. 7c). The preparation of AAm-pregel solution consisted of mixing acrylamide, acrylic acid (AAC), *N*,*N*-methylene-bis-acrylamide (BIS), and densified gold nanoparticle (GNP) solution in phosphate-buffered saline (PBS) solution. Dimethyl sulfoxide (DMSO) was added with photo-initiator (PI) hydroxycyclohexyl phenyl ketone in pregel solution. Silanization of the optical fiber tip was done by soaking it in HCl for surface activation and subsequent treatment in 3-(trimethoxysilyl) propyl methacrylate and nitrogen-purged octamethylcyclotetrasiloxane for 10 min. The fiber optic probe tip was then treated with PI and squalane drop before transferring the pregel solution through a pipette. The precursor solution was subjected to 365 nm UV exposure for 10 min and then immersed in pentene for 5 s to remove impurities. Overall, LSPR sensing technology is advantageous compared to SPR sensing as it can offer increased nano-particle availability in the sensing region. At the same time, density control of NPs is also precise in this set-up as NPs are dispersed in a 3D aqueous environment.[235]

Despite having significant advantages, the challenges of SPR-based sensing include the necessity of improved fabrication technology without the cladding removal process, as it hampers the fibers' structural strength and mechanical performance. Additionally, LSPR-based sensors improve sensitivity by increasing nanoparticles. However, integrating noble metal nanostructures and controlling uniform nanoparticle density remain a challenge.

5.4. Fluorescence-based hydrogel optical fiber sensors

In recent years, quantum dot (QD)-based fluorescence spectrometry has attracted significant interest due to its rapid response, high sensitivity, and high selectivity in ion sensing.[162,163] Previously, QDs were required to be mixed with target aqueous samples for fluorescence-based sensing, limiting the ability for on-site sensing.[236,237] Thus, the utilization of porous media like hydrogels,[238,239] which are permeable to surrounding analytes, has enabled the usage of immobilized QDs in a suitable matrix.[240–242] Nevertheless, on-site fluorescence sensing was prone to analyte-independent interferences, which hampers the detection ability of the sensor.[237] Therefore, ratiometric fluorescence-based ion sensing involving hydrogels has been proposed with two different QDs to overcome this limitation. The methodology involved using thioglycolic acid (TGA) as a reference owing to the insensitivity to metal ions and a quencher material (*N*-acetyl-L-cysteine) for high selectivity towards Fe^{3+} ions.[243] The fabrication process included mixing 30% w/v PEGDA (700 Da) and 1% w/v 2-hydroxy-2-methyl-propiophenone in DI water individually with two different QDs and injecting the solutions in a silicone tube mold simultaneously with syringes to fabricate the fiber core. At the same time, a silica MMF was pigtailed into a hydrogel fiber by inserting a 5 mm portion of it into the center of the tube mold. The photo cross-linking process was employed to induce polymerization with a UV lamp (365 nm, 5 mW cm^{-2}). After removing the pigtailed silica MMF with hydrogel from the tube mold, it was coated with Ca-alginate. A similar methodology has been adopted for detection by integrating various fluorescence indicators like EuNDC, fluorescein, lumogallion, and up-conversion nanoparticles.[39,244–246]

Despite recent advancements, NP-induced scattering of the incident light presents a significant drawback for the fluorescence method as scattering loss increases sharply with increasing particle diameter.[247]

5.5. Interferometry-based hydrogel optical fiber sensors

Interferometry-based fiber optic sensors involving hydrogels have experienced rapid growth due to their highly accurate measurements in various fields to sense physical phenomena such as temperature, pressure, pH, and curvature.[248–251] A novel optical fiber sensor with a spherical sensing region was developed utilizing the Fabry–Perot interferometric technique for examining the swelling degrees in different salt solutions using acrylamide-integrated hydrogels with the cationic monomer *N*-(3-dimethylaminopropyl) acrylamide.[252] A similar methodology also has been utilized for pH sensing;[252,253] however, maintaining a spherical shape while cross-linking brought difficulty in the fabrication process. Another interferometry-based humidity sensing structure was proposed to remove this complexity using hydroxypropyl methylcellulose (HPMC) coating at the sensor end face.[147] HPMC is a hydrophilic hydrogel polymeric material with excellent hygroscopic properties, enabling it to be a superior material for fiber optic humidity sensors.[254] Even though several hydrogel-integrated humidity sensing materials have been reported, namely, chitosan,[255] agarose,[256] CA,[257] and PVA,[258] HPMC demonstrates superior biocompatibility.[259] The proposed sensor comprised of three parts – 100 μm HCF fused with SMF through a fiber fusion splicer and a 10 μm HPMC hydrogel covering at the end face of HCF (Fig. 7d). An HPMC film coating was placed at the end of HCF to create a Fabry–Perot interferometer (FPI) structure. But the fusing process remains challenging as it may cause transmission loss and interference through the collapse of the welding surface. Although the reflection spectrum of the sensor was designed to have three reflection beams, due to the non-uniform waveguide property of HPMC, HPMC/air end face reflection does not contribute to interference phenomena.

Moreover, the faster dynamic response of the designed sensor is partially dependent on the decreasing thickness of HPMC. The technological limitation for HPMC hinders the coating thickness below 10 μm due to mechanical strength. The calcium alginate (CaAlg) hydrogel was also used to replace HMPC in similar structures owing to its excellent water absorption, retention, and expansion property.[260] However, the diameter of the interconnected nano-channels of the cross-linked hydrogel polymer was not uniform, which caused multiple reflections and scattering. Furthermore, the fabricated sensor was reported to accumulate stress at the hydrogel end face with increasing temperature, limiting the sensing up to 50 °C. Nevertheless, roughening treatment at the end face is reported to increase the sensing limit. Multiple efforts have been

 This journal is © The Royal Society of Chemistry 2023

Published on 13 June 2023. Downloaded by Bilkent University on 12/9/2023 12:01:00 PM.

focused on fabricating Fabry–Perot-based interferometric sensors, despite the requirement of complex post-processing of the interference spectrum for demodulating the optical path length changes. Moreover, to observe interference fringes within a reasonable bandwidth, a minimum gel coating thickness is needed (approximately 60 μm), which can limit the responsive property of the sensor.[261]

Mach–Zehnder interferometry (MZI)-based hydrogel fibers as a heavy metal cation sensor with a simple set-up and easy coating procedure have been reported, which are fabricated by splicing a 30 mm segment of the PCF (10.1/125 μm) between two SMFs (8.2/125 μm) using an electric arc splicer.[161,262] The precursor solution for coating was prepared by adding PVA and PAA in de-ionized water to make a polymer blend which was left to cool overnight with continuous stirring. The PCF segment was separately immersed in piranha solution (sulphuric acid and hydrogen peroxide in 7 : 3 volume ratio) at 80 °C for 60 min to remove any organic residue and hydroxylates from the fiber surface and later rinsed and dried with purified nitrogen gas. Afterward, the spliced structure was immersed in a dip coater at 100 mm min^{-1}, dried at room temperature, and heated at 130 °C. Finally, it was submerged in de-ionized water to remove the excess polymer. The PVA/PAA hydrogel-coated fiber was immersed in pH 6 phosphate buffer as a finishing process for chemical modification. Recently, another MZI-based novel humidity sensor has been developed for superior sensitivity where two MMF fibers were spliced between three SMF fibers, as demonstrated in Fig. 7e.[263] The sensor was fabricated by etching the upper layer of the MMF using hydrofluoric acid and coating the MMF with CaAlg. Later, the MMFs were spliced between three SMFs to manufacture the designed sensor with high sensitivity, good repeatability, stability, and fast response time. The key to improving sensitivity was the novel use of a superior hygroscopic material like CaAlg (which can absorb water more than ten times its weight) as a cladding layer with an MZI-based humidity sensor.[264]

Interferometry-based hydrogel sensors offer a platform with high sensitivity for detecting chemicals with high concentration resolution, low cost, remote detection ability, and good application prospects. However, the biomedical use of hydrogel-based biosensors necessitates the use of bioreceptors, and methods for immobilizing bioreceptors on hydrogels must be optimized.

5.6. Hydrogel optical fibers as Bragg grating sensors

Various FBG-based sensors have been fabricated utilizing the wavelength-shifting property of FBGs due to external perturbations such as pH, electric and magnetic fields, light, salt concentrations, and specific ions.[265–267] Recently, a Bragg grating-based fiber optic sensor was fabricated for pH measurement, where a blend of PVA and PAA was used to prepare the core (Fig. 7f).[268] The preparation process of PVA-PAA included mixing PVA and PAA in hot water of 90 °C for 7 h, followed by 5 h of stirring until a uniform blend of translucent gel was achieved. The periodic change of the refractive index in the core can be achieved by indenting an intense interferometric pattern formed by UV light, the point-by-point method, or the phase mask method. To combine the strain and stimuli sensing behavior of FBGs, a sensing head was prepared by coating the hydrogel over an optical fiber's unclad region. Cross-linking between PVA hydroxyl groups and PAA carboxyl groups is ensured by drying the hydrogel-coated fiber at 80 °C for 20 min, followed by annealing in a tubular furnace for 1 h at 130 °C.

Moreover, the sensitivity of these sensors was reported to be increased by 66% using a coating of elastomeric material below the hydrogel coating.[178] However, the accuracy of the FBG sensor depends on the linear response of hydrogel swelling with respect to pH change. Thus, non-uniform hydrogel cross-linking significantly hampers the detection accuracy of the FBG-based sensors.

5.7. Fiber optic probes based on asymmetric microlens arrays

Fiber optic probe-based sensors have emerged as suitable candidates for detecting devices in diverse fields like biosensing, industrial biotechnology, and environmental monitoring. Various methods have been implemented, such as interferometry, fluorescence, and SPR-based sensing. But these previous devices have several requirements, including coherent light sources and output signal processing.[269] To overcome the drawbacks of the existing fiber optic probe, an asymmetric microlens array-based glucose sensor has been developed where a light diffuser is imprinted on stimuli-responsive hydrogels for glucose, pH, and alcohol monitoring.[75,269,270] By cross-linking glucose-responsive PBA with acrylamide, a sensing probe containing an asymmetric microlens array was developed, which can reach equilibrium within 15 min.[271]

The precursor solution for fiber tip functionalization was prepared from acrylamide, MBAm, and 3-APBA mixed with DMPA. As shown in Fig. 8a, the precursor solution was drop-cast on the asymmetric microlens array surface. It was later covered with a salinized glass piece and UV cured for 5 min. Thus, an inverse replica of the master was prepared. The polymerized structure was preserved with PBS at pH 7.4. The hydrogel fiber's fabrication procedure included preparing the hydrogel precursor by mixing PEGDA with 2-hydroxy-2-methylpropiophenone (2-HMP) in DI water. The prepared solution for fiber was injected into a PVC tube mold and subjected to polymerization by UV-induced cross-linking. Finally, the biocompatible PEGDA-hydrogel fiber was extracted (Fig. 8b-(i–v)). Finally, the functionalized light-diffusing microlens (LDMs) with sensing material was attached separately with the PEGDA-hydrogel fiber and silica optical fiber for a comparative study (Fig. 8c(i–v)). In the presence of glucose, LDMs implanted on the fabricated biocompatible hydrogel bend due to the volumetric shift (osmotic Donnan pressure) of the hydrogel network when immobilized 3-APBA forms anionic boronate. Due to this glucose-induced swelling, the curvature of the asymmetric microlens array was modified, affecting the power transmitted through the hydrogel. Moreover, a faster glucose diffusion rate is the key to reaching equilibrium in the shortest possible time. Thus, other geometries such as the

Published on 13 June 2023. Downloaded by Bilkent University on 12/9/2023 12:01:00 PM.

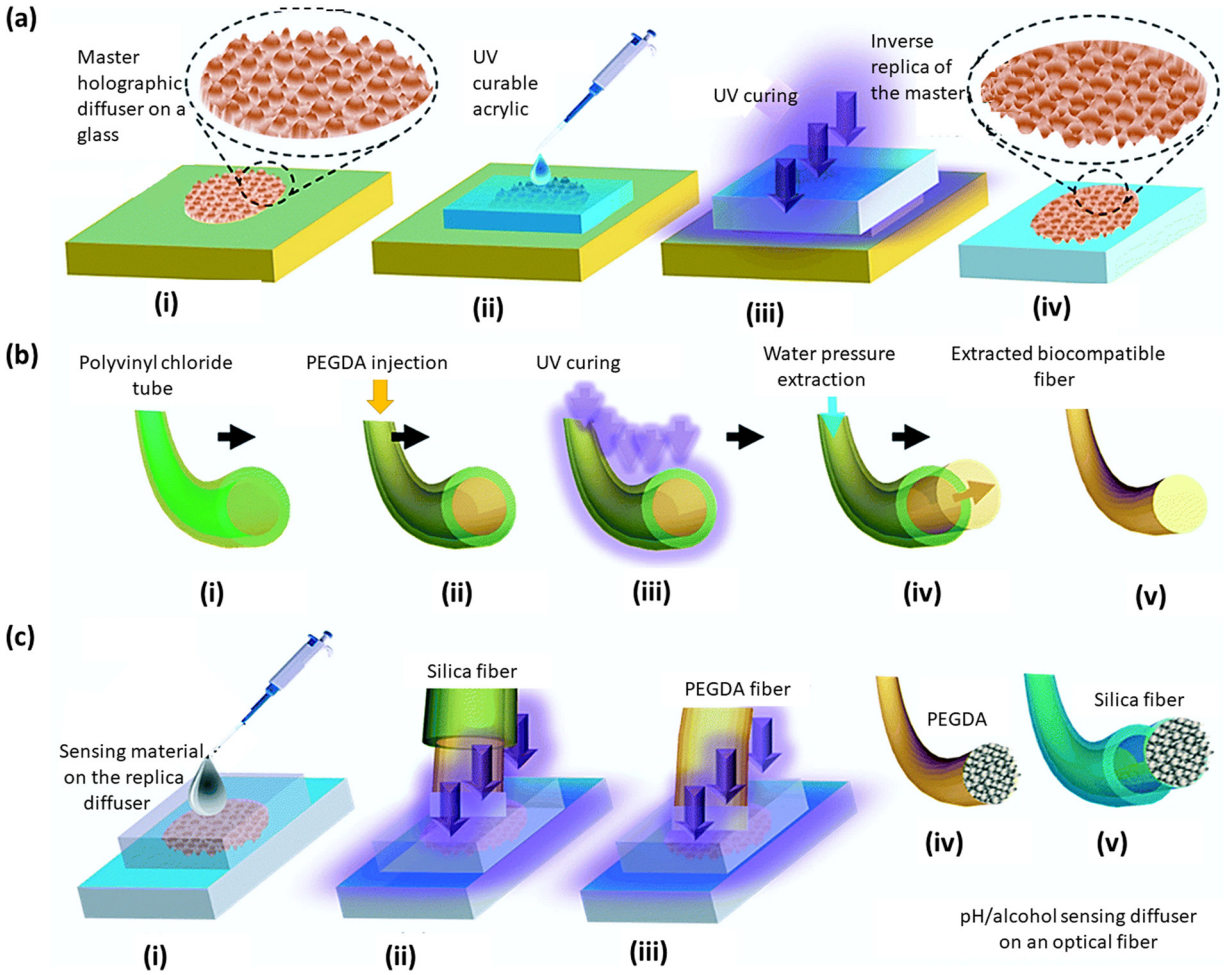


Fig. 8 Fabrication procedure of the glucose-responsive hydrogel probe based on light-diffusing microlens arrays. (a) Preparation of asymmetric microlens arrays on a glass slide stamped on a glucose-responsive hydrogel and (b and c) functionalization process done on the hydrogel and silica optical fiber. Reproduced with permission from ref. 268, Copyright © 2019 Royal Society of Chemistry.

porous structure[272,273] of the sensing region and microgel particles[274,275] can significantly reduce the sensing time.

The functionalization approach at the fiber tip has become advantageous over previously developed fluorescence- and SPR-based fiber optic probes. The fluorescent glucose sensor involves a multi-step process with time-consuming synthesis and purification.[276] On the other hand, SPR-based probes need a complex fabrication process with pretreatment, de-cladding, depositing the thin metal layer, and immobilizing the glucose-sensitive layer.[222,277,278] However, the cladding layer was not integrated with the fabricated hydrogel in this designed sensor, which resulted in a higher loss (1 dB cm^{-1} for 50% precursor concentration at 532 nm).[75] Coating a bio-compatible hydrogel layer as cladding can significantly increase the guiding efficiency.[201]

6. Sensor applications

The stimuli-response characteristics and the capability of incorporating functional recognition motifs into the hydrogel matrix have made hydrogel-integrated optical fibers a considerable candidate for various sensing applications. Many hydrogels like PVA, PAAm, and PEGDA have been employed in biomedical and biosensing applications. Hydrogels have been used both actively, where stimuli-responsive hydrogels are the sensing elements and exhibit phase or volume alterations proportional to environmental changes, or passively, where hydrogels act as matrices to host main sensing elements (nanoparticles, biomolecules, *etc.*) that respond to the corresponding changes. The use of hydrogel materials in sensing applications can improve bio-mechanical compatibility owing to their pivotal features, such as improved softness, lower friction, and flexibility.[192]

6.1. Glucose biosensors

Diabetes – the elevation of blood glucose (hyperglycemia) caused by insulin deficiency – has been a serious concern for millions worldwide. Today, it is incurable and if not controlled properly, it can cause long-term issues like kidney failure, cardiovascular complications, diabetic nephropathy,

 This journal is © The Royal Society of Chemistry 2023

Published on 13 June 2023. Downloaded by Bilkent University on 12/9/2023 12:01:00 PM.

and atherosclerosis due to its central role in homeostasis.[75,279,280] Moreover, there have been reports of hyperglycemia among intensive care patients such as those suffering from high-degree burns, shock, sepsis, and hypoxia, who had no prior history of diabetes, which is due to the stress of acute illness that results in increased glucose production, insulin resistance, and insulin deficiency.[281–284] Therefore, developing systems that can monitor blood glucose to control the level and evaluate the effectiveness of the implemented treatment is necessary.[285]

Enzyme-based sensing mechanisms have been majorly applied to glucose sensors through electrochemical or colorimetric modalities.[286–289] A glucose sensor was proposed where pH-sensitive chitosan-based microspheres, immobilized in optical fibers, were incorporated with a pair of FRET fluorophores and glucose oxidase (GOD).[290] The oxidation of glucose catalyzed by GOD produces gluconic acid and hydrogen peroxide, leading to a drop in the pH value from approximately 6.8 to 3.8, proportional to a glucose concentration increment from 0 to 12 000 μg. At lower pH, NH_3^+ groups formed, and electrostatic repulsion between cationic chains increased. Subsequently, the polymer became more hydrophilic, causing an increment in the hydration of the polymer chain that caused microsphere swelling, resulting in a FRET signal shift, and the opposite happened at higher pH. PNIPAAm, a temperature-sensitive hydrogel with an LCST of ~32 °C in an aqueous solution, was reported with GOD immobilized on nanoparticles like SiO_2 for glucose detection.[291–294] Hydrogel swelling at a lower LCST temperature allowed the enzyme to contact the substrate, causing an enzymatic catalysis reaction. On the other hand, when the temperature was higher than the LCST, the PNIPAAm/GOD complex (PIGC) was not able to perform enzymatic catalysis due to the isolation of the capsulated GOD from the substrate because of the shrinkage of the hydrogel. This caused an on-off switch-like effect through temperature for glucose oxidation, which is useful for multifunctional sensors.

An optical fiber-based glucose sensor was prepared using this PIGC-based approach and multiparameter sensing capability could be implemented in the sensor (with cholesterol oxidase for cholesterol sensing). The sensor exhibited a detection limit of 11.8 mg dL^{-1} for glucose and a response time of 200 seconds in the glucose concentration range of 50–700 mg dL^{-1} with an optimal detection condition of pH 6.5 and temperature 35 °C.[293] GOD immobilized Fe_3O_4@SiO_2(F)@*meso*-SiO_2 nanoparticles combined with the poly(*N*-isopropylacrylamide-*co*-acrylamide) complex could improve the performance.[292,293] Adding the AAm segment to PNIPAAm increased the LCST closer to the temperature of the human body. The developed sensor showed a linear increment in the phase delay change with increasing glucose concentration in the range of 50–700 mg dL^{-1}. However, the sensor could not detect glucose at 38 °C due to the failure to perform glucose oxidation. The sensor demonstrated a detection limit of 8.33 mg dL^{-1} with a response time of 200 s.[292] Since a healthy person typically has a glucose concentration of 70.1–109.7 mg dL^{-1}, this type of sensor has practical potential. In addition, this system could be used to develop a multiparameter sensor (for instance, with cholesterol) using temperature regulation as a switch. P(NIPAAm-*co*-AAm) could shrink above the LCST, separating GOD from the analyte. This isolation of GOD prevented the catalysis of glucose. Another enzyme was immobilized, capable of performing sensing activity for another analyte, such as cholesterol, at temperature above the LCST for glucose sensing, and the temperature was used as a regulator to activate and deactivate the enzymes sequentially.[293] However, these sensors had some drawbacks, including inferior long-term performance, lower sensitivity in low-concentration glucose, and instability regarding enzymes, which necessitated regular calibration and they showed incompatibility for long-term applications.

Phenylboronic acid derivatives, as another example, can regulate the fiber's optical properties by forming a glucose–boron complex and have demonstrated potential as glucose sensors (Fig. 9a).[295] Cationic boronic acid and anionic fluorescent dye-containing hydrogels were added to the PMMA fiber optic cable tip to develop a glucose sensor.[296] The electrostatic interaction between boronic acid and the dye resulted in the diminution of the fluorescent dye. Upon glucose addition into the system, the interaction between the glucose and the boronic acid groups generated negative boronate complexes leading to fluorescence recovery.

PAAm and PEGDA hydrogels, in combination with phenylboronic acid, were used to develop fiber optic glucose sensors. A fiber optic hydrogel was prepared by using p(AM-*co*-PEGDA) as the core and Ca alginate as the cladding and was functionalized with 3-(acrylamido) phenylboronic acid (3-APBA) (Fig. 9b). PEGDA resisted the adsorption of proteins like fibrinogen, albumin, and fibronectin, which reduced inflammatory cell interactions. This hydrogel optical fiber sensor was able to provide a readout rate of 1.33 mmol L^{-1} min^{-1} for a glucose concentration shift of 8.0 to 15.0 mmol L^{-1}, a 17-fold higher rate than the requirement for a typical diabetic patient (0.078 mmol L^{-1} min^{-1}). However, the p(AM-*co*-PEGDA-*co*-3-APBA) fiber required a relatively long time (almost 45 min) to reach the glucose complexion equilibrium.[76] 3-APBA cross-linked with acrylamide to formulate a glucose-sensing hydrogel, followed by the imprinting of asymmetric microlens (LDMs), was proposed to address this impediment. These microlens arrays controlled the beam shape of both monochromatic and white light and thus could consistently detect glucose concentrations for both monochromatic and broadband white light. Then, this glucose-responsive hydrogel was chemically attached to the tip of the optical fiber derived from the PEGDA (60 v%) monomer using the photopolymerization process.[75] The hydrogel could form anionic boronate leading to an osmotic Donnan pressure that caused a volumetric shift. This consequently modified the asymmetric microlens array curvature stamped on the hydrogel's surface, which changed the focal lenses of the microlenses, and eventually affected the maximum transmitted/reflected power. The sensor exhibited a linear response for a glucose concentration range of 0–20 mM. The output signal increment was 48 μW increasing from 602 to

Published on 13 June 2023. Downloaded by Bilkent University on 12/9/2023 12:01:00 PM.

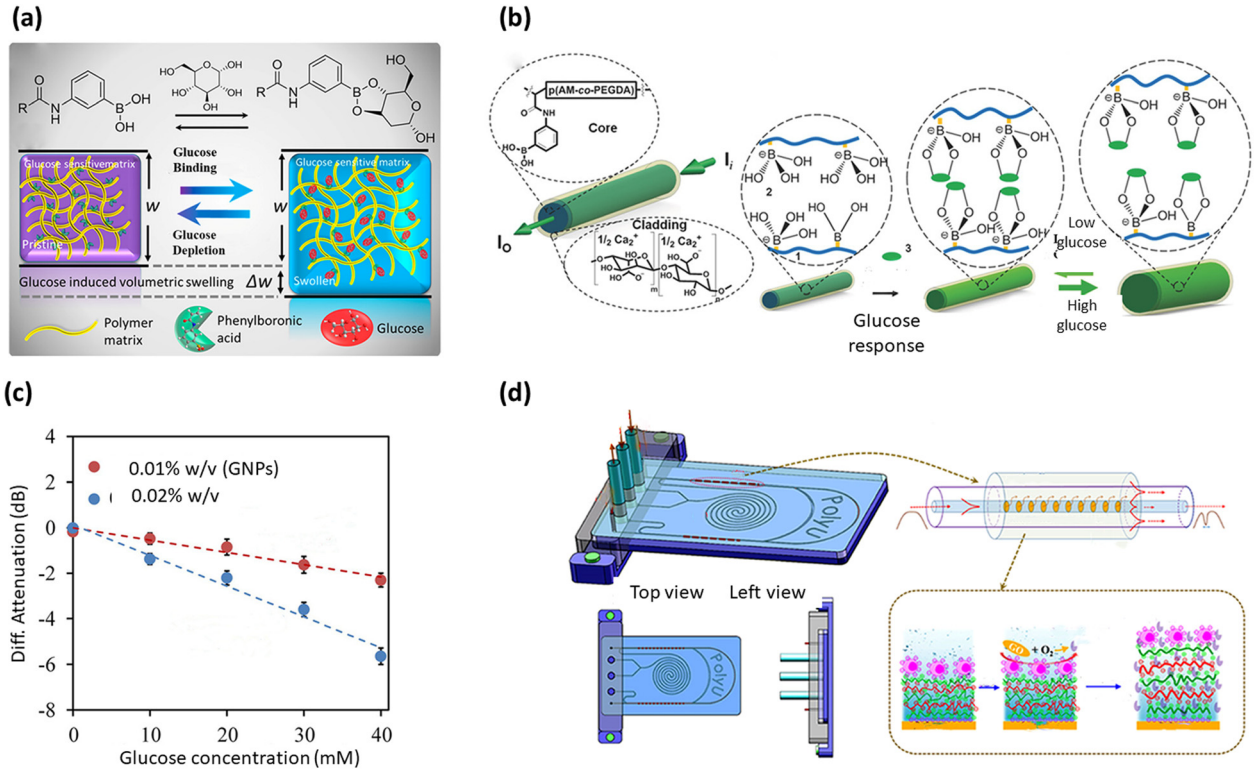


Fig. 9 Hydrogel-based optical fiber sensors for glucose sensing. (a) Glucose-binding process and volumetric shift of the hydrogel due to the addition or removal of glucose. Reproduced with permission from ref. 295, Copyright © 2018 American Chemical Society. (b) 3-APBA functionalized hydrogel matrix (1 → polyacrylamide hydrogel crosslinked with PEG, 2 → charged tetrahedral state of 3-APBA, 3 → glucose) and its response to glucose. Reproduced from ref. 76, Copyright © 2017 The Author. Published by John Wiley & Sons, Inc. (c) Differential light attenuation (at 528 and 700 nm) for different glucose concentrations of 0.01 wt% and 0.02 wt% gold nanoparticle doping. Reproduced with permission from ref. 137, Copyright © 2021 Walter de Gruyter GmbH. (d) Design of a microfluidic chip integrated with an optical fiber glucose biosensor with the mode coupling and optical resonance of the sensor and the glucose sensing and signal enhancing mechanism of the film. Reproduced with permission from ref. 301 Copyright © 2016 The Optical Society.

650 μW, when the glucose concentration was increased from 0 to 20 mM. However, for an increase in concentration from 20 mM to 50 mM, the output signal increment was lower (30 μW), indicating a sensitivity reduction. The limited availability of boronate binding sites and reduced elasticity of the hydrogel matrix competing against the volumetric swelling required for the detection mechanism were the reasons behind declined sensitivity at higher concentration.[297] The developed device had a readout rate of 0.66 mM min^{-1}, whereas the required readout rate for a diabetic patient is 0.078 mM min^{-1}. Moreover, it took one-third of the equilibrium time (15 min) compared to a previous study (45 min). However, the hydrogel fiber still exhibited less sensitivity compared to silica fiber performance due to the higher light loss than the silica fiber.[76]

A similar approach has also been reported for an acrylamide-integrated hydrogel, which was incorporated at the end of an optical fiber forming a Fabry–Perot cavity by curing a pre-gel solution using a photoinduced polymerization-crosslinking process.[261] PBA and dimethyl-amino-propyl-acrylamide (DMAPAA) were incorporated as the sensing material. It exhibited excellent sensitivity performance and compatibility with *in vivo* sensing due to its smaller size and faster swelling. 3-Acrylamido phenylboronic acid has a pK_a of 8.2–8.6, making it difficult to detect glucose at the physiological pH level (pH 7.4),[295] and further adding the amino group ameliorated this problem. The electrostatic interaction between boronic acid and the amino group (creates aminophenylboronic acid) stabilized the boronic acid moiety.[298] Another issue was that hydrogel sensors containing boronic acid suffered from a higher affinity towards other carbohydrates like fructose, mannose, and galactose than glucose. With only boronic acid, the addition of glucose showed an optical path length change of 117 nm mM^{-1} through swelling.

In contrast, fructose showed an optical path length change of 4416 nm mM^{-1} (galactose 595 nm mM^{-1} and mannose 366 nm mM^{-1}). The incorporation of DMAPAA could help with this noise issue. A decrease in the sensitivity towards fructose (also galactose and mannose) and an increase in the sensitivity towards glucose were observed with increasing mol% of DMAPAA. When 4 mol% was used, the optical path length reduced from 117 nm mM^{-1} to −692 nm mM^{-1}, indicating shrinkage, whereas the other carbohydrates still exhibited swelling. This behavior endowed the system with increasing sensitivity towards glucose and decreasing sensitivity towards fructose, galactose, and mannose. However, the use of DMAPAA beyond 10 mol% reduced the selectivity for glucose due to the increase

 This journal is © The Royal Society of Chemistry 2023

Published on 13 June 2023. Downloaded by Bilkent University on 12/9/2023 12:01:00 PM.

in the response magnitude towards other carbohydrates. This phenomenon might be due to DMAPAA resulting in charged boronic acid groups that suppressed the stabilization of fructose or increased charged groups due to DMAPAA causing an increased ionic and mixing contribution for swelling, producing a highly swollen gel, and additional negative charges from fructose-stabilized boronic acid groups, which were less impactful since the gel was already highly swollen.[261]

Cladding the optical fiber with a low refractive index material like CaAlg was also considered as a solution to this sensitivity problem.[76] The cladded hydrogel fiber reported an optical loss range of 1 to 6 dB cm^{-1} compared to the loss of the bare fiber core of 2–11 dB cm^{-1}. Besides, the longer ray propagation distances before reflecting off light from the core–air interface resulted in higher light transmission than thinner fibers. Integrating more 3-APBA and using a tertiary amine-like dimethylaminopropyl acrylamide improved the sensitivity and selectivity.[299] Yet, the issue with direct dependence on transmitted light intensity was that fiber deformation and environmental changes interfered with the transmitted light intensity; this resulted in light loss and interfered with the precision of the glucose sensing. The use of covalently immobilized gold nanoparticles improved the device's sensitivity due to the LSPR effect. A higher amount of gold nanoparticle doping (0.02% w/v) achieved superior sensitivity (0.13 dB mM^{-1}) in comparison to the lower amount of doping (0.05 dB mM^{-1} for 0.01% w/v) due to the LSPR effect (Fig. 9c).[137] Viologen-substituted boronic acid has also been used as a glucose recognition element.[300]

Another intriguing application area for developing sensors is microfluidics. As an example, a long-period grating-based single-mode fiber (SMF) optical refractive sensor was implemented in a microfluidic device (Fig. 9d).[301] The sensor was developed using a layer-by-layer assembly of poly(ethylenimine) (PEI) and PAA, with GOD as the outer layer sensing element that was integrated into a PDMS-based microfluidic chip. Although the sensitivity did not change upon microfluidic integration (sensing capability of 1 nm glucose concentration), the microfluidic device showed an increase in the detection range (from 2 μM to 10 μM). Also, the requirement of much less glucose volume for testing in the microfluidic device enabled a fast reaction between glucose and GOD, resulting in a quicker swelling/deswelling equilibrium. This significantly decreased the response time of the sensing system from 6 min to 70 s.

6.2. pH sensor

The pH value is another pivotal parameter in the field of chemistry and also medical science. The pH value is related to different electrolyte concentrations in the human body and is a crucial biomarker for indicating physiological conditions and diseases. So, substantial research has been done in developing reliable pH sensors, and also developing optical fiber-based pH sensors has been attempted. Optical fiber-based pH sensors are loosely divided into two categories: fluorescent dye-based sensors, which measure the absorption, and pH-sensitive material-based hydrogels, which measure the volume and refractive index change.[302–304] In fluorescence-based sensing methods, porous matrices have been coated on the optical fiber (surface or fiber tip), and the pH-sensitive fluorescents have been integrated on the coated matrices. Encapsulating pH-sensitive dyes in nanocapsules has also been attempted to develop pH sensors (Fig. 10a).[305] Fluorescence methods could provide simple operations and faster response time, but they also came with several issues. These sensors had a short shelf-life and poor fluorescence collection efficiency and exhibited temperature interference, excitation light intensity fluctuation, indicator leaching, limited evanescent field penetration depth, and short light–matter interaction distance. Evaluation of a ratiometric fluorescence-based pH sensor showed that increasing the molecular diameter of the fluorescent probe could be considered as way to improve the long-term stability of the sensor. Sensors with a higher core/clad diameter exhibited lower propagation loss. A thick core diameter with thin cladding could also be a considerable approach to achieve stability (thick cladding could increase the response time).

The sensor was designed by integrating dextran labeled with fluorescein (DLF), which exhibits pH-sensitive fluorescence, and Pt(II) *meso*-tetraphenyl tetrabenzoporphine (PtTPTBP) as the reference dye incorporated with the hydrogel optical fiber.[166] Tapered multimode quartz optical fibers modified with CdSe/ZnS quantum dots exhibited a minimum sensitivity of 0.5 pH units in the pH range of 4–12, and a point-of-care system was developed with the capability of smartphone detection and analysis of the fluorescence signal.[306] Another fluorescence-based pH sensor with photo-polymerized 1 : 1 HBMA/DMAEA (4-hydroxybutyl methacrylate/dimethylaminoethyl acrylate) hydrogel was applicable in measuring the pH across the ovine lung and distinguishing between normal and tumorous tissue.[167] The sensor was operational in the pH range of 5.5 to 8 with a linear performance, a response time below 30 s and an average precision of 0.10 pH units. The MZI has been another viable option for optical fiber pH sensors owing to its simple structure and good stability.[106,307] The SMF–PCF–SMF interferometer coated with a pH-sensitive hydrogel (poly(2-hydroxyethyl methacrylate-*co*-2-(dimethylamino) ethyl methacrylate)) enabled the system to achieve 1.71 nm pH^{-1} in the pH range of 6.75–8.25 pH with a detection limit of 0.004. However, cross-sensitivity due to temperature was a critical issue in such sensors. Fiber Bragg grating (FBG) sensors were considered a potential solution to this temperature cross-sensitivity. A hydrogel coated (synthesized from methacrylic acid, acrylamide, ammonium persulphate, *N*,*N*′-methylene bisacrylamide (BAAM), and tetraethyl ethylenediamine)) Mach–Zehnder interferometer with FBG was reported for sensing pH (along with temperature).[88] The sensor could operate in the pH range of 2 to 12 and exhibited a pH sensitivity of −0.27 nm pH^{-1}. The PCF-MZI combination had a higher sensitivity than the FBG; however, this also made it more vulnerable to vibration, light source intensity, and other disturbances. PVA-integrated hydrogels have been able to exhibit good film-forming properties and could be made insoluble by cross-linking with PAA.[308] PVA/PAA-based sensors were capable

Published on 13 June 2023. Downloaded by Bilkent University on 12/9/2023 12:01:00 PM.

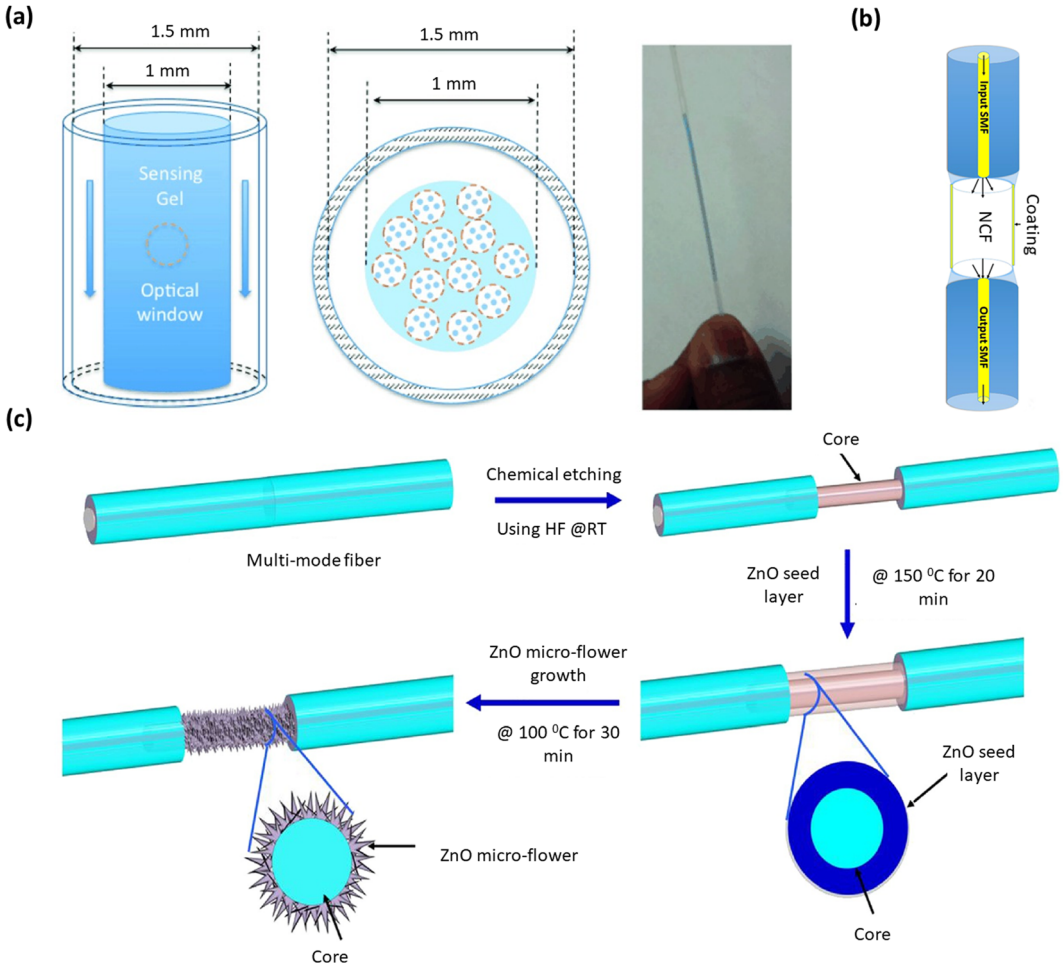


Fig. 10 Hydrogel-based optical fiber sensors for pH monitoring. (a) Demonstration of a capillary optode including nanocapsule loaded sensing gel at the core. Reproduced with permission from ref. 305, Copyright © 2015 John Wiley & Sons, Inc. (b) Illustration of the SMF-no core-SMF fiber coated with SiO_2 embedded PVA/PAA. Reproduced with permission from ref. 313, Copyright © 2021 The Optical Society. (c) Fiber optic probe fabrication through ZnO microflower growth. Reproduced with permission from ref. 304, Copyright © 2018 Elsevier Ltd.

of faster response and higher repeatability. This PVA/PAA hydrogel has been implemented in an FBG-based fiber optic sensor.[268,309,310]

An FBG coated with the cross-linked PVA/PAA hydrogel could achieve a linear sensing performance between the pH of 3 and 7 with a sensitivity of 12.16 pm pH^{-1}.[268] Developing a thin multilayer structure on the FBG achieved 53 pm pH^{-1} for the pH range of 6 to 9.[311] The use of a PMMA-based microstructured polymer optical fiber Bragg grating coated with a pH-responsive hydrogel even achieved a sensitivity of 73 pm pH^{-1} for the pH range of 5 to 7.[179] However, the performance of these sensors in most cases was limited to a specific small range of pH. A sensor with a spiral coating layer of continuous and uniform structure on an FBG with a hydrogel developed from *N*-isopropylacrylamide and NaAlg was capable of performing with a uniform wavelength shift for the overall pH range (0 to 14) and could achieve up to 23.6 pm pH^{-1}.[312]

The long-period fiber had the advantage of light coupling capability between core and cladding modes. Coating the LPFG with a hydrogel facilitated a sensitivity of 0.66 nm pH^{-1} in the pH range of 2 to 12.[181] However, the long-period grating was incapable of multipoint sensing and showed broad transmission resonance; leaky modes also resulted in multiple peaks leading to less accuracy. Combining the performance of hydrogels with different components has also been attempted to broaden the operating pH range. A single mode-no-core-single mode fiber configuration no-core fiber interferometer (NCFI) with diverse no-core fiber diameter achieved by HF etching for enhanced evanescent fields and sensitivity was coated with PVA/PAA for the measurement of pH in the range of 1 to 7 and SiO_2 embedded PVA/PAA for measuring in the range of pH 8 to 14 (Fig. 10b).[313] The sensor achieved a sensitivity of 3.42 nm pH^{-1} for the acidic range (pH 1–7) and 3.2 nm pH^{-1} for the basic range (pH 8–14).

SPR has been another well-reported pathway for developing pH sensors.[314] SPR sensors based on pH-sensitive hydrogels could offer advantages such as ultra-high sensitivity, fast response time, and the requirement of fewer samples. An LSPR-based fiber optic system with immobilized GNPs was developed for pH sensing.[315] A fiber-optic system was

 This journal is © The Royal Society of Chemistry 2023

Published on 13 June 2023. Downloaded by Bilkent University on 12/9/2023 12:01:00 PM.

developed using a single-mode waist-enlarged fiber with a tantalum pentoxide outer layer and by coating it with the PVA/PAA hydrogel.[107] The enlarged waist prevented Fabry–Perot interference refractive index mismatch at the splicing interface. It exhibited a sensitivity of 1.58 nm pH^{-1} for a pH range of 2.48 to 6.47. It has been reported that using a dielectric thin film as the top layer for an SPR configuration improved the sensitivity of the sensor.[224] A pH sensor was developed based on this concept by implementing a pH-sensitive hydrogel layer on an unclad core coated with a combined layer of silver and silicon, where adding a high refractive index material like Si improved the sensitivity of the sensor.[220] The sensor could achieve a maximum sensitivity of 12.5 nm pH^{-1}. However, this particular sensor could only perform at a higher (9–12) or lower (3–6) range of pH and could not show necessary sensitivity performance in the middle pH range (7–9) hypothetically due to the ionic group ionization in this range. Though the optical fiber core was generally coated with gold or silver, ITO integration led to superior properties and higher sensitivity.[223] It achieved a maximum sensitivity of 19.5 nm pH^{-1} but with a similar performance trend, *i.e.*, inadequate performance in the middle range. The sensor showed a broad SPR curve resulting in inferior detection accuracy of the resonance wavelength, which could have been avoided by implementing a thin layer of aluminum between the hydrogel and ITO. Even though the ITO-based sensor achieved higher sensitivity, it had several shortcomings such as non-biocompatible, less flexible, and costly since it worked in the infrared region with higher spectrometry cost. Stimuli-responsive hydrogels with imprinted asymmetric microlens structures functioning as the light diffuser integrated on the tips of the optical fibers (silica) showed a maximum sensitivity in the acidic region, especially in the pH range of 5–7, but poor performance in the basic region. The sensitivity of the system in the acidic region was found to be 40 nW pH^{-1}.[269] The use of silica in practical applications is unsuitable since it may cause inflammation and infection at the implant site. Hence, a biocompatible fiber based on PEGDA was also considered in developing the pH sensor. The PEGDA optical fiber has exhibited cell viability against the NIH-3T3 fibroblast cell line in another work, where a glucose sensor was developed.[76] The PEGDA-based setup for pH sensing exhibited a similar but inferior performance trend, achieving 10 nW pH^{-1} in the range of pH 5–pH 7 due to insufficient light guiding of the biocompatible bare core fiber. Enveloping the core with a biocompatible low refractive index cladding improved the performance by decreasing guided loss.[269]

The evanescent wave excitation and SPW stimulation through cladding removal at the interface between the environment medium and the metal film resulted in decreased mechanical strength.[316] A multimode-single mode-multimode fiber splicing structure solved this problem by enabling propagation along the interface between the cladding and metal layer.[35] The used hydrogel was synthesized from AAM, BAAM, *N*,*N*,*N*,*N*-tetramethylethylenediamine (TEMED), and methacrylic acid. The system showed excellent stability and reproducibility. It could work with a wide range of pH (1 to 12) and exhibited a maximum sensitivity of 13 nm pH^{-1} (for a pH range of pH 8 to pH 10). Even though the sensor exhibited temperature sensitivity (−0.15 nm pH^{-1}), the performance was insignificant compared to the pH sensitivity within the range of 20–40 °C. Hydrothermally grown ZnO micro flowers on tapered multimode optical fibers have also been used to enhance the evanescent wave (Fig. 10c).[35] The high surface-to-volume ratio of ZnO microflowers was complementary to pH sensing and improved the response time, and the sensor achieved a sensitivity of 2.59 nm pH^{-1} for a pH range of 3 to 7 and a sensitivity of 0.7 nm pH^{-1} for a pH range of 7 to 11.

Developing the PVA/PAA hydrogel on a photonic crystal fiber interferometer has been attempted to fabricate pH sensors.[106,253] This FPI sensor achieved a maximum sensitivity of 11 nm pH^{-1} while maintaining a linear performance in the pH range of 4.1 to 6.9.[253] However, a screen effect resulted from the high ionic strength and consequently led to critical hysteresis, limiting the potential of the sensor in biological applications beyond pH 9 (with a high concentration of Na^{+}). Implementing ionizable NaAlg (working pH range of up to 10.55) was considered as a potential solution to this issue. This exhibited a low-temperature cross-sensitivity of 0.011 pH $°C^{-1}$, mainly attributed to the thermal instability of the hydrogel. But, even with higher sensitivity, having a short pH operating range limited the sensor's potential in practical applications. This practicality issue was addressed in another Fabry–Perot-based interferometric sensor, where fiber-Bragg grating embedded single-mode fiber was inserted into a fused silica capillary, and the pH-sensitive hydrogel was coated on the tip of this fused silica.[317] The sensor achieved an average sensitivity of 0.3 nm pH^{-1}, which, although relatively inferior in comparison, exhibited a linear sensing performance for a much longer pH range (for a pH range of 1 to 7) with a fast response time. However, the reported cross-temperature sensitivity was relatively high (−1.87 pH $°C^{-1}$).

Systems other than hydrogel optical fiber-based approaches like the Fresnel lens were also considered to develop optical sensors for pH measurements.[318] The pH-responsive hydrogel was developed using HEMA, EGDMA (ethylene glycol dimethacrylate), DMPA photo-initiator (2,2-dimethoxy-2-phenylacetophenone), and isopropanol, which was dropped on an acrylic polymer-based Fresnel lens to develop the sensor. The developed sensor had an operating pH range of 4.5 to 7 with a negligible temperature cross-sensitivity between 20 °C and 40 °C. The sensitivity performance of this sensor was nonlinear and showed the highest sensitivity in the pH range of 4.5 to 5.5. Moreover, a longer storage time (in a PBS buffer solution of pH 7.4) resulted in improved sensitivity and performance consistency.[318]

6.3. Humidity sensors

Humidity is an important environmental condition in many fields, such as agricultural production, food storage and preservation, biomedicine, and corrosion monitoring in the construction and manufacturing industry (such as automobile and aerospace). Relative humidity is the parameter that is used in

Published on 13 June 2023. Downloaded by Bilkent University on 12/9/2023 12:01:00 PM.

quantifying the humidity measurement. It is a measure of water vapor content in an air–water vapor mixture. It is expressed as the ratio of the humidity of a specific air–water vapor mixture and the saturation humidity at a given temperature.[319] Numerous attempts have been made to develop low-cost, reliable, and robust humidity sensors based on various principles such as physical changes (surface acoustic wave), electrical responses (resistance and capacitance), and optical responses (reflection, diffraction, transmittance, and fluorescence); along with that various materials have also been considered such as polymers, electrolytes, porous metal oxides, and ceramics.[320,321] Although electrical sensors have been widely used for humidity sensing, they have several inherent disadvantages, such as vulnerable electromagnetic interference and cross-sensitivity. Fiber optic sensors have addressed these limitations and have advantages like low cost, lightweight, corrosion resistance, better stability, and higher sensitivity. Thus, fiber optic systems for humidity sensing have been getting strong attention, and extensive research has been done in this field over the last few decades. Internal reflection spectroscopy was utilized in a humidity sensor developed by coating an optical fiber with cobalt chloride.[322] Another cobalt chloride-coated plastic-clad silica fiber humidity sensor utilized the evanescent wave absorption spectroscopy.[323]

Hydrogels have exceptional water absorption, swelling property, film-forming ability, and adhesiveness, making them an excellent candidate for humidity sensing. The agarose gel has been an attractive option for developing relative humidity sensors due to their better performance, superior stability, and lower response time compared to the other hydrogels used in humidity sensing (like poly(hydroxyethyl methacrylate), PAAM, and poly(*N*-vinyl pyrrolidinone)).[324] It was used for the first time in developing an optical fiber humidity sensor to coat a biconically tapered SMF utilizing the biconically tapered optical fiber as a refractometer (Fig. 11a).[325] The refractive index changed with humidity, which changed the transmitted optical power. The sensor operated at a % RH range of 30–80%

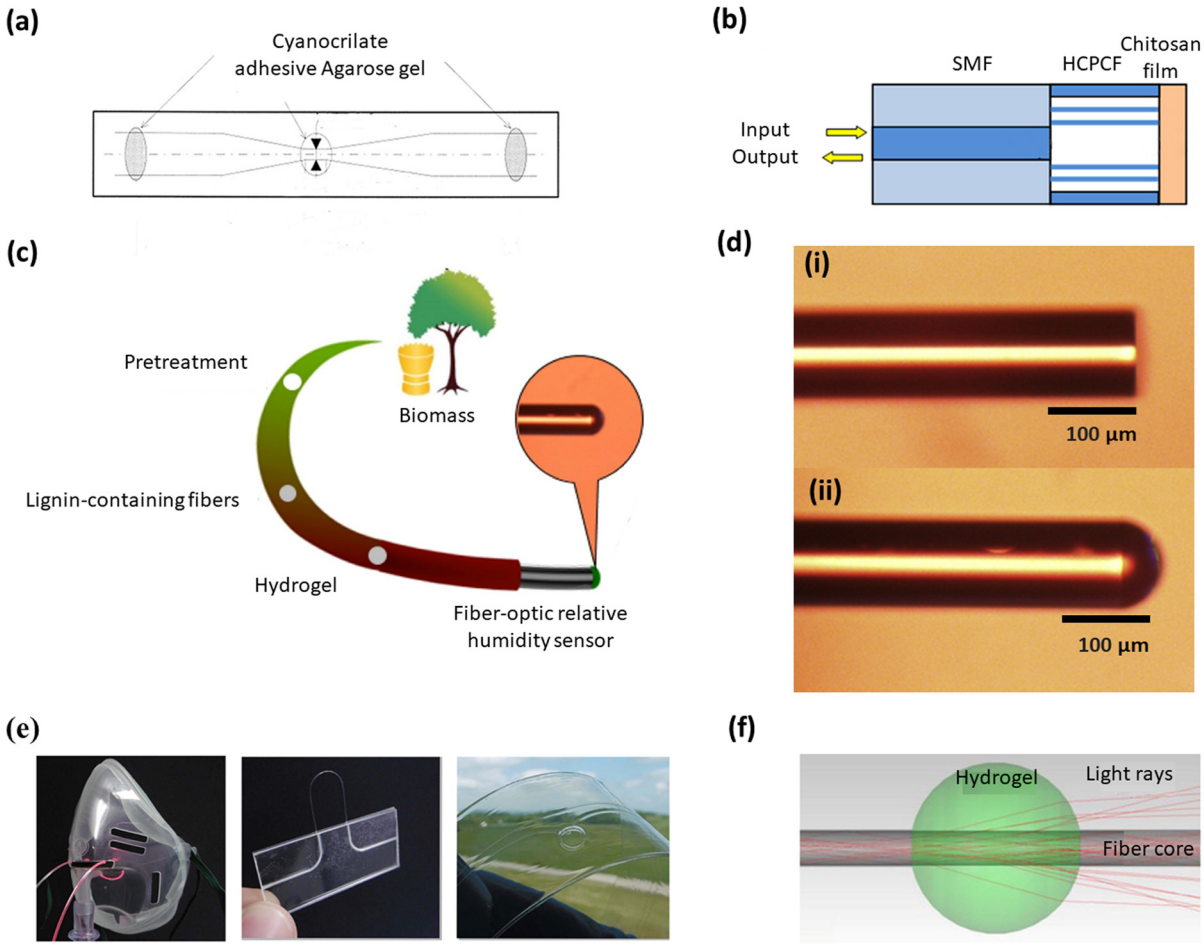


Fig. 11 Hydrogel-based optical fiber sensors for humidity sensing. (a) Schematic of a biconically tapered optical fiber. Reproduced with permission from ref. 325, Copyright © 2000 Elsevier Ltd. (b) FPI-based sensor with chitosan hydrogel. Reproduced with permission from ref. 327, Copyright © 2015 Taylor & Francis Ltd. (c) Preparation of hydrogel from renewable biomass for fiber optic humidity sensor. (d) Microscopic images of (i) a cut fiber end and (ii) an optical fiber sensor with cellulose film at the tip. (c and d) Reproduced with permission from ref. 26, Copyright © 2021 Elsevier Ltd. (e) Practical application of the U-bend fiber optic RH sensor (sensor implemented oxygen mask, cladding stripped plastic optical fiber U-bend sensor, and a polymer bare fiber laminated flexible device between two PMMA substrate layers). Reproduced from ref. 331, Copyright © 2017 The Author. Published by MDPI. (f) Illustration of the hydrogel sphere-based fiber optic sensor. Reproduced with permission from ref. 339, Copyright © 2015 Elsevier Ltd.

 This journal is © The Royal Society of Chemistry 2023

Published on 13 June 2023. Downloaded by Bilkent University on 12/9/2023 12:01:00 PM.

with a dynamic range of 6.5 dB and a response time of less than 1 min. The agarose hydrogel integrated with FBG hollow-core fibers (HCF) provided enhanced sensitivity through the influence of the coating thickness and the concentration of the hydrogel at the cost of increased response time.[326] The HPMC hydrogel demonstrated desired properties (like dispersion suspension, emulsifying, thickening, biocompatibility, stability, and adhesiveness) for developing humidity sensors by coating with HCF/SMF.[147] The sensor had an operating range of 40–99% RH with an excellent response time of 2.25 s. Another FBG humidity sensor with polyimide coating had a sensitivity of $(2.21 \pm 0.10) \times 10^{-3}$ nm per % RH for 10–90% RH.[323] A chitosan hydrogel film-coated FPI-based humidity sensor was developed using a hollow-core photonic crystal fiber (HCPCF) spliced SMF, where the refractive index and thickness change with humidity changed the reflected interference spectrum of the FPI (Fig. 11b).[327] The developed sensor measured an RH of 35–95% with a response time of 1 min. However, the performance was non-linear, and an interference fringe shift towards a shorter wavelength (maximum sensitivity 0.28 nm per % RH) and a decrease in fringe contrast (maximum sensitivity 0.5 dB per % RH) were observed with increasing % RH.

The utilization of renewable resources such as lignocellulose biomass has also been attempted in developing humidity-sensitive hydrogels by novel methods (Fig. 11c).[26] Lignin-containing fibers (LFs) were extracted from lignocellulose by combining a recyclable p-TsOH and ultrasonic treatment. The LFs were used in developing the hydrogel by reinforcing PVA.[26] Fig. 11d(i and ii) shows the tip of a cut fiber end and LF-reinforced PVA hydrogel deposited fiber end, respectively. This hydrogel coated on an SMF-based RH sensor showed a sensitivity of 4.7 dB within the humidity range of 45–80%.

CaAlg is another hydrogel (crosslinked NaAlg and calcium ion) with relevant properties that has been used in developing fiber optic humidity sensors. A humidity sensor was developed by crosslinking CaAlg on an HCF–SMF spliced structure which operated in the range of 20 to 90% RH.[260] In many cases, the indirect sensing method of FBG resulted in an inferior sensitivity performance. On the other hand, the FPI-based humidity sensor has been reported to need a high amount of coating, increasing the complexity of the sensor. In contrast, the MZI could provide higher sensitivity and the involved coating process was easier. More importantly, the process of sensing material incorporation could also complement the sensitivity improvement. A PVA-coated PCF-MZI-based humidity sensor exhibited a humidity resolution of 0.13% RH with an RH range of 30–95% and also measured temperature simultaneously.[328] A CaAlg-coated MZI fabricated with two sections of hydrofluoric acid-etched MMF (MMF cladding removed and replaced with the CaAlg hydrogel for sensitivity enhancement) and spliced between three sections of SMF exhibited a sensitivity of 0.48346 dB per % RH within the humidity range of 15–80%.[38]

A RH sensor fabricated by dip-coating the multimode silica fiber optic tip with core–shell polystyrene-PNIPAM nanosphere-based colloidal photonic crystals showed a maximum sensitivity of 6 nm per % RH.[329] But the sensor exhibited a non-linear performance, where the sensitivity increased with the relative humidity (30 pm per % RH for 30% RH, 300 pm per % RH for 80% RH, and 6 nm per % RH for 95% RH). Dip-coating of hydroxyethyl cellulose/polyvinylidene fluoride (HEC/PVDF) on a no-core optical fiber spliced between two SMFs was also reported. The power transfer from the guided modes to the leaky modes of this no-core fiber structure gave more power to the sensing region to interact with the analyte resulting in high sensitivity with less interaction. The sensor exhibited the maximum sensitivity (0.196 dB per % RH) at a wavelength of 1310 nm for a 2 cm no-core fiber length between the two applied wavelengths (1310 nm and 1550 nm), and the performance was better in the RH range of 40% to 70%. Although thinner coating increased the sensitivity, it also caused a higher loss of transmitted light, making the measurements difficult.[330] Dip coating was also attempted in combination with cross-linking. A U-bend fiber optic humidity sensor was developed using a hydrogel-implemented plastic optical fiber, where the hydrogel poly(dimethylacrylamide) (PDMAAm) was first dip-coated on the fiber and then cross-linked by UV-irradiation.[331] The developed humidity sensing system was used for respiratory monitoring in a medical oxygen mask and the possibility of using the sensor in flexible microelectromechanical systems (MEMS) was also considered (Fig. 11e).

Hydrogel-coated (based on acrylic acid, vinyl pyridine, benzoyl peroxide, and dimethyl bisacrylamide) long-period grating humidity sensors were developed that could achieve 99.5% linearity with ±2.3% accuracy for an RH range of 38.9 to 100%.[332,333] When hydrogel-coated cascaded LPG was used to develop an RH sensor that was based on Mach–Zehnder interference, it showed a sensitivity of 9.9×10^{-3} per % RH and an accuracy of 0.39% RH.[334] However, the linear performance range for this sensing setup was smaller (60% RH to 100% RH), and the accuracy decreased below the range. In another attempt, two different configurations, *e.g.*, hydrogel coating of the entire length and hydrogel coating of the separation section between two LPGs, were attempted for a sensing system.[335] The configuration with hydrogel coating on both the gratings and the separation between fibers was able to exhibit higher sensitivity (7.71×10^{-3} per % RH) compared to the separation section coating configuration (7.08×10^{-3} per % RH) due to the change of fringe visibility at a higher magnitude. Both configurations had an operating range of 50–100% with linearity. The first configuration had an accuracy of ±0.45%, and the second configuration had an accuracy of ±0.32%. The long period grating based gelatin-coated fiber optic RH sensors exhibited a sensitivity of 1.2 dB per % RH with soil relative humidity application measurement for agriculture and geology (soil % RH range is 90–100%) since gelatin is sensitive to humidity of only 90% and above.[336] Another RH sensor was also implemented for the same application based on optical time domain reflectometry, which sends short laser pulses through the optical fiber and measures the light scattered back, with the hydrogel (poly(ethylene oxide)-*co*-poly(propylene oxide) block copolymer polyurethaneurea) coating that was able to detect RH from 70 to almost 100% with an operating temperature range of 5 to 60 °C.[337] Implementation of PVA led to non-

Published on 13 June 2023. Downloaded by Bilkent University on 12/9/2023 12:01:00 PM.

linear performance and showed superior performance only in the higher region with a shorter RH range.[338] The performance of the sensor was 0.066 dB per % RH for 55–85% RH and 0.53 dB per % RH for 72–85% RH. A hydrogel sphere-integrated optical fiber RH sensor has been reported to exhibit better performance compared to hydrogel coating (Fig. 11f).[339] When poly(ethylene glycol) dimethacrylate (PEGDMA) hydrogel sphere was incorporated with a bare optical fiber core, transmittance decreased from 62.9% to 9%, with the increase of sphere diameter from 0.6 mm to 2 mm, showing that the superior capability of the sphere to couple out the light from the fiber than the coating resulted in higher sensitivity. However, other possible alternatives to PEGDMA are needed to be researched due to its narrow operation range of 70–90%.

6.4. Ion sensing

Water plays a significant role in the biological systems of all living creatures; hence, ensuring the purity of water is a critical issue. However, in recent years, due to environmental pollution and increased usage of heavy metal ions such as chromium and lead, impurities have increased in the aquatic and terrestrial environment.[340] Chromium is a hazardous and carcinogenic element and can have a detrimental effect on the human body. In the environment, it exists in two primary oxidation forms, trivalent chromium Cr^{3+} and hexavalent chromium Cr^{6+}. A controlled amount of Cr^{3+} is vital for the proper functioning of the biological system, while Cr^{6+} is known to be up to 1000 times more toxic than the Cr^{3+} ion.[176] A fiber optic sensor probe containing three layers of coating on the core (Fig. 12a), silver (Ag), indium-tin-oxide (ITO), and hydrogel with ATAC ((3-acrylamidopropyl)-trimethylammonium chloride), was used to detect the CrO_4^{2-} ion in the aqueous medium through polymerization reaction.[341] Here changing the concentration of CrO_4^{2-} around the probe led to the polymerization of ATAC on the hydrogel, which eventually caused a change in the refractive index of the medium. It also led to a red shift in

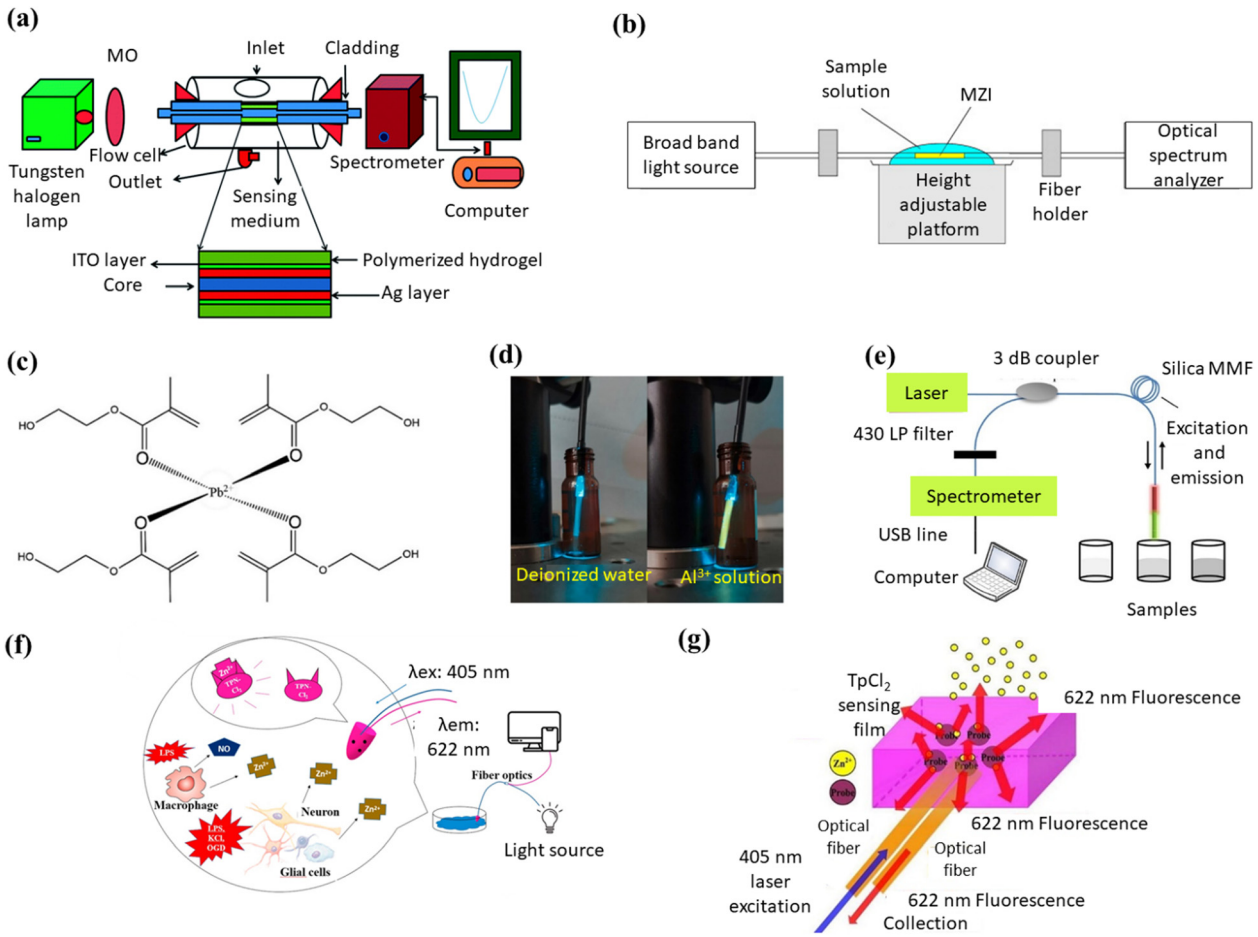


Fig. 12 Hydrogel-based optical fiber sensors for ion sensing. (a) Schematic representation of the experimental design. Reproduced with permission from ref. 341, Copyright © 2014 Royal Society of Chemistry. (b) Experimental design of the sensing equipment. Reproduced with permission from ref. 262, Copyright © 2014 Elsevier Ltd. (c) Interaction between Pb^{2+} ions and probe molecules. Reproduced with permission from ref. 161, Copyright © 2022 Elsevier Ltd. (d) Change of fluorescence intensity after Al^{3+} immersion. Reproduced with permission from ref. 349, Copyright © 2021 Elsevier Ltd. (e) Experimental setup for the ratiometric sensing of the probe molecule. Reproduced with permission from ref. 74, Copyright © 2018 Elsevier Ltd. (f) Mechanism of sensing with double fibers. Reproduced with permission from ref. 352, Copyright © 2020 Elsevier Ltd. (g) The working mechanism of the sensing film with two fibers. Reproduced with permission from ref. 355, Copyright © 2015 Elsevier Ltd.

 This journal is © The Royal Society of Chemistry 2023

Published on 13 June 2023. Downloaded by Bilkent University on 12/9/2023 12:01:00 PM.

the SPR spectra, further confirming the hydrogel's role in detecting Cr^{6+}. Subsequently, this sensor was found to show optimum performance at pH 7.0 with a background electrolyte (NaCl) concentration of 10^{-3} M, and the limit of detection (LOD) for this sensor was found to be 0.5×10^{-5} M with a sensitivity of 6.67×10^{10} nm M^{-1}. Another approach involved a phase-modulated fiber optic sensor for detecting the lead ion (Pb^{2+}), and the fiber sensor was coated with an AM-integrated smart hydrogel between two no-core-fiber (NCF) (Fig. 12b). The HEMA used in the hydrogel allows the trapping of the Pb^{2+} ion in the hydrogel *via* forming an "O–Pb–O" crosslink structure with the help of the oxygen atom in the structure (Fig. 12c).[342] This sensor showed a relatively high sensitivity of 8.155×10^5 nm mol^{-1} L^{-1} and a low standard deviation of $\leq 1.28 \times 10^{-8}$ mol L^{-1}.

Moreover, the estimated LOD was 2.452×10^{-8} mol L^{-1}, with a spectral resolution of 0.02 nm.[161] The spliced few-mode MZI, prepared by intertwining a photonic crystal fiber (PCF) between two single-mode fibers (SMF), was also used for monitoring heavy metal Ni^{2+} ions and pH with high sensitivity.[262] The hydrogel composition included PVA/PAA, which induces cross-linkage between hydroxyl and carboxyl groups upon further heating and eliminates the need for crosslinkers and initiators.[343] Subsequently, the swelling and deswelling rate of the hydrogel decreased upon further modification with 8-hydroxyquinoline (8-HQ) and it acted as a receptor for Ni^{2+} ions.

The hydrogel also demonstrated a pH responsiveness of 3.14 nm pH^{-1} in the pH range of 3 to 5, whereas the responsiveness of the 8-HQ modified hydrogel declined. Furthermore, in the concentration range of 50 μM, the modified hydrogel exhibited a sensitivity of 0.214 nm μM^{-1} with a LOD of 1 nM, which is lower than the limit for drinking water.[344] Additionally, the hydrogel composition affected the sensitivity, *i.e.*, the PVA/PAA ratio of 12 : 3 to 12 : 6 was more sensitive than other ratios.

The FBG demonstrated better sensitivity to Cr^{6+} detection utilizing a chemo-mechanical approach.[176] The highly responsive hydrogel prepared from the blend of ATAC, azobisisobutyronitrile (AIBN), and AM mixed with tetraalkylammonium salt was highly sensitive to the metal Cr^{6+} ion. When the hydrogel-coated FBG tip was submerged in Cr solutions, the FBG peaks shifted due to mechanical strain on the sensor brought on by the hydrogel's swelling and shrinkage properties. Moreover, the sensor was 5 to 10 times more sensitive toward Cr^{6+} compared to other heavy metals such as lead (Pb), mercury (Hg), arsenic (As), and cadmium (Cd).[345] The sensitivity level of 10 pm ppb^{-1} with a standard deviation of 0.0027 and a resolution of 0.83 ppb provided evidence for this sensor's high sensitivity, repeatability, and selectivity. This sensor also showed a comparatively shorter response time for swelling and deswelling time of 5 min and 6.1 min, respectively. The sensitivity of this sensor was further improved by reducing the diameter of the cladding of the sensor and thereby reducing the loss of forces on the hydrogel.[37,176] The etching of cladding improved sensitivity and resolution to 13.9 pm ppb^{-1} and 0.072 ppb, respectively. Additionally, this proposed sensor affected the response time, with a mean swelling time of 4.9 min and a mean deswelling time of 5.8 min.[37,177]

FBG-based chemical sensors for monitoring water salinity using the hydrophilic PAA hydrogel as an active element have also been reported.[265,346] The hydrogel shrank when the sensor was submerged in NaCl, which shifted the grating's Bragg wavelength to blue, and different concentrations correspond to different Bragg wavelengths. Additionally, by using hydrofluoric acid (HF) etching to reduce the diameter of the FBG cladding, it was possible to achieve a sensitivity of 0.07 nm M^{-1}, which is 8 times greater than that of the FBG without coating.

An LPFG sensor improves the response time while enabling water salinity monitoring with a strong ion-responsive hydrogel.[180] The hydrogel was prepared by layer-by-layer dip-assisted deposition of 37% quaternized poly(4-vinylpyridine) (37qP4VP) and PAA, followed by crosslinking with glutaraldehyde. This resulted in a linear response ($R^2 = 0.999$) with a good swelling/deswelling ability at a concentration of 0.4 M to 0.8 M at a pH of about 8.1. Besides, the fabricated sensor showed a high sensitivity of 7 nm resonance wavelength (RW)/M, which is 3 times higher than that of pristine LPFGs, and a fast response time of about 5 s.

Excessive aluminium (Al) accumulation is also harmful and may cause Parkinson's disease, amyotrophic lateral sclerosis, and Alzheimer's illness.[344,347,348] A lumogallion-doped hydrogel-containing optical fiber probe can detect Al^{3+} ions using the fluorescence method.[349] The optical fiber structure, containing a core with a refractive index of 1.465 and a cladding refractive of 1.395, was coated with the PEGDA-integrated hydrogel, where the chemical lumogallion functions as a fluorescence indicator. Metal ions of Pb^{2+}, Cr^{6+}, Cu^{2+}, Zn^{2+}, Mn^{2+}, Na^{+}, Fe^{3+}, and Al^{3+} having a concentration of 15 μM were added to lumogallion solutions of 150 μM concentration. The fluorescence intensity ratio of the lumogallion solution did not change for other ions except Al^{3+} (Fig. 12d). Additionally, fluorescence intensity decreased with the increased concentration of Al^{3+} ions, and the sensor showed high linearity ($R^2 = 0.991$) in the concentration range of 0 to 35 mM.

Another vital element, iron (Fe), can be found in the human body (total 4 to 5 g) in a wide variety of forms, and an excess amount of this element can lead to organ or tissue damage due to hemochromatosis, hepatitis, and neurodegenerative diseases.[350,351] QDs with a comparable or larger size than the pore of hydrogels can be immobilized in the polymer hydrogel.[238,239] A QD-doped hydrogel fiber has been used in fluorescence sensors for detecting Fe^{3+} ions in water solution (Fig. 12e).[74] A core-clad structure with a refractive index difference of 0.048 allowed the effective guidance of light along the fiber and provided effective excitation and collection of the emission laser in water. Green emissive QDs (gQDs) coated with TGA were insensitive to ions and exhibited a green emission signal and were used as a reference. *N*-Acetyl-L-cysteine (NAC) coated red emissive QDs (rQDs) showed a red emissive signal and demonstrated fluorescence quenching when exposed to

Published on 13 June 2023. Downloaded by Bilkent University on 12/9/2023 12:01:00 PM.

Fe^{3+} ions. When gQDs and rQDs were stimulated with a single wavelength, it resulted in two well-resolved emission band peaks at 520 nm and 628 nm. While the gQDs showed stable fluorescence emission in all the metal ions, the rQDs exhibited selective quenching towards Fe^{3+} ions.[74] Fluorescence ratiometric sensing showed a linearity of 0.9866 and a LOD of 14 nM throughout the 0 to 35 μM concentration range.

Although there is a relatively low amount of zinc ion (Zn^{2+}) in the human body, it plays a significant role in physiology. The Zn^{2+} ion activates approximately 300 enzymes and has roles in males' reproduction and nervous system.[352] For instance, researchers have reported the release of the Zn^{2+} ion in higher concentration during acute brain injuries such as seizure, trauma, and ischemia.[353,354] Hence, the Zn^{2+} ion is an excellent biochemical indicator for monitoring neural injury. A hydrogel material was mixed with probe molecules TPN-Cl_2 (meso-2,6-dichlorophenyltripyrrinone) for Zn^{2+} detection.[352] The fluorescence of the probe molecule increased with the concentration of Zn^{2+} ions released by artificial stress of rodent neural cells. To prevent probe molecule degradation, the optical diffuser in the sensor converted the high peak intensity at 405 nm near the fiber end into a moderate intensity at 622 nm. This variation in intensity was monitored by the optical sensor.[352] A tip-shaped solid-state sensor allowed the real-time detection of Zn^{2+} ions under aqueous conditions (Fig. 12f).[355] The sensor consisted of two parallel fibers covered with a hydrogel film made of poly-HEMA attached to a fluorescence probe of TPN-Cl_2. The probe molecule TPN-Cl_2 is sensitive to the Zn^{2+} ion, and it increases red fluorescence in solution (Fig. 12g).[356] This sensor was proven to work in a living organism such as an oyster that has a complex body fluid and was capable of sensing Zn ion (Zn^{2+}) concentrations of 10^{-6} M with traceable signal for 10^{-7} M. Additionally, the time-resolution was found to be 5 min for 10^{-4} M concentration, and it decreased to 1 min as the concentration decreased to 10^{-5} M. Such low limit of detection makes it suitable for the sensing of low concentration of Zn^{2+} ions released due to stress in neural cells induced by ischemia, intoxication, and inflammation.

6.5. Other sensing applications

Despite being an alcoholic chemical, ethanol is crucial for forensic and clinical analyses of substances, including blood, serum, urine, and saliva.[357,358] An optical transducer containing a hydrogel made of PAA and bisacrylamide with nanostructured gold (Au) (Fig. 13a) can detect ethanol concentrations between 0 and 30 vol%.[359] It demonstrated a reaction time of 5.2 min and a 10 day operational life. The sensor showed a red shift of the resonance wavelength as the refractive index was increased, and the predicted sensitivity of the probe was 287 nm per RIU (refractive index unit).

An SPR-based sensing probe for the detection of ethanol was fabricated by coating Ag and Si films on the unclad parts of optical fibers and further immobilizing an enzyme (ADH) and a coenzyme (NAD) in a layer of PAA hydrogel (Fig. 13b).[221] This sensor worked on the spectral mode of interrogations, where the increase in ethanol concentration from 0 to 10 mM showed a total shift of 30 nm in the resonance wavelength. Moreover, the sensor showed a maximum sensitivity of 21.70 nm mM^{-1} at close to zero ethanol concentrations. In addition, the LOD and limit of quantification (LOQ) were reported to be 29.63 μM and 15.34 μM, respectively. Additionally, a silicon layer of 8 nm thickness improved the efficacy of the sensing probe, increasing the maximum shift of resonance wavelength to 30 nm. The optimum performance was in ethanol solutions with a pH of 7.0.

A fiber optic sensor based on a chitosan and silver nanoparticle (AgNP) doped hydrogel was used to detect trichloroacetic acid (TCA).[360] When TCA comes in contact with AgNPs, the interactions between the positive amino group of chitosan and the negative group of TCA allow the transfer of electrons altering the refractive index of the nanocomposite hydrogel layer. The sensor exhibited linearity (R^2 = 0.99481) at concentrations ranging from 40 to 100 μM with a sensitivity of 0.587 nm μM^{-1}. The peak extension wavelength similarly showed a shift of around 42 nm when the concentrations of TCA were increased from 0 to 120 μM, and the device also demonstrated a quick response time of 10 s.

Nitric oxide (NO) is a vital small molecule that works as a chemical messenger and can transfer information between cells. It affects the nervous system and plays various pathological and physiological roles, such as controlling cerebral blood flow and inducing vasodilation.[221,361] A NO-detecting tip was fabricated by introducing the 1,2-diaminoanthraquinone (DAQ)-doped poly-HEMA hydrogel into two parallel optical fibers with a 1 mm length difference (Fig. 13c).[362] When the probe molecule (DAQ) captured the target molecule (NO), it shifted the waveguide's resonance frequency and enabled signal detection. This fabricated 1.2 mm-diameter sensing tip identified changes in NO concentrations in about 5 min with a LOD of 1 μM with a resolution time of around 5 min. It could detect nitrite ions (NO^{2-}) only under hypothetical physiological circumstances.

An FPI covered with a crosslinked hydrogel based on PVA and PAA was utilized to identify dangerous compounds like ammonia.[363] PVA/PAA hydrogel films were dip coated on the fiber ends to enable the binding of ammonia or volatile acids (Fig. 12d). Due to the inherent characteristics of the hydrogel, the pH changes with volume, resulting in a shift in the wavelength, enabling the detection of ammonia. The sensor demonstrated consistent linearity (R^2 = 0.99705) and a sensitivity of 20.85 nm ppm^{-1}.

The term ''dissolved oxygen'' (DO) refers to the amount of oxygen molecules dissolved in water. Measuring DO concentrations in living organisms is essential for disease diagnosis and therapy. An optical fiber coated with the PEGDA-made hydrogel precursor doped with different concentrations of a fluorescence indicator in both the core and the cladding was used for detecting DO using fluorescence quenching (Fig. 12e).[364] The sensor reduced the response time from 15 min to 10 min while reducing the optical loss from 4.2468 ± 0.1396 dB cm^{-1} to 1.3193 ± 0.0355 dB cm^{-1}. However, weak interactions between the evanescent wave and the fluorescent indicator

 This journal is © The Royal Society of Chemistry 2023

Published on 13 June 2023. Downloaded by Bilkent University on 12/9/2023 12:01:00 PM.

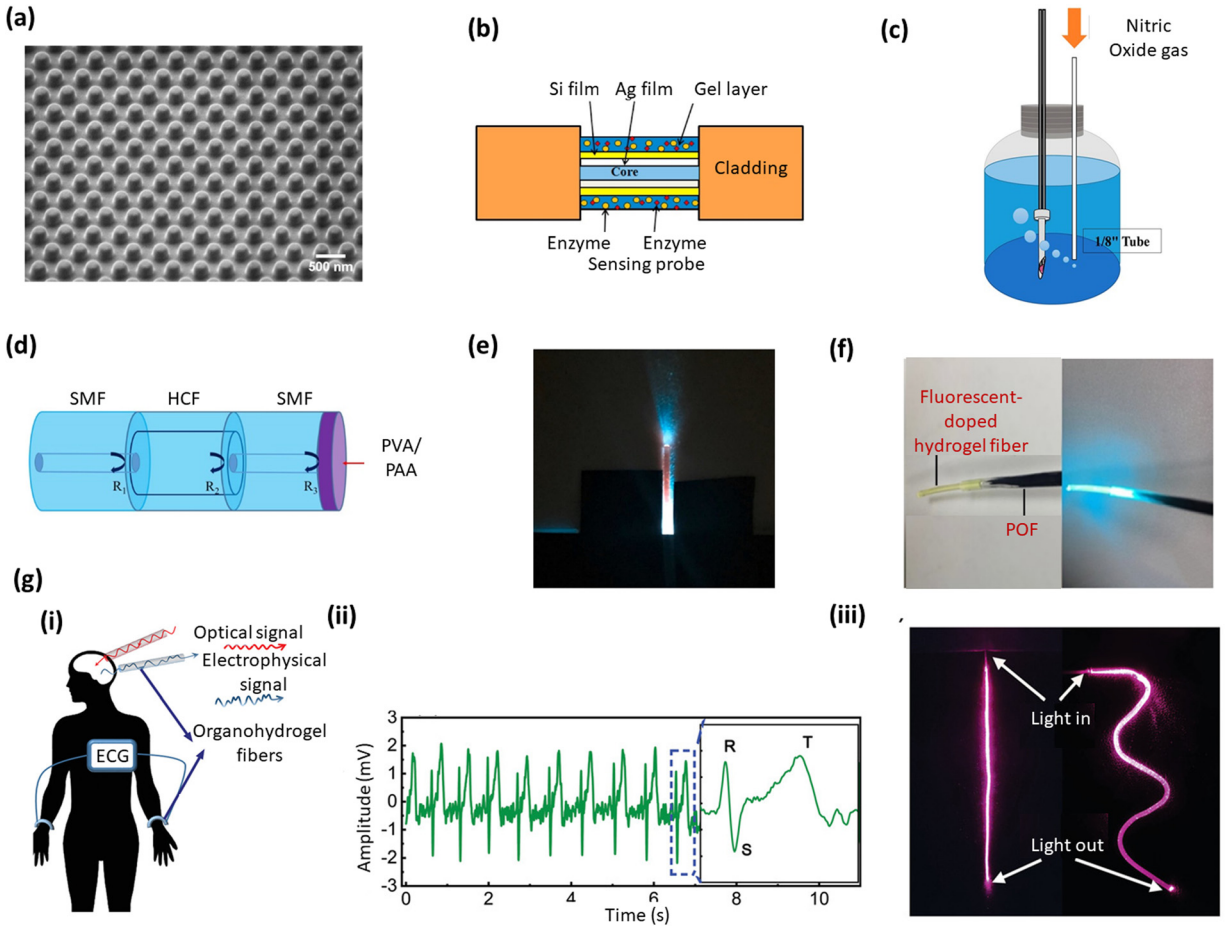


Fig. 13 Hydrogel-based optical fiber sensors for miscellaneous sensing applications: (a) scanning electron micrograph of nanopillars fabricated by lithography. Reproduced from ref. 359, Copyright © 2019 The Author. Published by MDPI. (b) Schematic representation of the designed sensing probe. Reproduced with permission from ref. 221, Copyright © 2016 Elsevier Ltd. (c) Sensing of NO gas by the prepared sensing tip. Reproduced with permission from ref. 362, Copyright © 2017 AIP Publishing LLC. (d) Fabrication schematic of the optical fiber. Reproduced with permission from ref. 363, Copyright © 2015 SPIE. (e) The variable scattering intensity along the fiber length. Reproduced with permission from ref. 364, Copyright © 2021 Elsevier Ltd. (f) Picture of the plastic optical fiber (POF) used for determining iodine concentrations. Reproduced with permission from ref. 245, Copyright © 2020 Elsevier Ltd. (g) Demonstration of real-life application of organohydrogel fibers in the biomedical field. (i) Schematic of organohydrogel's potential application in photogenetics and ECG. (ii) ECG signal collected using an organohydrogel electrode integrated device. (iii) Laser light guiding through the organohydrogel fiber. Reproduced with permission from ref. 215, Copyright © 2020 John Wiley & Sons, Inc.

reduced the sensitivity value (I/I_0) from 3.47 to 2.12.[364] The oxygen fluorescence indicator (dichlorotris(1,10-phenanthroline) ruthenium(II)) doped PEGDA hydrogel detected dissolved oxygen at different temperatures while maintaining linearity.[246] The sensor demonstrated an increased sensitivity from 2 mg mL^{-1} to 8 mg mL^{-1} fluorescent indicator concentration and later experienced a loss of sensitivity. The sensor featured a low LOD of 0.126 mg mL^{-1}, with high linearity (R^2 = 0.9863) and a fast response time of 10 s.

A chemical sensor was used to detect the explosive substance 2,4,6-trinitro toluene (TNT) using a molecularly imprinted polymer (MIP) hydrogel that displayed superior sensitivity.[365–367] The MIP was prepared using the standard method by mixing TNT, MAA, and divinylbenzene (DVB) followed by sputtering of gold film.[365,367] This sensor showed linear performance up to 1.3 × 10^{-4} M, where the linearity is R^2 = 0.92, and LOD is 5.1 × 10^{-5} M. Additionally, this sensor showed a sensitivity of 2.7 × 10^4 nm M^{-1} or 118 nm mg^{-1} mL^{-1}.

A molecularly imprinted acrylamide hydrogel integrated with colloidal crystals to create SPR-based optical fibers was proposed for vitamin B3 molecule detection.[366] The SPR spectra revealed a red shift as the interaction with the vitamin B3 molecule increased. For concentrations ranging from 0 to 10 mg mL^{-1}, the wavelength experienced a total shift of 16.651 nm. The sensor also had a sensitivity of 1.48 nm mg^{-1} mL^{-1}.

Detecting iodine in the human body is crucial. Iodine shortage can lead to conditions such as cretinism and goiter. A PEGDA-based hydrogel optical fiber doped with fluorescein was used to detect iodine ions (Fig. 12f).[245] The unclad hydrogel fiber showed a loss of 1.669 dB cm^{-1} ± 0.4 dB cm^{-1}, and the core-cladding hydrogel exhibited a loss of 0.597 dB cm^{-1} ± 0.2 dB cm^{-1}. Although the sensitivity of the hydrogel optical

Published on 13 June 2023. Downloaded by Bilkent University on 12/9/2023 12:01:00 PM.

Table 1 Hydrogel optical fiber-integrated sensors and their sensing performance

Sensor	Sensing principle	Optical setup	Hydrogel	Sensitivity	Range	Limit of detection	Response time	Ref.
Glucose	Microlens array	Silica MMF	PEGDA	2.6 μW mM^{-1}	5–20 mM	—	30 s	75
Glucose	Fluorescence	—	PNIPAAm	8.33 mg dL^{-1}	50–700 mg dL^{-1}	8.33 mg dL^{-1}	200 s	292
Glucose	Fluorescence	—	PNIPAAm	11.8 mg dL^{-1}	50–700 mg dL^{-1}	5.3 mg dL^{-1}	200 s	293
Glucose	Fluorescence	PMMA fiber optic	HEMA	—	—	—	—	296
Glucose	Fluorescence	—	PEGDA	1.33 mmol L^{-1} min^{-1}	8.0–15.0 mmol L^{-1}	—	—	76
Glucose	LSPR	—	PAAm	−0.13 dB mM^{-1}	0–40 mM	0.75 mM	—	137
pH	Fluorescence	MMF	HBMA/DMAEA	0.10 pH units	5.5–8 pH	—	30 s	167
pH	MZI	PCF spliced between two SMFs	Poly(2-HEMA-*co*-2-(dimethylamino)ethyl methacrylate)	1.71 nm pH^{-1}	6.75–8.25 pH	pH 0.004	—	307
pH	FBG + MZI	PCF spliced between two SMFs	Synthesized from MAA, acrylamide, ammonium persulphate, BAAM (N,N′-methylene acrylamide) and tetraethyl ethylenediamine	−0.27 nm pH^{-1}	2–12 pH	—	—	88
pH	FBG	SMF	PVA/PAA	12.16 pm pH^{-1}	3–7 pH	—	—	268
pH	FBG	—	—	52 pm pH^{-1}	6–12 pH	—	—	311
pH	FBG	PMMA-based microstructured polymer optical fiber	HEMA	73 pm pH^{-1}	5–7 pH	—	—	179
pH	FBG	SMF	Developed from *N*-isopropylacrylamide and NaAlg	23.6 pm pH^{-1}	0–14 pH	—	1.33 min pH^{-1}	312
pH	LPG	SMF	—	0.66 nm pH^{-1}	2–12 pH	—	< 2 s	181
pH	NCFI	SMF-no-core-SMF	PVA/PAA, SiO_2 embedded PVA/PAA	3.42 nm pH^{-1}, 3.2 nm pH^{-1}	1–7 pH, 8–14 pH	—	—	313
pH	Waist enlarged bitaper SMF interferometer	Waist-enlarged SMF	PVA/PAA	1.58 nm pH^{-1}	2.48–6.47 pH	—	—	107
pH	SPR	MMF	Hydrogel with a combined layer of silver and silicon	12.5 nm pH^{-1}	Higher (9–12 pH) or lower (3–6 pH)	—	1 min	220
pH	SPR	MMF–SMF–MMF	Synthesized from acrylamide, *N*,*N*′-BAAM, *N*,*N*,*N*,*N*-TEMED, and MAA	13 nm pH^{-1} (8–10)	1–12 pH	—	—	35
pH	Microflower	Tapered MMF	Hydrogel + ZnO microflowers	2.59 nm pH^{-1}, 0.7 nm pH^{-1}	3 to 7 pH, 7 to 11 pH	—	—	304
pH	FPI	HCPCF	PVA/PAA	11 nm pH^{-1}	4.1 to 6.9 pH	—	—	253
pH	FPI + FBG	SMF	—	0.3 nm pH^{-1}	1 to 7 pH	—	15–20 s	317
Humidity	Refractometer	Biconically tapered SMF	Agarose gel	6.5 dB	30–80% RH	—	<1 min	325
Humidity	FPI	HCF–SMF	HPMC	—	40–99% RH	—	2.25 day	147
Humidity	FPI	HCPCF spliced SMF	Chitosan hydrogel	0.28 nm per % RH	35–95% RH	—	1 min	327
Humidity	RI shift	SMF	Lignin-containing fibers	4.7 dB	45–80% RH	—	—	26
Humidity	RI shift	HCF spliced with an SMF	CaAlg	—	20–90% RH	—	—	260
Humidity	MZI	PCF	PVA	−99.5 pm per % RH	30–95%	—	∼2 s	328
Humidity	MZI	Two HF etched MMF spliced between three SMFs	CaAlg	0.48346 dB per % RH	15–80% RH	—	—	38
Humidity	RI shift	No-core optical fiber spliced between two SMFs	HEC/PVDF	0.196 dB per % RH	40–75% RH	—	10–60 s	330
Humidity	LPG-MZI	SMF	—	9.9×10^{-3} per % RH	60–100%	—	—	334
Humidity	LPG	—	—	7.71×10^{-3} per % RH	50–100%	—	—	335
Humidity	LPG	SMF	Gelatin	1.2 dB per % RH	90% and above	—	—	336
Humidity	RI shift	SMF	PVA	0.066 dB per % RH, 0.53 dB per % RH	55–85% RH, 72–85% RH	—	—	338
Humidity	RI shift	—	PEGDMA sphere	—	70–90%	—	—	339

 This journal is © The Royal Society of Chemistry 2023

Published on 13 June 2023. Downloaded by Bilkent University on 12/9/2023 12:01:00 PM.

Table 1 (*continued*)

Sensor	Sensing principle	Optical setup	Hydrogel	Sensitivity	Range	Limit of detection	Response time	Ref.
Cr ion	SPR	—	Acrylamide + bis-acrylamide	6.67×10^{10} nm M^{-1}	—	0.5×10^{-5} M	—	341
Pb ion	MZI	FMF	Acrylamide	8.155×10^{5} nm mol^{-1} L^{-1}	—	2.452×10^{-8} mol L^{-1}	—	161
Ni^{2+} ion	MZI	SMF	PVA/PAA	0.214 nm μM^{-1}	3–5 pH	1 nM	—	262
Cr ion	FBG	—	Acrylamide	1.2 pm ppb^{-1}	—	10 ppb	—	176
NaCl	FBG	SMF	Acrylamide + bis-acrylamide	0.07 nm M^{-1}			—	265 and 346
NaCl	LPFG	SMF	PAA	7 nm RW/M	—	—	< 5 s	180
Al ion	Fluorescence	—	PEGDA	—	0–35 mM	—	—	349
Fe^{3+} ions	Fluorescence	MMF	PEGDA	—	0–3.5 μM	14 nM	—	74
Zn^{2+} ions	Fluorescence	Parallel fibers covered with the hydrogel	Poly-HEMA	—	—	0, 1, 2, and 5 μM	—	352
Zn^{2+} ions	Fluorescence	SMF	Poly-HEMA	—	—	10^{-6} M	—	355
Ethanol	Plasmonic sensor	—	PAA and bisacrylamide	287 nm per RIU	—	—	—	359
Ethanol	SPR	MMF	PAA hydrogel	21.70 nm mM^{-1}	0–10 mM	29.63 μM	—	221
(TCA)	SPR	Multimodal plastic clad silica	Acrylamide	0.587 nm μm^{-1}	0–120 μm	—	10 s	360
(NO)	SPR	—	Poly-HEMA	—	—	1 μM	5 min	362
Ammonia	FPI	SMF + HCF + SMF	PVA/PAA	28.85 nm ppm^{-1}	—	—	—	363
Dissolved oxygen	Fluorescence	Plastic optical fiber (POF)	PEGDA	—	—	0.18 mg L^{-1}	10 min	364
Dissolved oxygen	Fluorescence	POF	PEGDA	0.003 mg^{-1} L^{-1}		0.126 mg mL^{-1}	10 s	246
TNT	SPR	POF	MAA	2.7×10^{4} nm M^{-1}	—	5.1×10^{-5} M	—	365
Vitamin B3	SPR-based	Multimodal POF	Acrylamide	1.48 nm mg^{-1} mL^{-1}			—	366
Iodine	Fluorescence	Core cladding bilayer structure	PEGDA/PMMA	—		26 nM	—	245

fiber was tested from 0 to 60 mM, the proposed sensor showed optimal performance in the concentration range of up to 36 mM. The sensor demonstrated high linearity (R^2 = 0.99545) with a detection limit of 26 nM.

Electrically conductive hydrogels or smart hydrogels, possessing high water content, biocompatibility, and electrical conductivity, have found their applications in diverse research fields, including tissue engineering and biomedicine,[368] energy storage,[369] sensing (capacitance, temperature, strain, humidity),[204,370–373] and flexible electronics.[374,375] However, their widespread application in optoelectronic devices is hampered by conductive hydrogel's poor optical guidance. In this respect, ionically conductive organohydrogels present a significant opportunity with their moderate conductivity along with superior optical transparency.[215] An organohydrogel fiber-based electrophysiological probe has been reported where the organogydrogel is used as an electrode for electrocardiogram (ECG) signal monitoring (Fig. 12g(i and ii)).[215] Organohydrogel fibers can provide a low modulus of elasticity while maintaining moderate conductivity, enabling them to fit on the skin's surface and provide a high signal-to-noise (SNR) ratio for electrophysiological measurements. Moreover, the fiber was also reported to demonstrate its potential for optogenetics as a flexible optical fiber with 90% optical transparency from 350 to 900 nm while maintaining light guiding property at 300% elongation (Fig. 12g(iii)).

7. Conclusion and outlook

Hydrogels have superior performance in terms of their biocompatibility and biodegradability, enabling immense leverage in biosensor development. In particular, hydrogels have been integrated with optical fibers to exploit various optical sensing principles. As elaborated by a zoo of examples in this review, hydrogel-integrated optical fiber sensors have demonstrated responsive properties toward biomarker detection and beyond, such as ion, pH, temperature, and humidity sensing. Table 1 compiles a list of some of these developments. Nevertheless, there are several major challenges to be addressed to realize more-advanced applications:

(I) Despite the availability of a large pool of natural and synthetic hydrogels, there is still a significant necessity for the exploration of newfangled hydrogel materials for integration with optical fibers. Further research on hydrogels to improve light guiding and polarization capabilities is crucial to increase the performance of fibers. Moreover, the mechanical properties of hydrogels require careful tailoring while maintaining optical properties and longer shelf life.

(II) Although the currently available methods to fabricate hydrogel-based optical fibers are relatively simple, scalability is a major concern. The thermal drawing process still dominates the manufacturing of optical fibers, and hydrogels are incompatible with this method. Exploration of hydrogel materials capable of preserving the physical and chemical properties at

Published on 13 June 2023. Downloaded by Bilkent University on 12/9/2023 12:01:00 PM.

elevated temperatures and high stress is of paramount importance for large-scale hydrogel fabrication. This will allow the fabrication of hydrogel optical fibers beyond step-index fibers with a core-clad structure. For instance, micro-structured hollow core optical fibers (PCFs and NCFs) are promising alternatives for low-loss guidance and higher power delivery. Integration of hydrogels in such fibers may allow the detection of biomolecules with higher sensitivity and selectivity.

(III) Integration of hydrogels in polymer and silica optical fibers requires complex step-by-step fabrication, primarily due to the dominant mechanism of hydrogel UV crosslinking. Crosslinking compatibility of hydrogels with visible light or infrared light and even with the guiding bandwidth of the optical fiber is essential to simplify the integration process.

(IV) Adaptation of sensing principles like SPR, LSPR, interferometry, and fluorescence phenomena in hydrogel-integrated optical fibers has significantly enhanced the performance of the sensors. However, adding these sensing principles requires nanomaterials and labels integrated within the hydrogel optical fiber structure, and detection is often performed through a complex experimental process. Developing optical fiber sensors with relatively less complicated optoelectronic circuitry is important for mass fabrication and wide usage of these sensors.

(V) Despite the superior sensitivity and selectivity of the optics and photonics-based sensors, the reliability and stability of the hydrogel-integrated sensor are critical. Hydrogel-integrated optical fiber sensors are inherently sensitive to environmental interferences such as temperature and humidity. Moreover, the hydrogel is also prone to structural degradation and loss of interfacial adhesion over time. Significant effort is required to ensure the development of hydrogel-integrated optical fiber sensors with long-time stability while maintaining the sensing performance in a dynamic environment.

(VI) The hydrogel-integrated sensors have demonstrated limited multi-functionalization capabilities. Although the optical detection principle provides higher precision, multiple analyte sensing capabilities are necessary to compete with recent advances in the realm of biosensing. Moreover, simultaneously detecting chemical and physiological signals will provide a significant advantage for wearable sensors. The combination of light-guided actuation and sensing may facilitate the fabrication of a lucrative platform for invasive surgery.

(VII) Very few studies have been conducted regarding hydrogel-based optoelectronic devices combining hydrogel fibers' electrical and optical properties. Electron-conductive hydrogel fibers demonstrate low optical transparency and low stretchability due to a high percentage of filler material. On the other hand, ion-conductive organohydrogel fibers provide an alternative option with superior optical transparency; however, the conductivity of ionically conductive hydrogel materials is still very low compared to that of conductive filler-based materials, limiting their applications in advanced optoelectronic devices. Thus, extensive investigation is required to improve organo-hydrogel fibers' optical and electrical properties. Moreover, dehydration and hysteresis of the conductive hydrogel fiber (CHF) are still a major concern. Thus, an effective strategy must be developed to fabricate hydrogel-based optoelectronic fibers with good water retention capacity, good optical transparency, high conductivity, preferable temperature tolerance, and stable mechanical properties.

(VIII) There has not been any reported work on hydrogel fiber-based semiconductor devices. Even though this field is largely unexplored, it has significant prospects as hydrogel-based semiconductor fibers can offer tunable optical properties allowing control over the wavelength, intensity, and transmission window. This tunability can make them an attractive option for displays, lighting, and optical sensor applications.

In conclusion, hydrogel-integrated optical fiber sensors present attractive opportunities for integrating sensors with biological tissues due to the high degree of their biocompatibility. Careful engineering of materials and precise device architectures are crucial factors to be considered for the realization of their potential. With the development of new hydrogels and optical fiber fabrication techniques, hydrogel-integrated optical fiber sensors would become an essential medium for the future of biosensing studies.

Conflicts of interest

There are no conflicts to declare.

Acknowledgements

Fatih Inci gratefully acknowledges support from the Scientific and Technological Research Council of Turkey (TÜBİTAK) 2232 International Fellowship for Outstanding Researchers (Project No. 118C254), the Turkish Academy of Sciences Outstanding Young Scientists Award Program (TÜBA-GEBİP), and the Young Scientist Awards Program (BAGEP) award from the Science Academy. Aykut Erbaş also acknowledges support from the Scientific and Technological Research Council of Turkey (TUBITAK) – 3501 Career Grant 119Z02. However, the entire responsibility of the publication/article belongs to the owner of the publication/article. The financial support received from TÜBİTAK does not mean that the content of the publication is approved in a scientific sense by TÜBİTAK.

References

1 S. Sharma and S. Tiwari, *Int. J. Biol. Macromol.*, 2020, **162**, 737–747.
2 L. M. D. L. Rodriguez, Y. Hemar, J. Cornish and M. A. Brimble, *Chem. Soc. Rev.*, 2016, **45**, 4797–4824.
3 Q. Chai, Y. Jiao and X. Yu, *Gels*, 2017, **3**, 6.
4 J. Tavakoli and Y. Tang, *Polymers*, 2017, **9**, 364.
5 N. A. Peppas and D. S. Van Blarcom, *J. Controlled Release*, 2016, **240**, 142–150.
6 A. Herrmann, R. Haag and U. Schedler, *Adv. Healthcare Mater.*, 2021, **10**, 2100062.

 This journal is © The Royal Society of Chemistry 2023

Published on 13 June 2023. Downloaded by Bilkent University on 12/9/2023 12:01:00 PM.

7 Y. Cheng, C. Huang, D. Yang, K. Ren and J. Wei, *J. Mater. Chem. B*, 2018, **6**, 8170–8179.
8 X. Du, J. Zhai, X. Li, Y. Zhang, N. Li and X. Xie, *ACS Sens.*, 2021, **6**, 1990–2001.
9 H. Yuk, B. Lu and X. Zhao, *Chem. Soc. Rev.*, 2019, **48**, 1642–1667.
10 G. Janarthanan and I. Noh, *J. Mater. Sci. Technol.*, 2021, **63**, 35–53.
11 A. Baranwal, A. Kumar, A. Priyadharshini, G. S. Oggu, I. Bhatnagar, A. Srivastava and P. Chandra, *Int. J. Biol. Macromol.*, 2018, **110**, 110–123.
12 N. Park and J. Kim, *Adv. Intell. Syst.*, 2020, **2**, 1900135.
13 J. A. Hunt, R. Chen, T. van Veen and N. Bryan, *J. Mater. Chem. B*, 2014, **2**, 5319–5338.
14 M. C. Catoira, L. Fusaro, D. Di Francesco, M. Ramella and F. Boccafoschi, *J. Mater. Sci.: Mater. Med.*, 2019, **30**, 115.
15 Y. Wang, *Biomaterials*, 2018, **178**, 663–680.
16 S. Kruss, L. Erpenbeck, M. P. Schön and J. P. Spatz, *Lab Chip*, 2012, **12**, 3285–3289.
17 B. Zhou, K. Fan, T. Li, G. Luan and L. Kong, *Sens. Actuators, B*, 2023, **380**, 133334.
18 G. Chen, S. Xu, Q. Zhou, Y. Zhang, Y. Song, J. Mi, Y. Liu, K. Hou and J. Pan, *Adv. Fiber Mater.*, 2023, **5**, 968–978.
19 C. A. Dreiss, *Curr. Opin. Colloid Interface Sci.*, 2020, **48**, 1–17.
20 M. J. Webber and E. T. Pashuck, *Adv. Drug Delivery Rev.*, 2021, **172**, 275–295.
21 Y. Min, R. Han, G. Li, X. Wang, S. Chen, M. Xie and Z. Zhao, *Adv. Funct. Mater.*, 2023, **33**, 2212803.
22 G. Yan, B. Chen, X. Zeng, Y. Sun, X. Tang and L. Lin, *Carbohydr. Polym.*, 2020, **244**, 116492.
23 A. J. Clasky, J. D. Watchorn, P. Z. Chen and F. X. Gu, *Acta Biomater.*, 2021, **122**, 1–25.
24 R. Curvello, V. S. Raghuwanshi and G. Garnier, *Adv. Colloid Interface Sci.*, 2019, **267**, 47–61.
25 X. Liu, J. Liu, S. Lin and X. Zhao, *Mater. Today*, 2020, **36**, 102–124.
26 X. Fu, H. Ji, X. Liu and W. Zhu, *Ind. Crops Prod.*, 2021, **173**, 114112.
27 S. Song, W. Li, H. Wen, X. Zeng and Y. Cao, in *10th International Symposium on Advanced Optical Manufacturing and Testing Technologies: Advanced and Extreme Micro-Nano Manufacturing Technologies*, SPIE, 2021, vol. 12073, pp. 18–24.
28 I. Ahmed, M. Elsherif, S. Park, A. K. Yetisen and H. Butt, *ACS Appl. Nano Mater.*, 2022, **5**, 7744–7753.
29 A. K. Yetisen, H. Butt, L. R. Volpatti, I. Pavlichenko, M. Humar, S. J. J. Kwok, H. Koo, K. S. Kim, I. Naydenova, A. Khademhosseini, S. K. Hahn and S. H. Yun, *Biotechnol. Adv.*, 2016, **34**, 250–271.
30 C. F. Guimarães, R. Ahmed, A. P. Marques, R. L. Reis and U. Demirci, *Adv. Mater.*, 2021, **33**, 2006582.
31 M. Loyez, M. C. DeRosa, C. Caucheteur and R. Wattiez, *Biosens. Bioelectron.*, 2022, **196**, 113694.
32 A. Ricciardi, M. Zimmer, N. Witz, A. Micco, F. Piccirillo, M. Giaquinto, M. Kaschel, J. Burghartz, M. Jetter, P. Michler, A. Cusano and S. L. Portalupi, *Adv. Mater. Technol.*, 2022, **7**, 2101681.
33 N. Polley, P. Werner, R. F. Balderas-Valadez and C. Pacholski, *Adv. Mater. Interfaces*, 2022, **9**, 2102312.
34 M. Choi, M. Humar, S. Kim and S.-H. Yun, *Adv. Mater.*, 2015, **27**, 4081–4086.
35 Y. Zhao, M. Lei, S.-X. Liu and Q. Zhao, *Sens. Actuators, B*, 2018, **261**, 226–232.
36 H. I. D. I. Muri and D. R. Hjelme, *Optical Fibers and Sensors for Medical Diagnostics and Treatment Applications XVI*, SPIE, 2016, vol. 9702, pp. 110–117.
37 X. Liu, X. Zhang, J. Cong, J. Xu and K. Chen, *Sens. Actuators, B*, 2003, **96**, 468–472.
38 C. Bian, Y. Cheng, W. Zhu, R. Tong, M. Hu and T. Gang, *IEEE Sens. J.*, 2020, **20**, 5759–5765.
39 L. Zhao, J. Gan, T. Xia, L. Jiang, J. Zhang, Y. Cui, G. Qian and Z. Yang, *J. Mater. Chem. C*, 2019, **7**, 897–904.
40 V. A. Maiorov, *Opt. Spectrosc.*, 2020, **128**, 367–386.
41 F. Pinelli, L. Magagnin and F. Rossi, *Mater. Today Chem.*, 2020, **17**, 100317.
42 X. Sun, S. Agate, K. S. Salem, L. Lucia and L. Pal, *ACS Appl. Bio Mater.*, 2021, **4**, 140–162.
43 K. Jang, J. H. Westbay and S. A. Asher, *ACS Sens.*, 2022, **7**, 1648–1656.
44 Z. Cai, N. L. Smith, J.-T. Zhang and S. A. Asher, *Anal. Chem.*, 2015, **87**, 5013–5025.
45 J. Maitra and V. K. Shukla, *Am. J. Polym. Sci.*, 2014, **4**, 25–31.
46 N. Bhattarai, J. Gunn and M. Zhang, *Adv. Drug Delivery Rev.*, 2010, **62**, 83–99.
47 S. W. Ali and S. A. R. Zaidi, *J. Appl. Polym. Sci.*, 2005, **98**, 1927–1931.
48 S. Bashir, M. Hina, J. Iqbal, A. H. Rajpar, M. A. Mujtaba, N. A. Alghamdi, S. Wageh, K. Ramesh and S. Ramesh, *Polymers*, 2020, **12**, 2702.
49 W. Wang, R. Narain and H. Zeng, in *Polymer Science and Nanotechnology*, ed. R. Narain, Elsevier, 2020, pp. 203–244.
50 X. Hu, M. Vatankhah-Varnoosfaderani, J. Zhou, Q. Li and S. S. Sheiko, *Adv. Mater.*, 2015, **27**, 6899–6905.
51 G. Zhang, Y. Chen, Y. Deng, T. Ngai and C. Wang, *ACS Macro Lett.*, 2017, **6**, 641–646.
52 Y. Hu, C.-H. Lu, W. Guo, M. A. Aleman-Garcia, J. Ren and I. Willner, *Adv. Funct. Mater.*, 2015, **25**, 6867–6874.
53 P. K. Nguyen, W. Gao, S. D. Patel, Z. Siddiqui, S. Weiner, E. Shimizu, B. Sarkar and V. A. Kumar, *ACS Omega*, 2018, **3**, 5980–5987.
54 H. Sai, A. Erbas, A. Dannenhoffer, D. Huang, A. Weingarten, E. Siismets, K. Jang, K. Qu, L. C. Palmer, M. O. de la Cruz and S. I. Stupp, *J. Mater. Chem. A*, 2020, **8**, 158–168.
55 J. L. Holloway, A. M. Lowman and G. R. Palmese, *Soft Matter*, 2012, **9**, 826–833.
56 J. L. Holloway, A. M. Lowman and G. R. Palmese, *Soft Matter*, 2012, **9**, 826–833.
57 M. Kobayashi and H. S. Hyu, *Materials*, 2010, **3**, 2753–2771.
58 J. A. Rowley, G. Madlambayan and D. J. Mooney, *Biomaterials*, 1999, **20**, 45–53.

Published on 13 June 2023. Downloaded by Bilkent University on 12/9/2023 12:01:00 PM.

59 H. Tan, C. Xiao, J. Sun, D. Xiong and X. Hu, *Chem. Commun.*, 2012, **48**, 10289–10291.
60 K. Y. Lee and D. J. Mooney, *Prog. Polym. Sci.*, 2012, **37**, 106–126.
61 B. Jeong, Y. H. Bae and S. W. Kim, *Macromolecules*, 1999, **32**, 7064–7069.
62 J. Zhang, T. Tokatlian, J. Zhong, Q. K. T. Ng, M. Patterson, W. E. Lowry, S. T. Carmichael and T. Segura, *Adv. Mater.*, 2011, **23**, 5098–5103.
63 X. Qu, A. Wirsén and A.-C. Albertsson, *Polymer*, 2000, **41**, 4589–4598.
64 H. C. Kolb, M. G. Finn and K. B. Sharpless, *Angew. Chem., Int. Ed.*, 2001, **40**, 2004–2021.
65 S. Piluso, B. Hiebl, S. N. Gorb, A. Kovalev, A. Lendlein and A. T. Neffe, *Int. J. Artif. Organs*, 2011, **34**, 192–197.
66 B. E. Mirzaei, S. A. Ramazani, M. Shafiee and M. Danaei, *Int. J. Polym. Mater. Polym. Biomater.*, 2013, **62**, 605–611.
67 X. Wu, C. He, Y. Wu and X. Chen, *Biomaterials*, 2016, **75**, 148–162.
68 P. Eiselt, K. Y. Lee and D. J. Mooney, *Macromolecules*, 1999, **32**, 5561–5566.
69 K. L. Shantha and D. R. K. Harding, *J. Appl. Polym. Sci.*, 2002, **84**, 2597–2604.
70 K. L. Shantha and D. R. K. Harding, *J. Appl. Polym. Sci.*, 2002, **84**, 2597–2604.
71 W. Wei, X. Qi, Y. Liu, J. Li, X. Hu, G. Zuo, J. Zhang and W. Dong, *Colloids Surf., B*, 2015, **136**, 1182–1192.
72 J.-Y. Wang, K. Wang, X. Gu and Y. Luo, *ACS Biomater. Sci. Eng.*, 2016, **2**, 887–892.
73 J. Guo, X. Liu, N. Jiang, A. K. Yetisen, H. Yuk, C. Yang, A. Khademhosseini, X. Zhao and S.-H. Yun, *Adv. Mater.*, 2016, **28**, 10244–10249.
74 M. Zhou, J. Guo and C. Yang, *Sens. Actuators, B*, 2018, **264**, 52–58.
75 M. Elsherif, M. U. Hassan, A. K. Yetisen and H. Butt, *Biosens. Bioelectron.*, 2019, **137**, 25–32.
76 A. K. Yetisen, N. Jiang, A. Fallahi, Y. Montelongo, G. U. Ruiz-Esparza, A. Tamayol, Y. S. Zhang, I. Mahmood, S.-A. Yang, K. S. Kim, H. Butt, A. Khademhosseini and S.-H. Yun, *Adv. Mater.*, 2017, **29**, 1606380.
77 K. S. Anseth, C. N. Bowman and L. Brannon-Peppas, *Biomaterials*, 1996, **17**, 1647–1657.
78 K. S. Anseth, C. N. Bowman and L. Brannon-Peppas, *Biomaterials*, 1996, **17**, 1647–1657.
79 Y. Cohen, O. Ramon, I. J. Kopelman and S. Mizrahi, *J. Polym. Sci., Part B: Polym. Phys.*, 1992, **30**, 1055–1067.
80 T. P. Davis and M. B. Huglin, *Macromolecules*, 1989, **22**, 2824–2829.
81 J. P. Baker, H. W. Blanch and J. M. Prausnitz, *J. Appl. Polym. Sci.*, 1994, **52**, 783–788.
82 H. Cui, H. Zhang, M. Yu and F. Yang, *Desalination*, 2018, **426**, 118–126.
83 H. Zhang, J. Li, H. Cui, H. Li and F. Yang, *Chem. Eng. J.*, 2015, **259**, 814–819.
84 H. Chen, Y. Gu, Y. Hu and Z. Qian, *PDA J. Pharm. Sci. Technol.*, 2007, **61**, 303–313.
85 A. Razmjou, M. R. Barati, G. P. Simon, K. Suzuki and H. Wang, *Environ. Sci. Technol.*, 2013, **47**, 6297–6305.
86 A. Erbaş and M. Olvera de la Cruz, *Macromolecules*, 2016, **49**, 9026–9034.
87 R. A. Siegel, M. Falamarzian, B. A. Firestone and B. C. Moxley, *J. Controlled Release*, 1988, **8**, 179–182.
88 M. Lei, Y.-N. Zhang, B. Han, Q. Zhao, A. Zhang and D. Fu, *IEEE Sens. J.*, 2018, **18**, 7499–7504.
89 S.-W. Seo, H. Rostami Azmand and Y. Song, *Opt. Fiber Technol.*, 2020, **58**, 102246.
90 N. Gizli, S. S. Çok and F. Koç, in *Advanced Materials for Sustainable Environmental Remediation*, ed. D. Giannakoudakis, L. Meili and I. Anastopoulos, Elsevier, 2022, pp. 195–229.
91 S. Mi Jung, D. Won Kim and H. Young Jung, *Nanoscale*, 2019, **11**, 17563–17570.
92 A. Reyad Raslan, Synthesis and characterization of metal-organic framework aerogels, 2015.
93 A. Bisson, A. Rigacci, D. Lecomte, E. Rodier and P. Achard, *Drying Technol.*, 2003, **21**, 593–628.
94 C. E. Kim, J. S. Yoon and H. J. Hwang, *J. Sol-Gel Sci. Technol.*, 2009, **49**, 47–52.
95 P. R. Aravind, P. Shajesh, P. Mukundan and K. G. K. Warrier, *J. Sol-Gel Sci. Technol.*, 2009, **52**, 328–334.
96 A. K. Yetisen, in *Holographic Sensors*, ed. A. K. Yetisen, Springer International Publishing, Cham, 2015, pp. 27–51.
97 P. J. Flory, *Principles of Polymer Chemistry*, Cornell University Press, 1953.
98 H. Li, A. Erbaş, J. Zwanikken and M. Olvera de la Cruz, *Macromolecules*, 2016, **49**, 9239–9246.
99 A. Erbas and M. Olvera de la Cruz, *ACS Macro Lett.*, 2015, **4**, 857–861.
100 A. C. Sharma, T. Jana, R. Kesavamoorthy, L. Shi, M. A. Virji, D. N. Finegold and S. A. Asher, *J. Am. Chem. Soc.*, 2004, **126**, 2971–2977.
101 H. Jiang, J. Markowski and J. Sabarinathan, *Opt. Express*, 2009, **17**, 21802–21807.
102 A. V. Goponenko and S. A. Asher, *J. Am. Chem. Soc.*, 2005, **127**, 10753–10759.
103 S. A. Asher, S. F. Peteu, C. E. Reese, M. Lin and D. Finegold, *Anal. Bioanal. Chem.*, 2002, **373**, 632–638.
104 V. Palodiya and S. K. Raghuwanshi, in *International Conference on Photonics Solutions 2015*, SPIE, 2015, vol. 9659, pp. 51–54.
105 L. Wang, C. Zhong, D. Ke, F. Ye, J. Tu, L. Wang and Y. Lu, *Adv. Opt. Mater.*, 2018, **6**, 1800427.
106 P. Hu, X. Dong, W. C. Wong, L. H. Chen, K. Ni and C. C. Chan, *Appl. Opt.*, 2015, **54**, 2647–2652.
107 W. C. Wong, C. C. Chan, P. Hu, J. R. Chan, Y. T. Low, X. Dong and K. C. Leong, *Sens. Actuators, B*, 2014, **191**, 579–585.
108 P. Russell, *Science*, 2003, **299**, 358–362.
109 H. Nguyen, J. Park, S. Kang and M. Kim, *Sensors*, 2015, **15**, 10481–10510.
110 R. Ahmed, M. O. Ozen, M. G. Karaaslan, C. A. Prator, C. Thanh, S. Kumar, L. Torres, N. Iyer, S. Munter, S. Southern, T. J. Henrich, F. Inci and U. Demirci, *Adv. Mater.*, 2020, **32**, 1907160.

 This journal is © The Royal Society of Chemistry 2023

Published on 13 June 2023. Downloaded by Bilkent University on 12/9/2023 12:01:00 PM.

111 F. Inci, U. Celik, B. Turken, H. Ö. Özer and F. N. Kok, *Biochem. Biophys. Rep.*, 2015, **2**, 115–122.
112 A. Mataji-Kojouri, M. O. Ozen, M. Shahabadi, F. Inci and U. Demirci, *ACS Nano*, 2020, **14**, 8518–8527.
113 H. Li and L. Zhang, *Curr. Opin. Green Sustainable Chem.*, 2017, **6**, 48–56.
114 P. Pattnaik, *Appl. Biochem. Biotechnol.*, 2005, **126**, 79–92.
115 S. A. Maier, *Plasmonics: Fundamentals and Applications*, Springer US, New York, NY, 2007.
116 O. Tokel, F. Inci and U. Demirci, *Chem. Rev.*, 2014, **114**, 5728–5752.
117 V. Semwal and B. D. Gupta, *Sens. Actuators, B*, 2019, **283**, 632–642.
118 X. Li, P. Gong, Q. Zhao, X. Zhou, Y. Zhang and Y. Zhao, *Sens. Actuators, B*, 2022, **359**, 131596.
119 I. Antohe, L.-I. Jinga, V.-A. Antohe and G. Socol, *Sensors*, 2021, **21**, 4218.
120 X. Zhou, S. Li, X. Li, X. Yan, X. Zhang, F. Wang and T. Cheng, *IEEE Trans. Instrum. Meas.*, 2020, **69**, 8494–8499.
121 R. Zhang, S. Pu and X. Li, *Sensors*, 2019, **19**, 4345.
122 E. Haque, Md. A. Hossain, F. Ahmed and Y. Namihira, *IEEE Sens. J.*, 2018, **18**, 8287–8293.
123 F. Wang, Y. Zhang, M. Lu, Y. Du, M. Chen, S. Meng, W. Ji, C. Sun and W. Peng, *Sens. Actuators, B*, 2021, **337**, 129816.
124 F. H. Suhailin, A. A. Alwahib, Y. M. Kamil, M. H. Abu Bakar, N. M. Huang and M. A. Mahdi, *Plasmonics*, 2020, **15**, 1369–1376.
125 Y. Chen and H. Ming, *Photonic Sens.*, 2012, **2**, 37–49.
126 P. Sharma, V. Semwal and B. D. Gupta, *Opt. Fiber Technol.*, 2019, **49**, 22–27.
127 F. Inci, C. Filippini, M. Baday, M. O. Ozen, S. Calamak, N. G. Durmus, S. Wang, E. Hanhauser, K. S. Hobbs, F. Juillard, P. P. Kuang, M. L. Vetter, M. Carocci, H. S. Yamamoto, Y. Takagi, U. H. Yildiz, D. Akin, D. R. Wesemann, A. Singhal, P. L. Yang, M. L. Nibert, R. N. Fichorova, D. T.-Y. Lau, T. J. Henrich, K. M. Kaye, S. C. Schachter, D. R. Kuritzkes, L. M. Steinmetz, S. S. Gambhir, R. W. Davis and U. Demirci, *Proc. Natl. Acad. Sci. U. S. A.*, 2015, **112**, E4354–E4363.
128 F. Inci, M. G. Karaaslan, A. Mataji-Kojouri, P. A. Shah, Y. Saylan, Y. Zeng, A. Avadhani, R. Sinclair, D. T.-Y. Lau and U. Demirci, *Appl. Mater. Today*, 2020, **20**, 100709.
129 F. Inci, O. Tokel, S. Wang, U. A. Gurkan, S. Tasoglu, D. R. Kuritzkes and U. Demirci, *ACS Nano*, 2013, **7**, 4733–4745.
130 K. M. Mayer and J. H. Hafner, *Chem. Rev.*, 2011, **111**, 3828–3857.
131 E. Petryayeva and U. J. Krull, *Anal. Chim. Acta*, 2011, **706**, 8–24.
132 S. Jia, C. Bian, J. Sun, J. Tong and S. Xia, *Biosens. Bioelectron.*, 2018, **114**, 15–21.
133 J. Chen, S. Shi, R. Su, W. Qi, R. Huang, M. Wang, L. Wang and Z. He, *Sensors*, 2015, **15**, 12205–12217.
134 Y. J. He, *Opt. Express*, 2013, **21**, 23498.
135 M. H. Tu, T. Sun and K. T. V. Grattan, *Sens. Actuators, B*, 2014, **191**, 37–44.
136 J. Ortega-Mendoza, A. Padilla-Vivanco, C. Toxqui-Quitl, P. Zaca-Morán, D. Villegas-Hernández and F. Chávez, *Sensors*, 2014, **14**, 18701–18710.
137 J. Guo, B. Zhou, Z. Du, C. Yang, L. Kong and L. Xu, *Nanophotonics*, 2021, **10**, 3549–3558.
138 M. Fox, *Quantum optics: an introduction*, Oxford University Press, Oxford, New York, 2006.
139 J. Stone and D. Marcuse, *J. Lightwave Technol.*, 1986, **4**, 382–385.
140 N. Ismail, C. C. Kores, D. Geskus and M. Pollnau, *Opt. Express*, 2016, **24**, 16366.
141 R. Cao, Y. Yang, M. Wang, X. Yi, J. Wu, S. Huang and K. P. Chen, *Opt. Lett.*, 2020, **45**, 3163.
142 Y. Cui, Y. Jiang, T. Liu, J. Hu and L. Jiang, *IEEE Access*, 2020, **8**, 80582–80587.
143 X. Lei and X. Dong, *IEEE Sens. J.*, 2020, **20**, 5292–5297.
144 M. Chen, Y. Zhao, F. Xia, Y. Peng and R. Tong, *Sens. Actuators, A*, 2018, **275**, 60–66.
145 N. A. Ushakov, A. A. Markvart and L. B. Liokumovich, *IEEE Sens. J.*, 2020, **20**, 11302–11312.
146 A. M. Shrivastav, D. S. Gunawardena, Z. Liu and H.-Y. Tam, *Sci. Rep.*, 2020, **10**, 6002.
147 J. Li, J. Zhang, H. Sun, D. Hong, L. Li, Y. Yang, X. Yong, C. Zhang and J. Cui, *Optik*, 2019, **195**, 163172.
148 X. Wu, H. Liu, X. Wang and H. Jiang, *IEEE Sens. J.*, 2018, **18**, 45–52.
149 J. S. Santos, I. M. Raimundo, C. M. B. Cordeiro, C. R. Biazoli, C. A. J. Gouveia and P. A. S. Jorge, *Sens. Actuators, B*, 2014, **196**, 99–105.
150 H. I. Muri, A. Bano and D. R. Hjelme, *J. Lightwave Technol.*, 2018, **36**, 1159–1167.
151 C. Jung, S.-J. Kim, J. Jang, J. H. Ko, D. Kim, B. Ko, Y. M. Song, S.-H. Hong and J. Rho, *Sci. Adv.*, 2022, **8**, eabm8598.
152 K. P. Zetie, S. F. Adams and R. M. Tocknell, *Phys. Educ.*, 2000, **35**, 46–48.
153 L. Li, L. Xia, Z. Xie and D. Liu, *Opt. Express*, 2012, **20**, 11109.
154 P. Lu, L. Men, K. Sooley and Q. Chen, *Appl. Phys. Lett.*, 2009, **94**, 131110.
155 Y. Wang, Y. Li, C. Liao, D. N. Wang, M. Yang and P. Lu, *IEEE Photonics Technol. Lett.*, 2010, **22**, 39–41.
156 Z. Tian, S. S.-H. Yam, J. Barnes, W. Bock, P. Greig, J. M. Fraser, H.-P. Loock and R. D. Oleschuk, *IEEE Photonics Technol. Lett.*, 2008, **20**, 626–628.
157 W. Liu, X. Wu, G. Zhang, S. Li, C. Zuo, W. Zhang and B. Yu, *Appl. Opt.*, 2020, **59**, 1786.
158 B. Sun, Y. Huang, S. Liu, C. Wang, J. He, C. Liao, G. Yin, J. Zhao, Y. Liu, J. Tang, J. Zhou and Y. Wang, *Opt. Express*, 2015, **23**, 14596.
159 S. Marrujo-Garcia, I. Hernandez-Romano, M. Torres-CIsneros, D. A. May-Arrioja, V. P. Minkovich and D. Monzon-Hernandez, *J. Lightwave Technol.*, 2020, 1.
160 S. Kadhim Al-Hayali, A. M. Salman and A. Hadi Al-Janabi, *Opt. Fiber Technol.*, 2022, **71**, 102944.
161 G. Li, Z. Liu, J. Feng, G. Zhou and X. Huang, *Opt. Laser Technol.*, 2022, **145**, 107453.
162 W. Xuan, L. Ruiyi, F. Saiying, L. Zaijun, W. Guangli, G. Zhiguo and L. Junkang, *Sens. Actuators, B*, 2017, **243**, 211–220.

Published on 13 June 2023. Downloaded by Bilkent University on 12/9/2023 12:01:00 PM.

163 X. Zhang, Z. Shi, X. Huang and X. Li, *Cont. Shelf Res.*, 2017, **143**, 1–8.
164 J. R. Lakowicz and B. R. Masters, *J. Biomed. Opt.*, 2008, **13**, 029901.
165 G. A. Jones and D. S. Bradshaw, *Front. Phys.*, 2019, **7**, 100.
166 L. Zhao, G. Li, J. Gan and Z. Yang, *J. Light Technol.*, 2021, **39**, 6653–6659.
167 J. Gong, M. G. Tanner, S. Venkateswaran, J. M. Stone, Y. Zhang and M. Bradley, *Anal. Chim. Acta*, 2020, **1134**, 136–143.
168 K. Ehrlich, T. R. Choudhary, M. Ucuncu, A. Megia-Fernandez, K. Harrington, H. A. C. Wood, F. Yu, D. Choudhury, K. Dhaliwal, M. Bradley and M. G. Tanner, *Sensors*, 2020, **20**, 6115.
169 C. G. Frankær, K. J. Hussain, T. C. Dörge and T. J. Sørensen, *ACS Sens.*, 2019, **4**, 26–31.
170 Y. Bai and Q. Bai, *Subsea Pipeline Integrity and Risk Management*, Elsevier, 2014, pp. 3–25.
171 P. Irving and C. Soutis, *Polymer composites in the aerospace industry*, Woodhead Publishing, 2019, p. 666.
172 X. Qiao, Z. Shao, W. Bao and Q. Rong, *Sensors*, 2017, **17**, 429.
173 G. Allwood, G. Wild and S. Hinckley, *Electronics*, 2017, **6**, 92.
174 V. P. Matveenko, I. N. Shardakov, A. A. Voronkov, N. A. Kosheleva, D. S. Lobanov, G. S. Serovaev, E. M. Spaskova and G. S. Shipunov, *Struct. Control Health Monit.*, 2018, **25**, e2118.
175 D. Tosi, *Sensors*, 2017, **17**, 2368.
176 P. V. N. Kishore, M. Sai Shankar and M. Satyanarayana, *Sens. Actuators, B*, 2017, **243**, 626–633.
177 P. V. N. Kishore, S. S. Madhuvarasu and S. Moru, *Opt. Eng.*, 2018, **57**, 017101.
178 I. Yulianti, A. S. M. Supa'at, S. M. Idrus, O. Kurdi and M. R. S. Anwar, *Meas. Sci. Technol.*, 2012, **23**, 015104.
179 J. Janting, J. K. M. Pedersen, G. Woyessa, K. Nielsen and O. Bang, *J. Light Technol.*, 2019, **37**, 4480–4486.
180 F. Yang, R. Hlushko, D. Wu, S. A. Sukhishvili, H. Du and F. Tian, *ACS Omega*, 2019, **4**, 2134–2141.
181 S. K. Mishra, B. Zou and K. S. Chiang, *IEEE J. Sel. Top. Quantum Electron.*, 2017, **23**, 284–288.
182 K. Chiang, Y. Liu, M. N. Ng and X. Dong, *Electron. Lett.*, 2000, **36**, 966–967.
183 M. Choi, J. W. Choi, S. Kim, S. Nizamoglu, S. K. Hahn and S. H. Yun, *Nat. Photonics*, 2013, **7**, 987–994.
184 G. I. Olivas and G. V. Barbosa-Cánovas, *LWT – Food Sci. Technol.*, 2008, **41**, 359–366.
185 B. Zeeb, A. Hossein Saberi, J. Weiss and D. Julian McClements, *Soft Matter*, 2015, **11**, 2228–2236.
186 A. F. Hassan, A. M. Abdel-Mohsen and M. M. G. Fouda, *Carbohydr. Polym.*, 2014, **102**, 192–198.
187 M. M. Ward Muscatello, L. E. Stunja and S. A. Asher, *Anal. Chem.*, 2009, **81**, 4978–4986.
188 B. Stuart, *Kirk-Othmer Encyclopedia of Chemical Technology*, John Wiley & Sons, Ltd, 2005.
189 C. H. Yang, M. X. Wang, H. Haider, J. H. Yang, J.-Y. Sun, Y. M. Chen, J. Zhou and Z. Suo, *ACS Appl. Mater. Interfaces*, 2013, **5**, 10418–10422.
190 H. Yuk, T. Zhang, S. Lin, G. A. Parada and X. Zhao, *Nat. Mater.*, 2016, **15**, 190–196.
191 C. Cha, E. Antoniadou, M. Lee, J. H. Jeong, W. W. Ahmed, T. A. Saif, S. A. Boppart and H. Kong, *Angew. Chem., Int. Ed.*, 2013, **52**, 6949–6952.
192 B. Liu, H. Zhu, D. Zhao, G. Nian, S. Qu and W. Yang, *Adv. Opt. Mater.*, 2021, **9**, 2101036.
193 M. Jin, X. Feng, J. Xi, J. Zhai, K. Cho, L. Feng and L. Jiang, *Macromol. Rapid Commun.*, 2005, **26**, 1805–1809.
194 Q. Liu, G. Nian, C. Yang, S. Qu and Z. Suo, *Nat. Commun.*, 2018, **9**, 846.
195 S. Deguchi, J. Hotta, S. Yokoyama and T. S. Matsui, *J. Micromech. Microeng.*, 2015, **25**, 097002.
196 M. A. Daniele, S. H. North, J. Naciri, P. B. Howell, S. H. Foulger, F. S. Ligler and A. A. Adams, *Adv. Funct. Mater.*, 2013, **23**, 698–704.
197 K. Hou, Y. Li, Y. Liu, R. Zhang, B. S. Hsiao and M. Zhu, *Polymer*, 2017, **123**, 55–64.
198 S. Nakajima, R. Kawano and H. Onoe, *Soft Matter*, 2017, **13**, 3710–3719.
199 S. Chen, W. Ma, Y. Cheng, Z. Weng, B. Sun, L. Wang, W. Chen, F. Li, M. Zhu and H.-M. Cheng, *Nano Energy*, 2015, **15**, 642–653.
200 Z. Zhang, L. Cui, X. Shi, X. Tian, D. Wang, C. Gu, E. Chen, X. Cheng, Y. Xu, Y. Hu, J. Zhang, L. Zhou, H. H. Fong, P. Ma, G. Jiang, X. Sun, B. Zhang and H. Peng, *Adv. Mater.*, 2018, **30**, 1800323.
201 G. Chen, G. Wang, X. Tan, K. Hou, Q. Meng, P. Zhao, S. Wang, J. Zhang, Z. Zhou, T. Chen, Y. Cheng, B. S. Hsiao, E. Reichmanis and M. Zhu, *Natl. Sci. Rev.*, 2021, **8**, nwaa209.
202 G. Chen, K. Hou, N. Yu, P. Wei, T. Chen, C. Zhang, S. Wang, H. Liu, R. Cao, L. Zhu, B. S. Hsiao and M. Zhu, *Nat. Commun.*, 2022, **13**, 7789.
203 C.-H. Choi, H. Yi, S. Hwang, D. A. Weitz and C.-S. Lee, *Lab Chip*, 2011, **11**, 1477–1483.
204 Y. Niu, H. Liu, R. He, M. Luo, M. Shu and F. Xu, *Small*, 2021, **17**, 2101151.
205 J. C. Knight, *Nature*, 2003, **424**, 847–851.
206 M. Ordu and A. E. Akosman, *Opt. Lett.*, 2022, **47**, 3039–3042.
207 Z. Cai, J.-T. Zhang, F. Xue, Z. Hong, D. Punihaole and S. A. Asher, *Anal. Chem.*, 2014, **86**, 4840–4847.
208 K. Jang, W. S. Horne and S. A. Asher, *ACS Appl. Mater. Interfaces*, 2020, **12**, 39612–39619.
209 J. H. Holtz and S. A. Asher, *Nature*, 1997, **389**, 829–832.
210 S. M. Wagalgave, S. S. Birajdar, J. N. Malegaonkar and S. V. Bhosale, in *Progress in Molecular Biology and Translational Science*, ed. R. S. Bhosale and V. Singh, Academic Press, 2021, vol. 185, pp. 199–223.
211 W. Li, J. Liu, J. Wei, Z. Yang, C. Ren and B. Li, *Adv. Funct. Mater.*, 2023, **33**, 2213485.
212 Y. Li and X. Zhang, *Adv. Funct. Mater.*, 2022, **32**, 2107767.
213 M. Zhang, S. Chen, N. Sheng, B. Wang, Z. Wu, Q. Liang, Z. Han and H. Wang, *J. Mater. Chem. A*, 2021, **9**, 12574–12583.

 This journal is © The Royal Society of Chemistry 2023

Published on 13 June 2023. Downloaded by Bilkent University on 12/9/2023 12:01:00 PM.

214 X. Zhao, F. Chen, Y. Li, H. Lu, N. Zhang and M. Ma, *Nat. Commun.*, 2018, **9**, 3579.
215 J. Song, S. Chen, L. Sun, Y. Guo, L. Zhang, S. Wang, H. Xuan, Q. Guan and Z. You, *Adv. Mater.*, 2020, **32**, 1906994.
216 S. K. Srivastava, R. Verma and B. D. Gupta, *Sens. Actuators, B*, 2011, **153**, 194–198.
217 R. C. Jorgenson and S. S. Yee, *Sens. Actuators, B*, 1993, **12**, 213–220.
218 B. D. Gupta and R. K. Verma, *J. Sens.*, 2009, 979761.
219 J. Homola, S. S. Yee and G. Gauglitz, *Sens. Actuators, B*, 1999, **54**, 3–15.
220 S. Singh and B. D. Gupta, *Sens. Actuators, B*, 2012, **173**, 268–273.
221 V. Semwal, A. M. Shrivastav, R. Verma and B. D. Gupta, *Sens. Actuators, B*, 2016, **230**, 485–492.
222 S. Singh and B. D. Gupta, *Sens. Actuators, B*, 2013, **177**, 589–595.
223 S. K. Mishra and B. D. Gupta, *Analyst*, 2013, **138**, 2640–2646.
224 A. Lahav, M. Auslender and I. Abdulhalim, *Opt. Lett.*, 2008, **33**, 2539–2541.
225 P. Bhatia and B. D. Gupta, *Appl. Opt.*, 2011, **50**, 2032–2036.
226 R. K. Verma and B. D. Gupta, *J. Opt. Soc. Am. A*, 2010, **27**, 846–851.
227 Y. Qian, Y. Zhao, Q. Wu and Y. Yang, *Sens. Actuators, B*, 2018, **260**, 86–105.
228 I. Hernández-Romano, M. A. Cruz-Garcia, C. Moreno-Hernández, D. Monzón-Hernández, E. O. López-Figueroa, O. E. Paredes-Gallardo, M. Torres-Cisneros and J. Villatoro, *Opt. Express*, 2016, **24**, 5654–5661.
229 Y. Yuan, L. Ding and Z. Guo, *Sens. Actuators, B*, 2011, **157**, 240–245.
230 J. R. Velázquez-González, H. Peregrina-Barreto, J. Rangel-Magdaleno and J. C. Ramírez-San-Juan, in *IEEE International Autumn Meeting on Power, Electronics and Computing (ROPEC)*, 2017, pp. 1–6.
231 Y. Zhao, Z. Deng and Q. Wang, *Sens. Actuators, B*, 2014, **192**, 229–233.
232 H.-H. Jeong, Y.-J. Son, S.-K. Kang, H.-J. Kim, H.-J. Roh, N. Erdene, J.-H. Park, D.-H. Jeong, H.-Y. Lee and S.-K. Lee, *IEEE Sens. J.*, 2013, **13**, 351–358.
233 M. Sanders, Y. Lin, J. Wei, T. Bono and R. G. Lindquist, *Biosens. Bioelectron.*, 2014, **61**, 95–101.
234 J. Cao, M. H. Tu, T. Sun and K. T. V. Grattan, *Sens. Actuators, B*, 2013, **181**, 611–619.
235 H. I. Muri and D. R. Hjelme, *Sensors*, 2017, **17**, 2723.
236 J. Qian, K. Wang, C. Wang, C. Ren, Q. Liu, N. Hao and K. Wang, *Sens. Actuators, B*, 2017, **241**, 1153–1160.
237 P. Wu, X. Hou, J.-J. Xu and H.-Y. Chen, *Nanoscale*, 2016, **8**, 8427–8442.
238 A. G. Lee, C. P. Arena, D. J. Beebe and S. P. Palecek, *Biomacromolecules*, 2010, **11**, 3316–3324.
239 J. Guo, M. Zhou and C. Yang, *Sci. Rep.*, 2017, **7**, 7902.
240 T.-W. Sung and Y.-L. Lo, *Sens. Actuators, B*, 2012, **165**, 119–125.
241 T.-W. Sung, Y.-L. Lo and I.-L. Chang, *Sens. Actuators, B*, 2014, **202**, 1349–1356.
242 H. M. R. Gonçalves, A. J. Duarte and J. C. G. Esteves da Silva, *Biosens. Bioelectron.*, 2010, **26**, 1302–1306.
243 I. I. Bessen, *US Pat.*, US2925497A, 1960.
244 S. Wen, J. Zhou, K. Zheng, A. Bednarkiewicz, X. Liu and D. Jin, *Nat. Commun.*, 2018, **9**, 2415.
245 L. Zhang, Z. Bian, A. Hu, J. Li, L. Liu and F. Chu, *Opt. Commun.*, 2020, **475**, 126225.
246 Z. Bian, C. Zhao, S. Feng, L. Xue, A. Hu, H. Yang and F. Chu, *Opt. Fiber Technol.*, 2021, **66**, 102659.
247 R. Acharya, in *Satellite Signal Propagation, Impairments and Mitigation*, ed. R. Acharya, Academic Press, 2017, pp. 57–86.
248 X. Hu, X. Shen, J. Wu, J. Peng, L. Yang, J. Li, H. Li and N. Dai, *Opt. Express*, 2016, **24**, 21693–21699.
249 S. Al-Ithawi and A. Hadi, *Defect Diffus. Forum*, 2020, **398**, 125–130.
250 S. Dong, B. Dong, C. Yu and Y. Guo, *J. Light Technol.*, 2018, **36**, 1125–1130.
251 B. Gu, M.-J. Yin, A. P. Zhang, J.-W. Qian and S. He, *Opt. Express*, 2009, **17**, 22296–22302.
252 S. Tierney, D. R. Hjelme and B. T. Stokke, *Anal. Chem.*, 2008, **80**, 5086–5093.
253 Y. Zheng, L. H. Chen, X. Dong, J. Yang, H. Y. Long, P. L. So and C. C. Chan, *IEEE J. Sel. Top. Quantum Electron.*, 2016, **22**, 331–335.
254 M. K. Pati and P. Nayak, *Mater. Sci. Appl.*, 2011, **2**, 1741–1748.
255 K. Ni, C. C. Chan, L. Chen, X. Dong, R. Huang and Q. Ma, *Opt. Fiber Technol.*, 2017, **33**, 56–59.
256 A. K. Mallik, D. Liu, V. Kavungal, Q. Wu, G. Farrell and Y. Semenova, *Opt. Express*, 2016, **24**, 21216–21227.
257 M. T. S. Chani, K. S. Karimov, S. B. Khan and A. M. Asiri, *Sens. Actuators, A*, 2016, **246**, 58–65.
258 Y. Wang, C. Shen, W. Lou and F. Shentu, *Opt. Commun.*, 2016, **372**, 229–234.
259 S. Feroz and G. Dias, *Heliyon*, 2021, **7**, e08294.
260 H. Luo, L. Liang, X. Ma, N. Liu, S. Huang and H. Sun, *IEEE Sens. J.*, 2018, **18**, 8022–8027.
261 S. Tierney, S. Volden and B. T. Stokke, *Biosens. Bioelectron.*, 2009, **24**, 2034–2039.
262 Z. Q. Tou, T. W. Koh and C. C. Chan, *Sens. Actuators, B*, 2014, **202**, 185–193.
263 S. Deng, H. Meng, X. Wang, X. Fan, Q. Wang, M. Zhou, X. Guo, Z. Wei, F. Wang, C. Tan and X. Huang, *Opt. Express*, 2019, **27**, 9232–9240.
264 X. Zhang, X. Wang, W. Fan, Y. Liu, Q. Wang and L. Weng, *Polymers*, 2022, **14**, 3227.
265 J. Cong, X. Zhang, K. Chen and J. Xu, *Sens. Actuators, B*, 2002, **87**, 487–490.
266 R. Rajini-Kumar, M. Suesser, K. G. Narayankhedkar, G. Krieg and M. D. Atrey, *Cryogenics*, 2008, **48**, 142–147.
267 P. Lu, L. Men and Q. Chen, *Appl. Phys. Lett.*, 2008, **92**, 171112.
268 V. N. K. Pabbisetti and S. S. Madhuvarasu, *Opt. Eng.*, 2016, **55**, 057107.

Published on 13 June 2023. Downloaded by Bilkent University on 12/9/2023 12:01:00 PM.

269 M. Elsherif, R. Moreddu, M. U. Hassan, A. K. Yetisen and H. Butt, *Lab Chip*, 2019, **19**, 2060–2070.
270 I. Ahmed, M. Elsherif, S. Park, A. K. Yetisen and H. Butt, *ACS Appl. Nano Mater.*, 2022, **5**, 7744–7753.
271 M. Elsherif, R. Moreddu, M. U. Hassan, A. K. Yetisen and H. Butt, *Lab Chip*, 2019, **19**, 2060–2070.
272 X. Zhang, Y. Guan and Y. Zhang, *Biomacromolecules*, 2012, **13**, 92–97.
273 X. Wang, Q. Li, Y. Guan and Y. Zhang, *Mater. Today Chem.*, 2016, **1–2**, 7–14.
274 Y. Zhang, Y. Guan and S. Zhou, *Biomacromolecules*, 2006, **7**, 3196–3201.
275 Z. Tang, Y. Guan and Y. Zhang, *Polym. Chem.*, 2014, **5**, 1782–1790.
276 J. V. Veetil, S. Jin and K. Ye, *Biosens. Bioelectron.*, 2010, **26**, 1650–1655.
277 D. Li, J. Wu, P. Wu, Y. Lin, Y. Sun, R. Zhu, J. Yang and K. Xu, *Sens. Actuators, B*, 2015, **213**, 295–304.
278 S. K. Srivastava, V. Arora, S. Sapra and B. D. Gupta, *Plasmonics*, 2012, **7**, 261–268.
279 C. Chen, Q. Xie, D. Yang, H. Xiao, Y. Fu, Y. Tan and S. Yao, *RSC Adv.*, 2013, **3**, 4473–4491.
280 S. K. Vashist, D. Zheng, K. Al-Rubeaan, J. H. T. Luong and F.-S. Sheu, *Anal. Chim. Acta*, 2011, **703**, 124–136.
281 V. R. Kondepati and H. M. Heise, *Anal. Bioanal. Chem.*, 2007, **388**, 545.
282 C. L. Thompson, K. C. Dunn, M. C. Menon, L. E. Kearns and S. S. Braithwaite, *Diabetes Spectrum*, 2005, **18**, 20–27.
283 S. J. Finney, C. Zekveld, A. Elia and T. W. Evans, *J. Am. Med. Assoc.*, 2003, **290**, 2041–2047.
284 V. M. Montori, B. R. Bistrian and M. M. McMahon, *J. Am. Med. Assoc.*, 2002, **288**, 2167–2169.
285 S. Viswanathan, T. N. Narayanan, K. Aran, K. D. Fink, J. Paredes, P. M. Ajayan, S. Filipek, P. Miszta, H. C. Tekin, F. Inci, U. Demirci, P. Li, K. I. Bolotin, D. Liepmann and V. Renugopalakrishanan, *Mater. Today*, 2015, **18**, 513–522.
286 C. Malitesta, F. Palmisano, L. Torsi and P. G. Zambonin, *Anal. Chem.*, 1990, **62**, 2735–2740.
287 P. D. Hale, L. I. Boguslavsky, T. Inagaki, I. Karan, H. S. Lee, T. A. Skotheim and Y. Okamoto, *Anal. Chem.*, 1991, **63**, 677–682.
288 D. A. Gough and T. Bremer, *Diabetes Technol. Ther.*, 2000, **2**, 377–380.
289 M. Zhang, A. Smith and W. Gorski, *Anal. Chem.*, 2004, **76**, 5045–5050.
290 A. C. Mack, J. Mao and M. J. McShane, *2005 IEEE Sensors*, 2005, p. 4.
291 J. Huang, M. Li, P. Zhang, P. Zhang and L. Ding, *Sens. Actuators, B*, 2016, **237**, 24–29.
292 J. Huang, P. Zhang, M. Li, P. Zhang and L. Ding, *Biochem. Eng. J.*, 2016, **114**, 262–267.
293 J. Huang, Y. Liu, P. Zhang, Y. Li and L. Ding, *Biochem. Eng. J.*, 2017, **125**, 123–128.
294 H. Lin, M. Li, L. Ding and J. Huang, *Appl. Biochem. Biotechnol.*, 2019, **187**, 1569–1580.
295 M. Elsherif, M. U. Hassan, A. K. Yetisen and H. Butt, *ACS Nano*, 2018, **12**, 2283–2291.
296 P. Thoniyot, F. E. Cappuccio, S. Gamsey, D. B. Cordes, R. A. Wessling and B. Singaram, *Diabetes Technol. Ther.*, 2006, **8**, 279–287.
297 M. Elsherif, M. U. Hassan, A. K. Yetisen and H. Butt, *ACS Nano*, 2018, **12**, 2283–2291.
298 I. Hisamitsu, K. Kataoka, T. Okano and Y. Sakurai, *Pharm. Res.*, 1997, **14**, 289–293.
299 S. Tierney, B. M. H. Falch, D. R. Hjelme and B. T. Stokke, *Anal. Chem.*, 2009, **81**, 3630–3636.
300 S. Gamsey, J. T. Suri, R. A. Wessling and B. Singaram, *Langmuir*, 2006, **22**, 9067–9074.
301 M. Yin, B. Huang, S. Gao, A. P. Zhang and X. Ye, *Biomed. Opt. Express*, 2016, **7**, 2067–2077.
302 W. C. Michie, B. Culshaw, I. McKenzie, M. Konstantakis, N. B. Graham, C. Moran, F. Santos, E. Bergqvist and B. Carlstrom, *Opt. Lett.*, 1995, **20**, 103–105.
303 B. J.-C. Deboux, E. Lewis, P. J. Scully and R. Edwards, *J. Light Technol.*, 1995, **13**, 1407–1414.
304 A. K. Pathak, D. K. Chaudhary and V. K. Singh, *Sens. Actuators, A*, 2018, **280**, 399–405.
305 A. Q. Maclin, M. D. Kim, S. A. Dergunov, E. Pinkhassik and E. Lindner, *Electroanalysis*, 2015, **27**, 733–744.
306 T. Liu, W. Wang, H. Ding and D. Yi, *IEEE Sens. J.*, 2019, **19**, 9441–9446.
307 Z. Q. Tou, C. C. Chan, J. Hong, S. Png, K. M. T. Eddie and T. A. H. Tan, *J. Biomed. Opt.*, 2014, **19**, 047002.
308 I. Manavi-Tehrani, M. Rabiee, M. Parviz, M. R. Tahriri and Z. Fahimi, *Macromol. Symp.*, 2010, **296**, 457–465.
309 S. M. M. Quintero, M. Cremona, A. L. C. Triques, A. R. d'Almeida and A. M. B. Braga, *Polymer*, 2010, **51**, 953–958.
310 P. V. N. Kishore and M. S. Shankar, in *Frontiers in Optics 2015 (2015)*, paper JW2A.6, Optica Publishing Group, 2015, p. JW2A.6.
311 X. Liang, S. Chen, H. Huang and W. Liu, *Photonic Sens.*, 2014, **4**, 28–33.
312 Y. Lin, S. Chen, M. Wang and W. Liu, *Opt. Eng.*, 2015, **54**, 057107.
313 T. A. Abdzaid and H. J. Taher, *Appl. Opt.*, 2021, **60**, 1587–1594.
314 S. Li and W.-D. Li, in Optical Sensing, Imaging, and Photon Counting: Nanostructured Devices and Applications *2017*, SPIE, 2017, vol. 10353, pp. 82–87.
315 H. I. Muri and D. R. Hjelme, *Sensors*, 2017, **17**, 2723.
316 J. S. Velázquez-González, D. Monzón-Hernández, D. Moreno-Hernández, F. Martínez-Piñón and I. Hernández-Romano, *Sens. Actuators, B*, 2017, **242**, 912–920.
317 A. A. Noman, J. N. Dash, X. Cheng, X. Cheng, C. Y. Leong, H.-Y. Tam, C. Yu and C. Yu, *Opt. Express*, 2020, **28**, 39640–39648.
318 Y. Alqurashi, M. Elsherif, A. Hendi, K. Essa and H. Butt, *Biosensors*, 2022, **12**, 40.
319 C. W. Callahan, A. M. Elansari and D. L. Fenton, in *Postharvest Technology of Perishable Horticultural*

 This journal is © The Royal Society of Chemistry 2023

Published on 13 June 2023. Downloaded by Bilkent University on 12/9/2023 12:01:00 PM.

Commodities, ed. E. M. Yahia, Woodhead Publishing, 2019, pp. 271–310.
320 T. L. Yeo, T. Sun and K. T. V. Grattan, *Sens. Actuators, A*, 2008, **144**, 280–295.
321 L. Alwis, T. Sun and K. T. V. Grattan, *Measurement*, 2013, **46**, 4052–4074.
322 A. P. Russell and K. S. Fletcher, *Anal. Chim. Acta*, 1985, **170**, 209–216.
323 S. K. Khijwania, K. L. Srinivasan and J. P. Singh, *Sens. Actuators, B*, 2005, **104**, 217–222.
324 F. J. Arregui, Z. Ciaurriz, M. Oneca and I. R. Matias, *Sens. Actuators, B*, 2003, **96**, 165–172.
325 C. Bariain, I. R. Matias, F. J. Arregui and M. Lopez-Amo, *Sens. Actuators, B*, 2000, **69**, 127–131.
326 D. Lo Presti, C. Massaroni, V. Piemonte, P. Saccomandi, R. D'Amato, M. A. Caponero and E. Schena, *IEEE Sens. J.*, 2019, **19**, 3335–3342.
327 X. Liu, M. Jiang, Q. Sui and X. Geng, *J. Mod. Opt.*, 2016, **63**, 1668–1674.
328 S. Zhang, X. Dong, T. Li, C. C. Chan and P. P. Shum, *Opt. Commun.*, 2013, **303**, 42–45.
329 P. D. Palma, C. Taddei, S. Campopiano, M. Giordano, A. Iadicicco and L. Sansone, in *26th International Conference on Optical Fiber Sensors (2018)*, paper ThE10, Optica Publishing Group, 2018, p. ThE10.
330 L. Xia, L. Li, W. Li, T. Kou and D. Liu, *Sens. Actuators, A*, 2013, **190**, 1–5.
331 C. Kelb, M. Körner, O. Prucker, J. Rühe, E. Reithmeier and B. Roth, *Sensors*, 2017, **17**, 517.
332 Y. Liu, L. Wang, M. Zhang, D. Tu, X. Mao and Y. Liao, *IEEE Photonics Technol. Lett.*, 2007, **19**, 880–882.
333 L. Wang, Y. Liu, M. Zhang, D. Tu, X. Mao and Y. Liao, *Meas. Sci. Technol.*, 2007, **18**, 3131–3134.
334 X. Yu, P. Childs, M. Zhang, Y. Liao, J. Ju and W. Jin, *IEEE Photonics Technol. Lett.*, 2009, **21**, 1828–1830.
335 X. Yu, M. Zhang, S. Liu, Y. Liao and W. Jin, in *21st International Conference on Optical Fiber Sensors*, SPIE, 2011, vol. 7753, pp. 1325–1328.
336 K. M. Tan, S. C. Tjin, C. C. Chan, L. Mohanty and C. M. Tay, in *17th International Conference on Optical Fibre Sensors*, SPIE, 2005, vol. 5855, pp. 375–378.
337 A. MacLean, W. C. Michie, S. G. Pierce, G. Thursby, B. Culshaw, C. Moran and N. B. Graham, in Smart Structures and Materials 1998: Sensory Phenomena and Measurement Instrumentation for Smart Structures and Materials, SPIE, 1998, vol. 3330, pp. 134–144.
338 A. Gastón, F. Pérez and J. Sevilla, *Appl. Opt.*, 2004, **43**, 4127–4132.
339 Z. F. Zhang and Y. Zhang, *Opt. Laser Technol.*, 2015, **74**, 16–19.
340 R. A. Kumbasar, *J. Hazard. Mater.*, 2010, **178**, 875–882.
341 S. K. Mishra and B. D. Gupta, *Anal. Methods*, 2014, **6**, 5191.
342 Y. Wang, J. Wu, J. Yuan, G. Sun and C. Pan, *J. Appl. Polym. Sci.*, 2002, **83**, 2883–2891.
343 H. Vázquez-Torres, J. V. Cauich-Rodríguez and C. A. Cruz-Ramos, *J. Appl. Polym. Sci.*, 1993, **50**, 777–792.
344 P. F. Good, C. W. Olanow and D. P. Perl, *Brain Res.*, 1992, **593**, 343–346.
345 O. Ozay, N. Aktas and N. Sahiner, *Sep. Sci. Technol.*, 2011, **46**, 1450–1461.
346 X. Liu, S. Zheng, X. Zhang, J. Cong, K. Chen and J. Xu, *Chin. Opt. Lett.*, 2004, **2**, 683–685.
347 T. P. Flaten, *Brain Res. Bull.*, 2001, **55**, 187–196.
348 S. R. Paik, J.-H. Lee, D.-H. Kim, C.-S. Chang and J. Kim, *Arch. Biochem. Biophys.*, 1997, **344**, 325–334.
349 F. Chu, P. Han, S. Feng, S. Wei, H. Ma and Z. Bian, *Optik*, 2021, **240**, 166875.
350 P. T. Lieu, M. Heiskala, P. A. Peterson and Y. Yang, *Mol. Aspects Med.*, 2001, **22**, 1–87.
351 A. A. Belaidi and A. I. Bush, *J. Neurochem.*, 2016, **139**, 179–197.
352 M.-J. Tsai, H. Cheng, H.-H. Ho, P.-W. Lin, D.-Y. Liou, T.-C. Fang, C.-W. Li, K. Kwan, Y.-C. Chen, C.-S. Huang, S.-F. Horng, C.-H. Hung, H.-W. Zan and H.-F. Meng, *Biosens. Bioelectron.*, 2020, **162**, 112230.
353 D. W. Choi and J. Y. Koh, *Annu. Rev. Neurosci.*, 1998, **21**, 347–375.
354 B. K. Y. Bitanihirwe and M. G. Cunningham, *Synapse*, 2009, **63**, 1029–1049.
355 H.-T. Su, M.-J. Tsai, G.-F. Chang, C.-H. Hung, H.-C. Lin, C.-Y. Chou, D.-W. Huang, C.-C. Liang, Y.-C. Lin, H.-F. Meng, H.-W. Zan, S.-F. Horng, D.-Y. Liou and H. Cheng, *Org. Electron.*, 2015, **26**, 429–438.
356 J.-H. Syu, Y.-K. Cheng, W.-Y. Hong, H.-P. Wang, Y.-C. Lin, H.-F. Meng, H.-W. Zan, S.-F. Horng, G.-F. Chang, C.-H. Hung, Y.-C. Chiu, W.-C. Chen, M.-J. Tsai and H. Cheng, *Adv. Funct. Mater.*, 2013, **23**, 1566–1574.
357 A. Hernández-Tobías, A. Julián-Sánchez, E. Piña and H. Riveros-Rosas, *Chem.-Biol. Interact.*, 2011, **191**, 14–25.
358 B. K. Logan and A. W. Jones, *Med., Sci. Law*, 2000, **40**, 206–215.
359 C. Kroh, R. Wuchrer, N. Steinke, M. Guenther, G. Gerlach and T. Härtling, *Sensors*, 2019, **19**, 1264.
360 V. Semwal, A. M. Shrivastav and B. D. Gupta, *Nanotechnology*, 2017, **28**, 065503.
361 R. M. J. Palmer, A. G. Ferrige and S. Moncada, *Nature*, 1987, **327**, 524–526.
362 C.-W. Chung, M.-J. Tsai, P.-W. Lin, D.-W. Huang, K.-H. Wang, Y.-A. Chen, H.-F. Meng, H.-W. Zan, H. Cheng, L. Tong, L. Zhang, S.-F. Horng and C.-H. Hung, *AIP Adv.*, 2018, **8**, 025207.
363 Y. Zheng, L. H. Chen, C. C. Chan, X. Dong, J. Yang, Z. Q. Tou and P. L. So, 24th International Conference on Optical Fibre Sensors, 2015, Vol. 9634, pp. 963467.
364 C. Fenghong, F. Shi, B. Zhenglan, Z. Chunpeng, X. Liang and H. Anduo, *Optik*, 2021, **247**, 168014.
365 N. Cennamo, G. D'Agostino, R. Galatus, L. Bibbò, M. Pesavento and L. Zeni, *Sens. Actuators, B*, 2013, **188**, 221–226.
366 R. Verma and B. D. Gupta, *Sens. Actuators, B*, 2013, **177**, 279–285.
367 Y. Taguchi, E. Takano and T. Takeuchi, *Langmuir*, 2012, **28**, 7083–7088.

Published on 13 June 2023. Downloaded by Bilkent University on 12/9/2023 12:01:00 PM.

368 M. Sasaki, B. C. Karikkineth, K. Nagamine, H. Kaji, K. Torimitsu and M. Nishizawa, *Adv. Healthcare Mater.*, 2014, **3**, 1919–1927.
369 C. Yang, P. Zhang, A. Nautiyal, S. Li, N. Liu, J. Yin, K. Deng and X. Zhang, *ACS Appl. Mater. Interfaces*, 2019, **11**, 4258–4267.
370 Y. Wei, L. Xiang, P. Zhu, Y. Qian, B. Zhao and G. Chen, *Chem. Mater.*, 2021, **33**, 8623–8634.
371 Z. Bai, X. Wang, M. Zheng, O. Yue, M. Huang, X. Zou, B. Cui, L. Xie, S. Dong, J. Shang, G. Gong, A. M. Blocki, J. Guo and X. Liu, *Adv. Funct. Mater.*, 2023, **33**, 2212856.
372 C. Cai, C. Wen, W. Zhao, S. Tian, Y. Long, X. Zhang, X. Sui, L. Zhang and J. Yang, *ACS Appl. Mater. Interfaces*, 2022, **14**, 23692–23700.
373 Z. Zhou and W. Yuan, *Composites, Part A*, 2023, **172**, 107603.
374 L. Hu, P. L. Chee, S. Sugiarto, Y. Yu, C. Shi, R. Yan, Z. Yao, X. Shi, J. Zhi, D. Kai, H.-D. Yu and W. Huang, *Adv. Mater.*, 2023, **35**, 2205326.
375 H. Liu, M. Li, S. Liu, P. Jia, X. Guo, S. Feng, T. J. Lu, H. Yang, F. Li and F. Xu, *Mater. Horiz.*, 2020, **7**, 203–213.

 This journal is © The Royal Society of Chemistry 2023